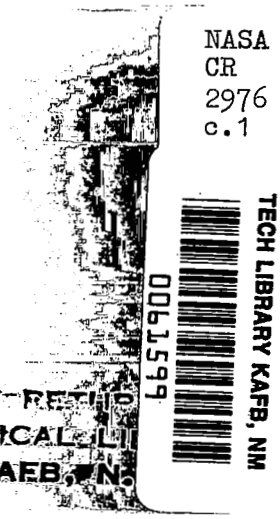

NASA Contractor Report 2976

Ball to Separator Contact Forces in Angular Contact Ball Bearings Under Thrust and Radial Loads

Lester J. Nypan

GRANT NSG-3065
APRIL 1978

NASA

NASA Contractor Report 2976

Ball to Separator Contact Forces in Angular Contact Ball Bearings Under Thrust and Radial Loads

Lester J. Nypan
California State University, Northridge
Northridge, California

Prepared for
Lewis Research Center
under Grant NSG-3065

NASA
National Aeronautics
and Space Administration

**Scientific and Technical
Information Office**

1978

Table of Contents

List of Figures

List of Tables

Introduction

Current developments in jet engine technology are placing more stringent demands on gas turbine design. There is a constantly increasing requirement for engines to develop greater thrust outputs. In addition to this increased loading the need to raise the thrust/weight ratio of engines and to improve the fuel consumption has led to higher rotor speeds and operating temperatures, lighter components and correspondingly increased structural flexibility. In anticipation of tomorrow's requirements, further advanced knowledge of engine component technology must be obtained.(1)*

In the case of rolling contact bearings there is a need for a better understanding of cage and rolling element dynamics, particularly in ultra-high speed applications.(2,3,4,5)

Recently developed, advanced bearing theories have resulted in computerized optimization of rolling element bearing designs and in some cases accurate prediction of bearing performance. These developments and advances by no means substitute for testing of rolling element bearings which for many years was the basis for bearing development. To the contrary, the need for more refined data gathering methods has become obvious. Tests are needed to verify the theories which form the foundation of these computer programs. Also, performance tests and studies will always be needed to refine bearing designs for critical applications.

The interaction between the rolling elements of a bearing with the raceways and separators is particularly difficult to measure due

---

*Numbers in parentheses designate references at end of report.

to the rapidity of their motion. The kinematic behavior and the resulting forces acting on a rolling element/separator/raceway assembly could in the past be measured only by tests where the operating conditions were drastically simplified.

Separator Study Machine

An optical bearing test rig has been constructed to operate the bearing and make photographic records of the rolling elements and separator behavior. Figure 1a shows an overall view of the machine as it is presently installed in the Dynamics Laboratory of the Engineering Building at California State University, Northridge. The machine was originally assembled by Industrial Tectonics, Inc., Compton, Calif., and has been used in industrial bearing research, and in a ball motion study reported in (6).

The bearing test rig is basically a shaft supported by a pair of preloaded ball bearings at one end and the test bearing at the other end. One face of the test bearing is exposed to allow free view of the balls and the separator. Radial load was applied to the test bearing by a hydraulic actuator through a cable loop over the bearing housing. The shaft was driven by a 75 hp hydraulic motor through a geared belt drive, giving speeds infinitely variable from 100 to 15,000 rpm. Figure 1b is a schematic of the shaft assembly.

Lubricating oil for under race cooling and test bearing lubrication is supplied through a series of orifices from the rear of the test bearing.

Due to the high tangential velocities present when a bearing is rotated at shaft speeds up to 15,000 rpm, conventional photograph techniques are inadequate. The difficulty lies in obtaining photo-

graphs having sufficient resolution for analysis when very short exposures are required to freeze the motion of the bearing elements. This problem has been overcome by eliminating the gross rotational motion using a derotation prism. The resulting image thus presents the differential motion between the separator and the rolling element, enabling observation and photographs to be made of an individual separator pocket. Derotation is accomplished by synchronizing the rotation of a Pechan prism at half-speed with the rotation of the ball separator, thus causing the apparent image rotation and the true separator rotation to coincide. This results in the derotated image of the area of interest being imaged on the film plane of a camera. Light rays from the illuminated bearing are collected through the front window of the instrument. This window is optically coated to reject ultraviolet energy produced by ultraviolet lamps, serving the circuit for the prism speed control. From the window, the rays travel through collimator lenses and the Pechan prism before they travel through the exit lenses. Their path is then deflected by mirrors which fold the image in different directions. Figure 1c shows light paths through the scanner.

One light trace travels to a beam splitter where approximately 15 % of the light is reflected to the eyepiece optics to provide an image observable to the operator. The balance of light enters the aperture of the pulse camera.

Alignment and positioning of the optical elements ensure that the eyepiece observes the same image quality and format as that which the film sees.

Another image is folded and demagnified in the transfer lens assembly before it enters the camera.

A derotated image of the luminous painted segment of the test bearing separator is optically folded out and directed toward an

image splitting mirror surface wedge which proportions the light entering two photomultiplier tube photocathodes. The electronic signals from these tubes are used by the tracking system to control the prism speed.

A tracking system holds the image of a selected point at the test bearing separator in the field of view. It will accommodate a variation of up to 10% of a fixed ratio of separator-to-shaft speed without loss of the ability to lock onto the proper position within one revolution of the bearing retainer.

It is necessary to sense the tracking error in angular position of the derotation prism to provide an input for the servo system. This error signal is provided in the form of the difference in output of two multiplier phototubes.

A sector on the bearing retainer is coated with fluorescent paint and illuminated with ultraviolet light. An image of the sector of arc is formed in a plane containing the apex of a mirror surface wedge. The light striking the two surfaces of the wedge is reflected and illuminates the photocathode of the photomultiplier tubes. Rotation of the prism results in a displacement of the image and a consequent increase in the output of one tube and decrease in the output of the other.

Electronic filtering is provided to discriminate between the steady signal due to the ultraviolet excitation of the phosphor and any intermittent excitation due to strobe lamps to reduce any interaction between the level of light striking the phosphor and the error signal produced by the photomultipliers.

Four Chadwick-Helmuth Strobex lamps are flashed at the 16-frame-per-second camera rate to illuminate the separator and to stop the images of the protractors on the inner and outer races of the bearing so that angular position information is recorded on the photographs.

Four mercury vapor spot lamps with ultraviolet filters illuminate the flourescent patch for the tracking system.

The camera used was a Neyhard Enterprises model G-4. The camera film magazine accepts 100 or 200 foot reels of 35 mm film. The camera has a data box, the image of which is projected onto each film frame.

Test Bearings

The bearings used in the ball to separator contact force investigation were mainshaft thrust bearings used in the Pratt and Whitney TF 30 gas turbine engine, part numbers PWA 506110 and PWA 506111. Dimensions and other characteristics of these bearings are given in Table 1.

Separator Force Transducer

A ball contact force transducer was constructed on the bearing separator by introducing a cantilever beam between two of the bearing balls. The cantilever beam replaced a rigid separating element so that cantilever beam deflection would give an indication of the ball contact force. A hole was drilled through one of the side rails of the separator to hold the fixed end of the cantilever beam. A notch to frame the deflected end of the cantilever was cut in the other side rail opposite the hole. Various beam cross sections were used depending on contact forces and deflections encountered. A Teflon

rubbing block was cemented to the center portion of the beam to make up the normal ball spacing dimension of the rigid separator element replaced by the ball force indicating beam. A duplicate modification was installed at 180° to the first to maintain separator balance.

With the shaft and test bearing operating at a speed and load condition to be investigated, the derotation prism was synchronized with the separator to produce a stationary image of the deflecting end of the cantilever beam as the balls and separator repeatedly moved through loaded and unloaded regions of the bearing. The 16 frame per second 35 mm instrumentation camera photographed the motions of the cantilever beam deflections relative to the notch in the separator. As ball contact forces may be expected to be a repetitive event from revolution to revolution the relatively slow framing rate can be extended to a very high effective framing rate by taking a large number of photographs over many revolutions of the bearing. This gives frames covering 0 to 360° to the applied load. The angle to the applied load was indicated by the position of the cantilever beam relative to a fixed protractor on the bearing outer race. Radial loads were applied vertically at the 360 (0) degree mark on the protractor. Static photographs with the cantilever beam at 90,180, and 270 degrees to the vertical clearly indicated positive, zero, and negative deflections consistent with the weight of 19.05 mm (0.750 in) steel balls.

Figure 3 shows one of the ball contact force transducers as constructed.

Force Transducer Calibration

The force transducing cantilever beam was assembled into the separator with epoxy resin with the Teflon spacing element also epoxied in place. The separator was held in a small vise and loaded with a wire hook positioned at the estimated ball contact location. A small weight pan and 6.35 mm (0.250 in.) balls were used to load the cantilever beam. Cantilever deflections were photographed. Figure 4 gives the force-deflection relation for the stiffest cantilever beam used (61.8 N/mm). The permanent deformation evident in Fig. 4 did not affect ball force measurements as forces encountered did not exceed 27.5 N (6.2lb.). Table 3 gives values of spring constant and bearings used in the course of investigation.

Experimental Procedure

The lubricating oil used throughout the tests was a 5-centistoke neopentyl polyol (tetra) ester. This is a type II oil which conforms to specification MIL-L-23699. Test bearing inlet oil was heated and controlled to 485° K (150±2°F).

The Separator Study Machine bearing rig was started with a 500 lb thrust load and brought up to speed, the desired load condition applied, the prism synchronized with the separator and 100 to 200 photographs taken. Film used was Kodak 2475 Recording Film. It was cut into lengths fitting stainless steel reels and developed in a small tank with HC 110 developer, dilution A, for 30 minutes at laboratory room temperature. This seemed to give images of adequate contrast, with background fog just beginning to be noticeable on fresh film.

Data Analysis

After chemical processing of the film was completed the film was respliced and each frame was numbered.

The film was read with a Benson-Lehner model N-2 film reader capable of indicating 4 digits with the least digit representing 0.005 mm (0.0002 in.) in the film image. The film images, however, varied in density and sharpness from frame to frame due to variation in Xenon flash intensity, duration, and jitter in flash initiation among the four Xenon flash tubes, as well as from oil splash in the bearing chamber and on the bearing chamber window.

Readings were taken by aligning a cross-hair onto the lowest edge of the notch for R1, the bottom of the beam end for R2, the top of the beam end for R3, and the top of the notch for R4. The computer program listed in Appendix I was used to calculate differences R2-R1, R3-R1, R4-R1, R3-R2, R4-R3, and R4-R2. From R4-R1 and R3-R2 a consistency check was available to pull out or correct obviously defective readings as the notch dimension and beam height should always be of constant value. After subtraction of undeflected (zero) readings, the other four differences give four separate indications of the beam deflection in that film frame.

The computer program also calculated average values of notch size for the photo set and normalized the deflection indications on the average notch size to compensate for image size variation with focus setting. It then scales the deflections to the lineal measured notch dimension. The deflection indications are then multiplied by the spring constant determined in the force transducer calibration, and are listed and plotted by a Calcomp plotter.

Figure 5 is representative of photographs obtained.

It was possible to determine cage to shaft speed ratio with some accuracy over 10 successive photographs of multiple shaft revolutions from the following considerations.

The derotating prism is synchronized to rotate at half the separator speed thus producing a stationary image of the separator to be photographed. Protractors which are mounted on the stationary outer race and on the rotating inner race are visible in the photographs. Four Xenon flash tubes with a flash duration of 50 microseconds permit clear instantaneous photographs of the stationary separator and stop the motion of the protractor images. Typically 100 to 200 photographs were taken at a cine frame rate of 16 per second for each case investigated.

In these photographs the angle turned through by the separator (cage) can be determined from the difference in angle on the stationary outer race protractor between two consecutive frames. Thus,

$$2\Delta\theta_p = \Delta\theta_c = \Delta\theta_o = \left(\frac{W_c}{W_s}\right) W_s \Delta t \qquad (1)$$

where:

$\Delta\theta_p$ = true prism angle turned through

$\Delta\theta_c$ = true cage angle turned through

$\Delta\theta_o$ = angle difference $+360^\circ$ x number of revolutions between photographs

$\frac{W_c}{W_s}$ = separator to shaft speed ratio in the operating bearing

W_s = shaft speed

Δt = time between photographs

The protractors are engraved with angle increasing in the direction of shaft rotation. The shaft turns through a greater angle than does the separator; consequently, the cage photographs centered on the transducer in the cage show the inner race angles decreasing. The

true angle that the shaft has turned through in the 1/16 second between successive frames may be determined from the protractor angles photographed by

$$\Delta\theta_s = \Delta\theta_o - \Delta\theta_{st} = \left(\frac{W_c}{W_s}\right) W_s \Delta t - W_s \Delta t \qquad (2)$$

where:

$\Delta\theta_s$ = angle difference on inner race protractor between photographs

($\theta_{s_{i+1}} - \theta_{s_i}$ with i being the frame number)

$\Delta\theta_{st}$ = true angle turned through by the shaft in time Δt

From equation 2, then $\Delta\theta_{st} = \Delta\theta_o - \Delta\theta_s$, and $W_c \Delta t = \Delta\theta_o$, $W_s \Delta t = \Delta\theta_{st}$ so:

$$\frac{W_c}{W_s} = \frac{\Delta\theta_o}{\Delta\theta_o - \Delta\theta_s} \qquad (3)$$

where $\Delta\theta_s$ is a negative number.

Care must be taken in calculating angle differences $\Delta\theta_o$ and $\Delta\theta_s$ between photographs and in using equation (3). Multiple revolutions of shaft and separator occur without this being apparent in the photographs. At 16 frames per second with a nominal value of 0.441 for W_c/W_s the ranges of angle differences given in Table 4 may be anticipated.

To obtain the true angle of rotation of the cage between successive frames, it is necessary to:

1. Subtract the angle read from the reference point of the separator in the photograph from that read in the i-1 frame.
2. Determine the number of full rotations between frames using Table 4.
3. Add the number of full rotations to the difference found in step 1.

These considerations led to the cage/shaft speed ratios that appear on the cage force figure captions and in the cage/shaft speed ratio versus load figures.

Results and Discussion

This investigation was undertaken to experimentally evaluate ball to cage contact forces. It was subsequently noted that information on cage to inner race land contact force, cage to inner race land operating clearance, and cage to shaft speed ratios could also be extracted from the data obtained.

Ball to Cage Contact Forces

The principal results of this investigation are the ball to cage contact forces shown in Figures 6-8. These show the ball force on the cage as a function of ball location in the bearing. Ball location is measured clockwise from the centerline of the radial load at 0° (360°). Table 2 summarizes the shaft speeds, loads, spring constants, figure identification system, and loads used in the investigation.

Different spring constants were necessary as the investigation progressed from 1000 to 4000 rpm and to higher speeds. Larger forces were

encountered and cantilever deflections approaching the ball to cage pocket clearance were observed.

Data was obtained at 1000 rpm with a spring constant of 1.49 N/mm (8.51 lb/in). These forces were small and of similar nature to those at higher speeds. The 1000 rpm results are not presented as they are too small to be visible on the scales used to present the higher speed results. Centrifugal force at 12000 rpm deflected the 17.2 N/mm (98.2 lb/in) beam out to contact the cage so that friction limited the motion of the cantilever.

All the data at 12000 rpm was taken with the 61.8 N/mm (353 lb/in) spring constant cantilever. Some lower speed cases were also run with the larger spring constant cantilevers.

Positive forces in the figures are those exerted by balls tending to accelerate the cage. Negative forces are those exerted by balls tending to retard or decelerate the cage. In general the stiffer cantilever beam deflecting elements indicate greater forces, with more scatter in the film readings.

There does appear to be a correlation between the magnitude of the ball-cage forces measured and the stiffness of the beam. For a given load and speed condition the range of ball-cage forces is always lowest for the 4.73 N/mm beam and reasonably equal for the 17.2 and 61.8 N/mm beams.

This may be a result of a "fixed displacement" aspect of ball motion whereby ball-cage forces are created when the cage constrains the ball from accelerating or decelerating as ball kinematic considerations dictate.

Apparently the 4.73 N/mm beam permits the ball to move as it will with only minor interactive forces generated by the beam. The forces generated by the 17.2 and 61.8 N/mm beams seem to be nearly

the same. This may be an indication that the maximum possible traction forces have been developed at the ball-raceway contacts for the particular load and speed condition.

Table 5 tabulates the variation in force range with spring constant.

Figures 9 and 10 summarize the variation of magnitude and location of cage forces with speed for radially loaded bearings. Figure 11 summarizes the variation of magnitude of cage forces with speed for thrust loaded bearings. As might be expected the equally loaded balls in thrust loaded cases do not show much variation in cage force with ball location within the bearing.

The approximately 1 lb. negative force in pure thrust loaded cases indicates the balls are decelerating (retarding) the cage uniformly. This is consistent with the cage being driven by the higher speed shaft surface on which the cage is guided.

Centrifugal force moves the tip of the cantilever beam out by a noticeable amount in photographs taken at 12000 rpm. It is felt that the radial centrifugal deflections do not affect the deflection characteristics of the beam in the tangential direction. It was reasoned that the portion of the beam that is bent by the ball is only that part extending from a fixed end in one rail of the cage to the center of the ball pocket where contact with the ball takes place. The larger portion of the beam extends from the center of the ball pocket and through the other rail of the cage. It is acting as a straight pointer to magnify the deflection at the center of the cage pocket. Over the part of the beam stressed in bending the radial deflection is small compared to beam dimensions.

Cage to Inner Race Land Contact Force

From the data of Figures 6, 7, and 8 it was possible to derive the force between the cage and its guiding contact with the inner race land. This was obtained by taking horizontal and vertical components of each force point as plotted in Figures 6, 7, and 8. Adding vertical and horizontal forces in an 18 degree sector, and dividing by the number of forces in the sector gave the average force one of the 20 balls would exert on the cage. The sum of the 20 ball forces should equal the resultant force that the inner race must exert on the cage. The angular location of the resultant force was obtained by taking the arc tangent of the ratio of horizontal to vertical force components. Figure 12 summarizes the magnitude and direction of the cage to inner race land force due to ball contact forces for various speeds and loads. It should be noted that this did not include the 3.5N (0.78 lb) weight of the cage.

Cage to Inner Race Land Operating Clearance

Figure 13 shows the separation between the cage and the inner race as a function of location from the zero degree index on the stationary outer race protractor. What appears in Figure 13 to be cage to inner race contact may actually be a close approach or small clearance that was shadowed by the optical angle and projection of the inner race image onto the cage image in the film plane. It appears that cage motion is somewhat erratic in the 12000 rpm speed case. The thrust loaded condition indicated an almost constant cage to inner race clearance. A clearance was visible in every one of the photographs read for the thrust loaded case.

The location of the cage to shaft contact indicated in Fig. 13a seems to agree with that of Fig. 12b. Figure 13c likewise agrees with

Fig. 12b. Figure 13b, however, indicates cage to shaft contact somewhere between 45 and 190 degrees, possibly centered at 120 degrees much of the time, while the corresponding point in Fig. 12b was found to be located at 40 degrees. It would seem that there are uncertainties in the cage force measurements and their locations that are not always averaged away by the simple device of calculating an average force per ball and adding the 20 ball to cage forces vectorially to arrive at a cage to shaft resultant force.

Cage to Shaft Speed Ratios

Figure 14 shows the cage to shaft speed ratios calculated by the method described in the section Data Analysis. It may be noted that data taken before January 12, 1977 (also identified by the spring constant of 4.7 N/mm) were taken with a PWA 506111 bearing while the balance of the data was taken with a PWA 506110 bearing. The different spring constants used may have influenced the cage motion through their effect on cage forces. It is also possible that internal bearing clearances changed due to changes in temperatures of bearing components. The bearings used were of split inner race construction with presumably some gothic arch to the inner race surfaces to prevent ball contact with radial oil passages between the races.

All data obtained fell between cage to shaft speed ratios of 0.465 and 0.433. There was a general trend for cage to shaft speed ratio to decrease with load. It would seem that the loads employed did not encourage skidding, and that the cage to shaft speed ratio variations observed were due to deflections of bearing components due to load and temperature.

Conclusion

Ball to cage contact forces were evaluated experimentally. They appear to be greatest in radially loaded bearings operating at high speed, and are of the order of 25 N (5 lb) at the maximum. Stiffer cantilever beam deflecting elements indicated larger forces, however, the 17.2 and 61.8 N/mm beams gave comparable results. Resultant cage to inner race land forces vary in a similar manner with values up to 20 N (4 lb). Resultant force as used here is the vector sum around the bearing of the average forces on each ball, and is equal to the vector sum of cage to shaft normal and tangential force components. Cage to shaft speed ratios indicated that the load conditions employed did not encourage skidding.

References

1. Brown, P.F., "Bearings and Dampers for Advanced Jet Engines", Paper 700318 SAE National Air Transportation Meeting, New York, New York, April 20-23, 1970.

2. Gupta, P.K., Transient Ball Motion and Skid in Ball Bearings

3. Harris, T.A., "An Analytical Method to Predict Skidding in Thrust Loaded Angular Contact Ball Bearings", Journal of Lubrication Technology, Trans. ASME, Series F, Vol. 73, 1971, pp. 17-24.

4. Poplawski, J.V., "Slip and Cage Forces in A High Speed Roller Bearing", Journal of Lubrication Technology, Trans. ASME, Series F, Vol. 72, pp.

5. Walters, C.T., "The Dynamics of Ball Bearings", Journal of Lubrication Technology, Trans. ASME, Series F, Vol. 93, 1971, pp. 1-10.

6. Signer, H.R., "Experimental Ball Bearing Dynamics Study", NASA CR 1345 28, October 1973.

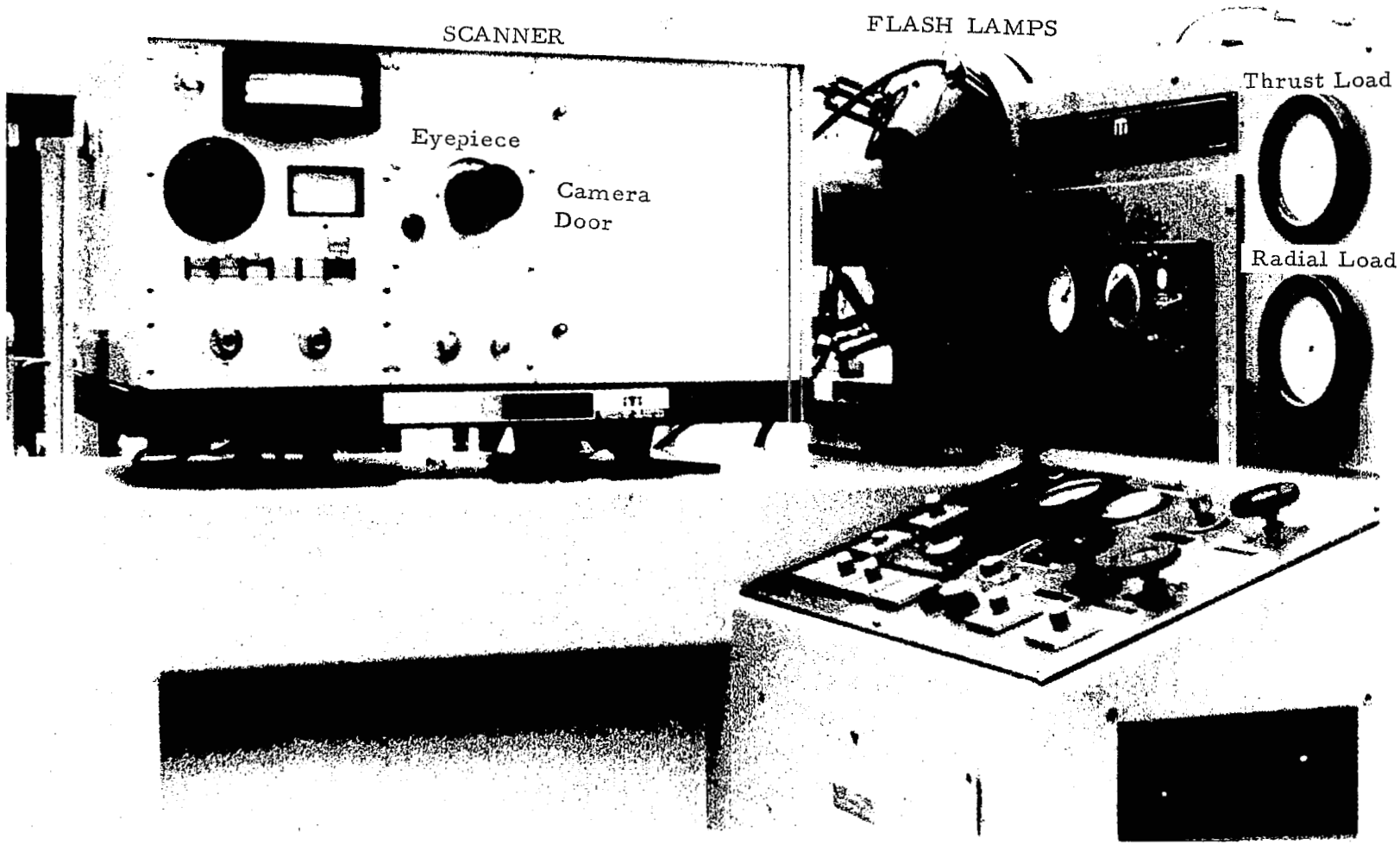

FIG. 1-A SEPARATOR
STUDY MACHINE

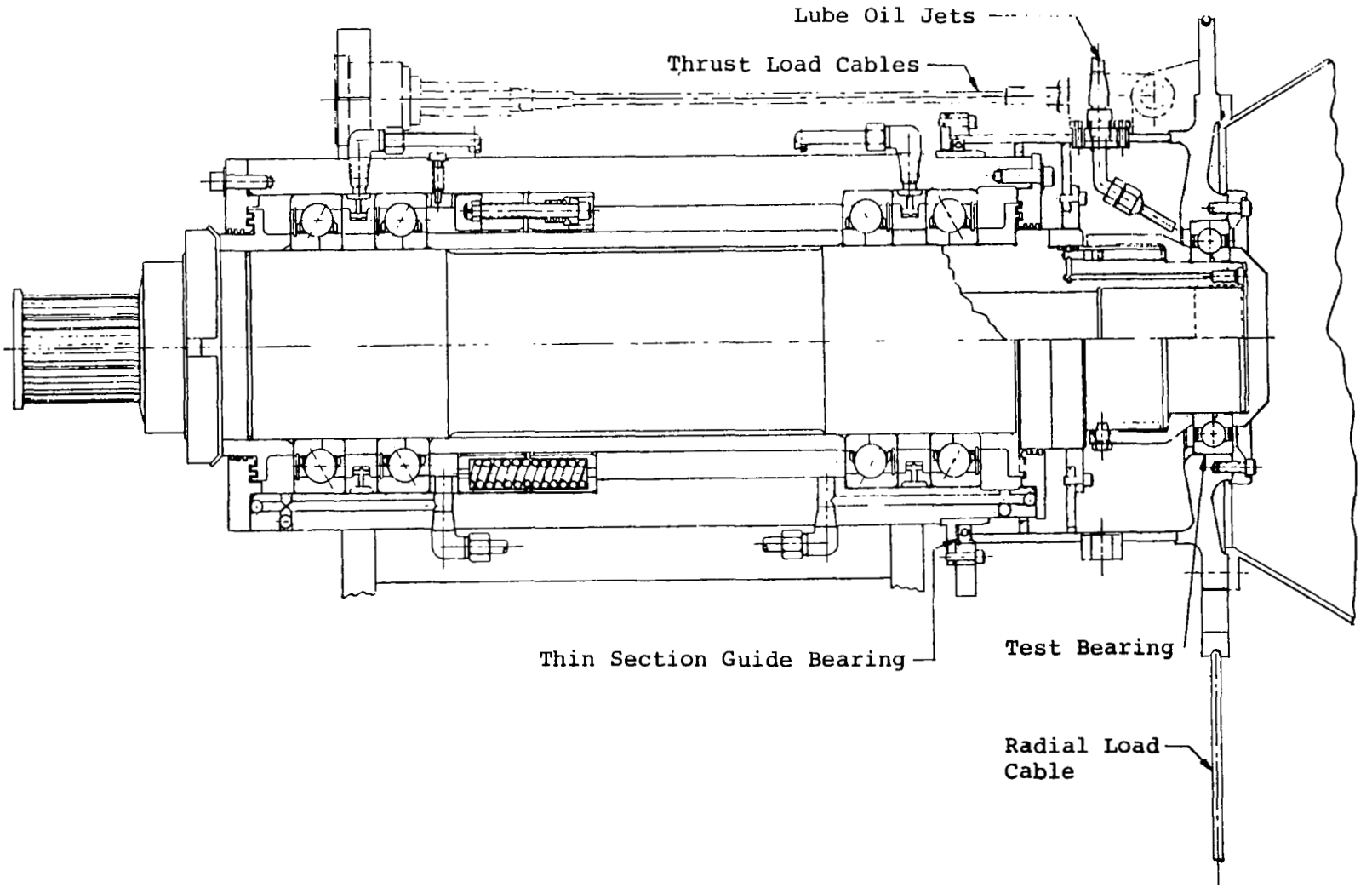

FIG. 1b SCHEMATIC OF SHAFT ASSEMBLY

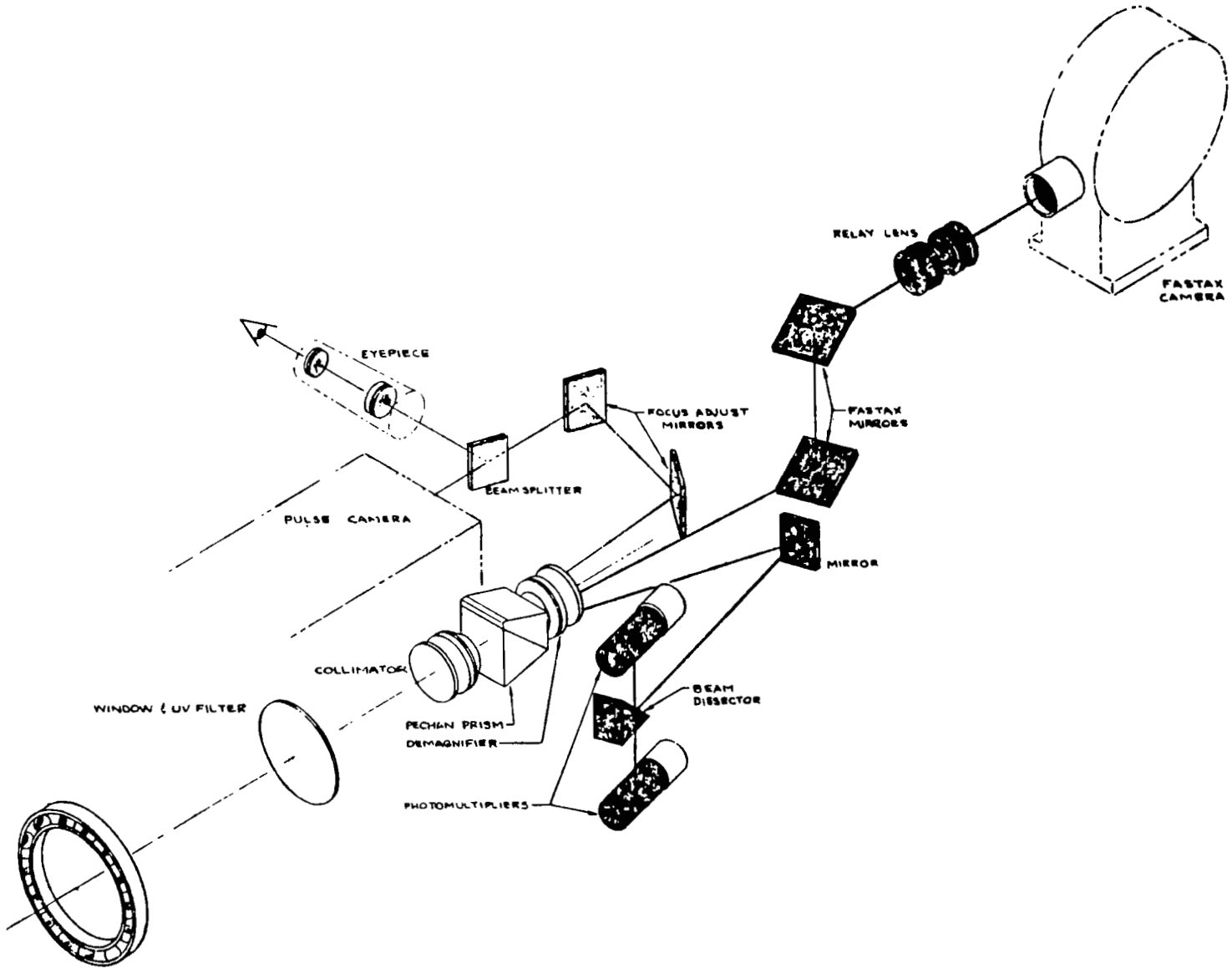

FIG. 1 c OPTICAL PATHS THROUGH THE BEARING SCANNER

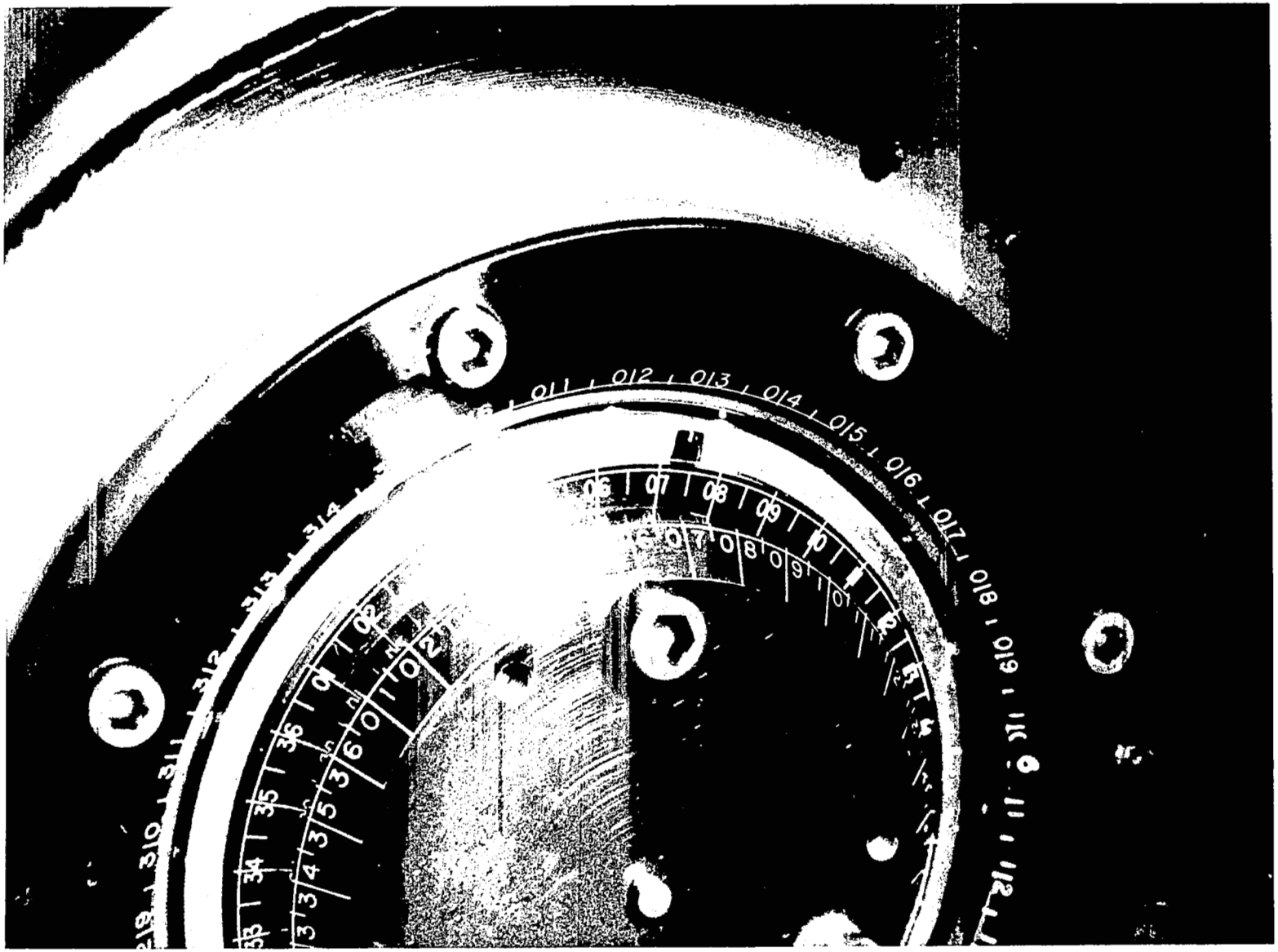

FIG. 2 TEST BEARING
IN SEPARATOR STUDY
MACHINE

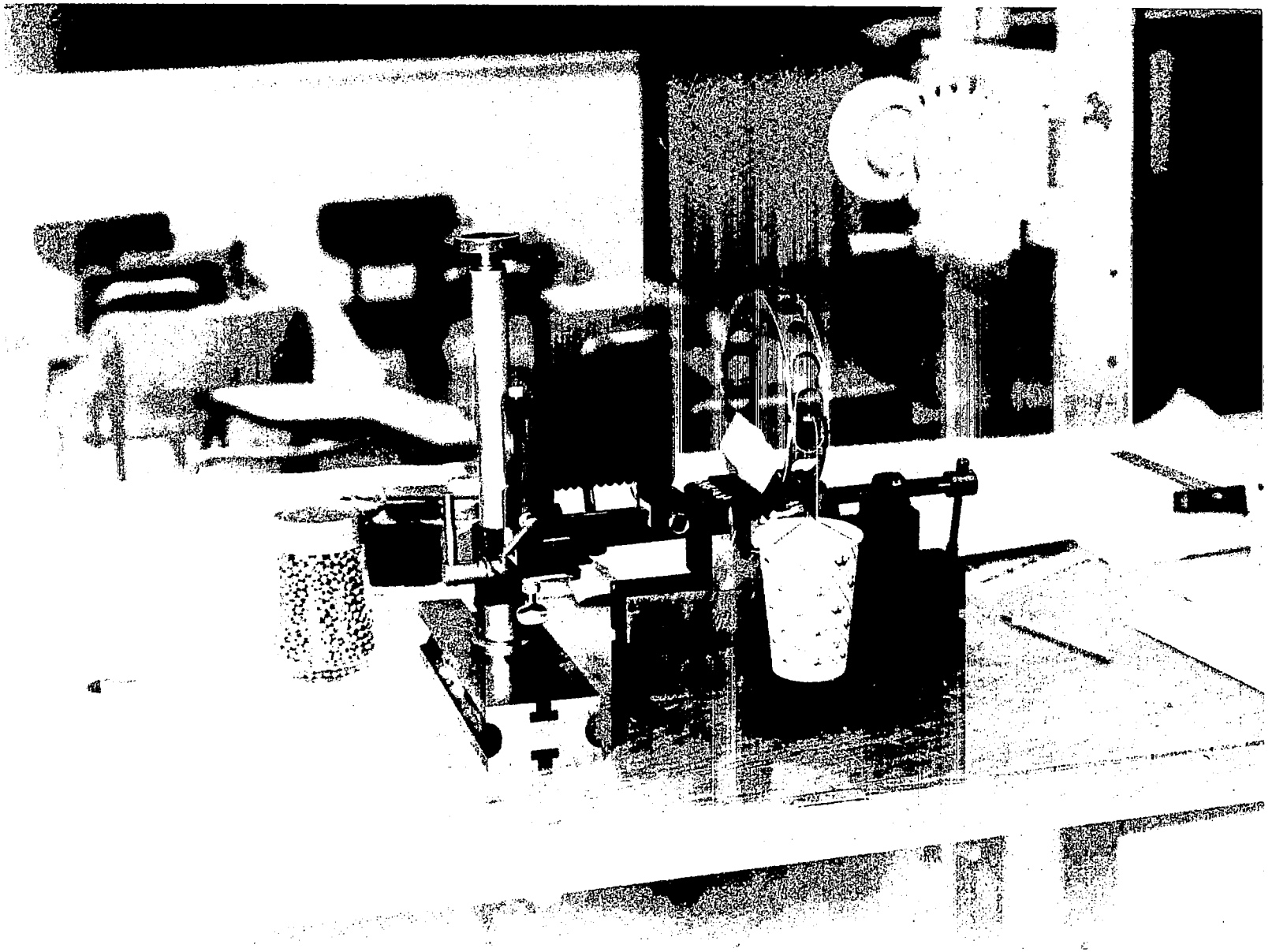

FIG. 3 BALL CONTACT
FORCE TRANSDUCER

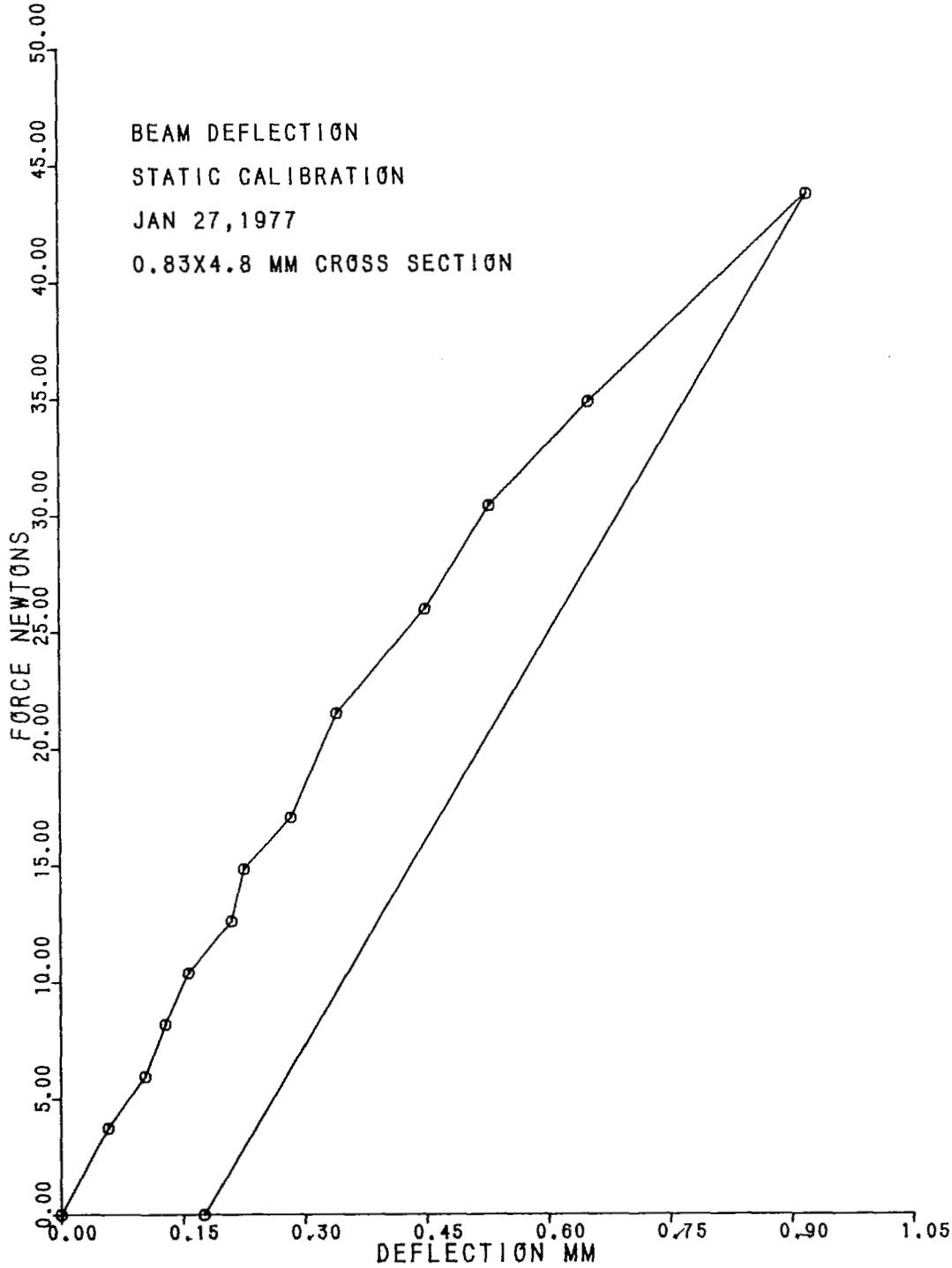

FIG. 4 SAMPLE FORCE TRANSDUCER CALIBRATION (61.8 N/mm BEAM)

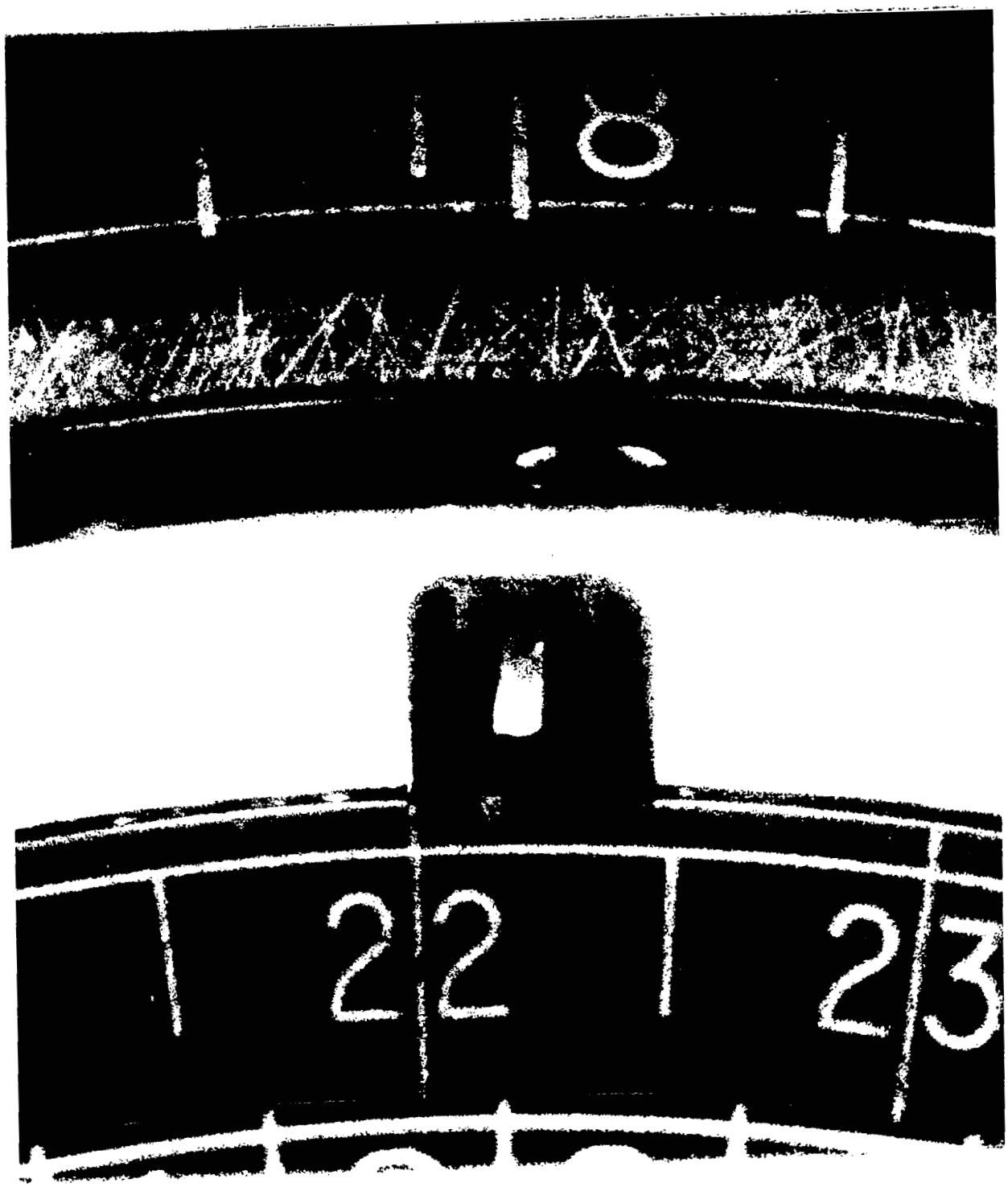

FIG. 5 EXAMPLE OF
PHOTOGRAPHS TAKEN

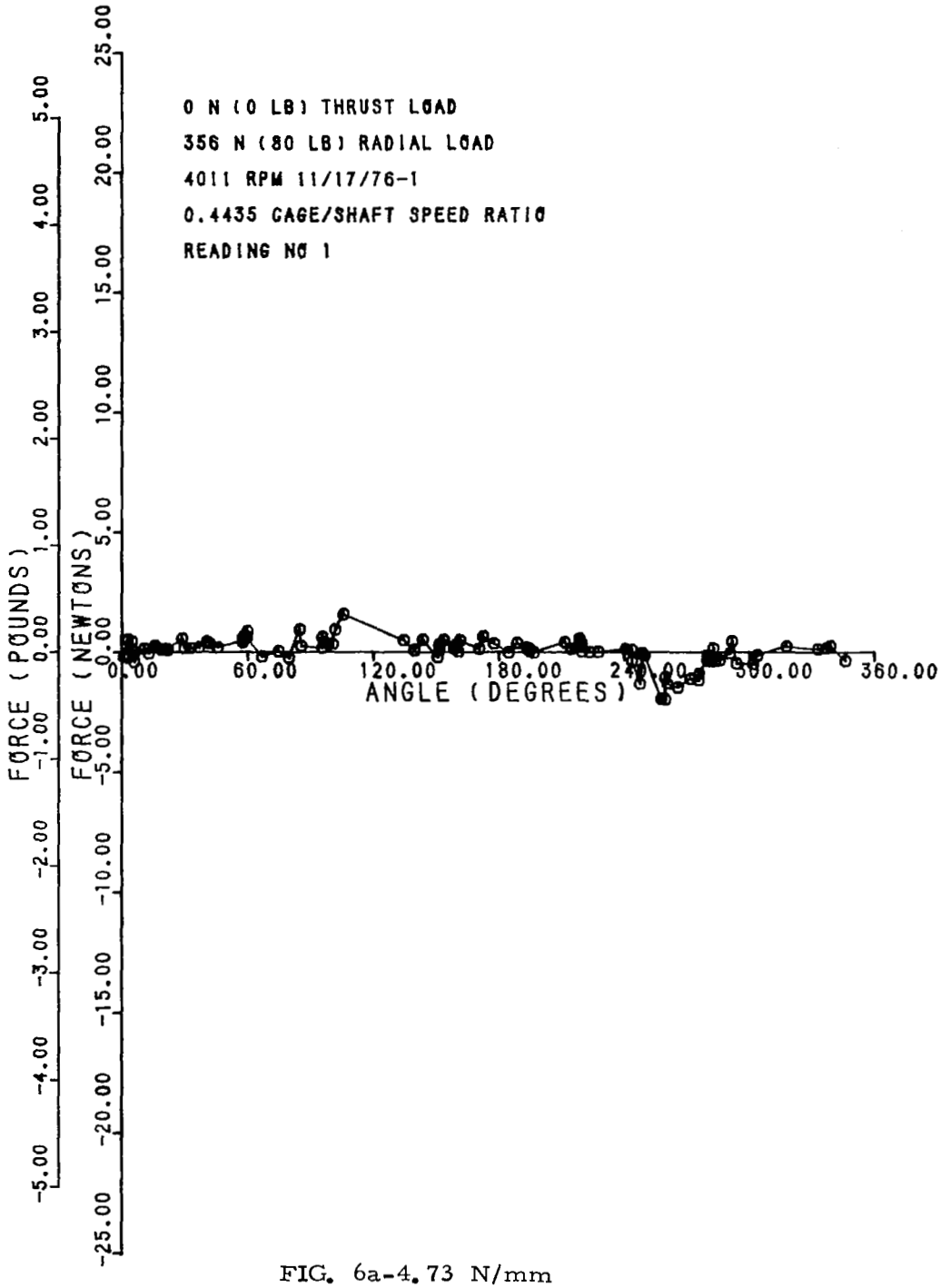

FIG. 6a-4.73 N/mm

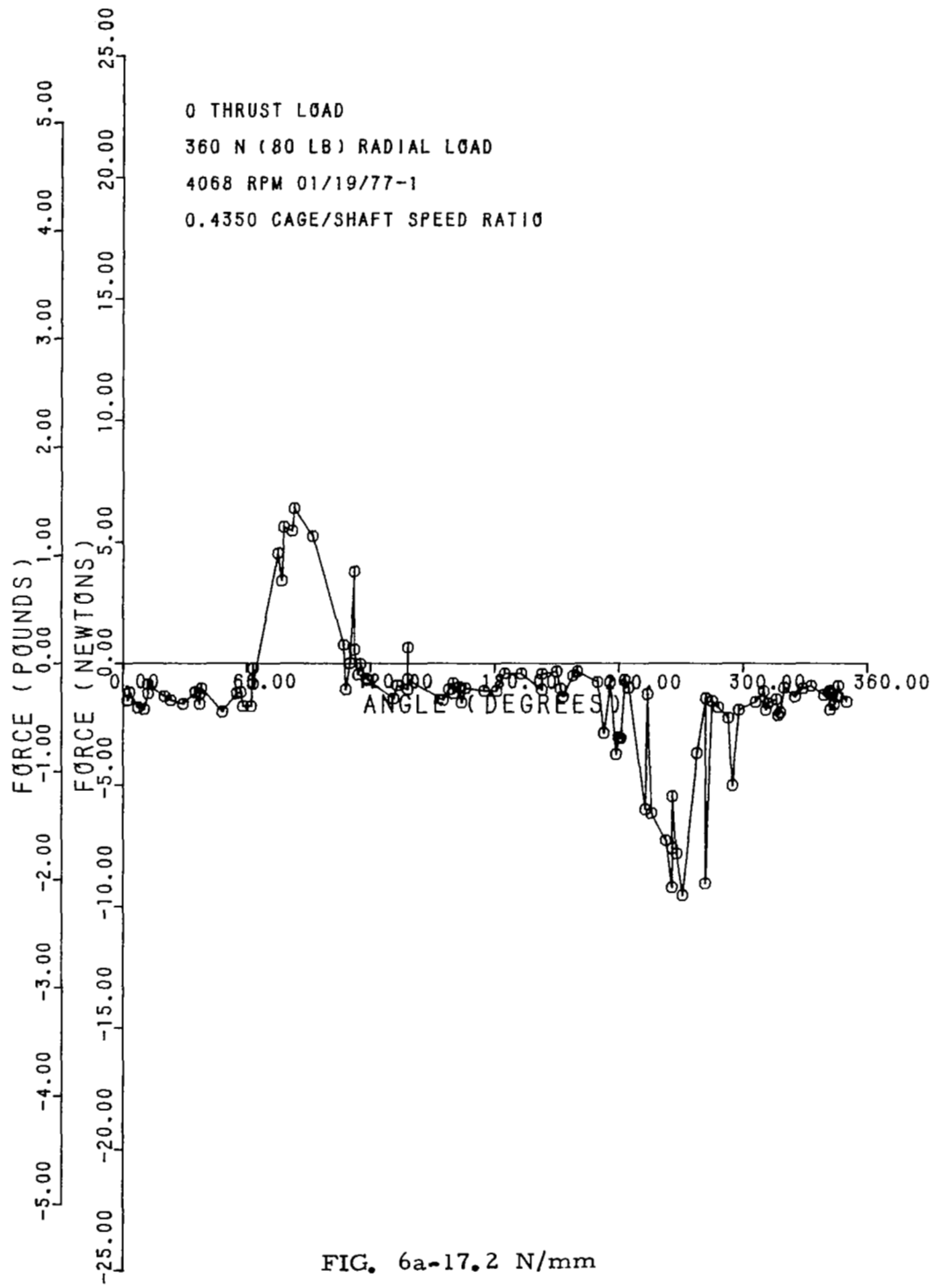

FIG. 6a-17.2 N/mm

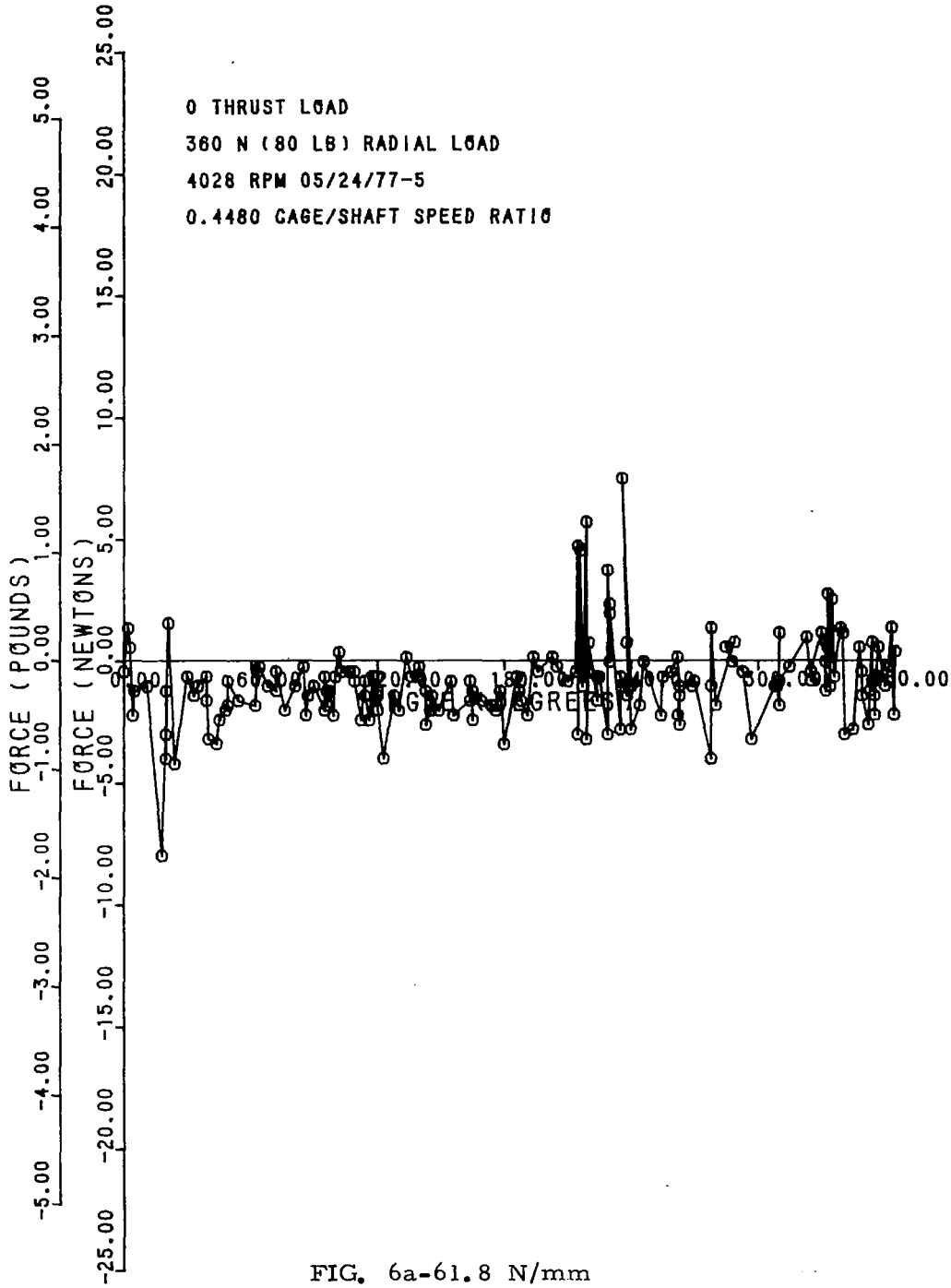

FIG. 6a-61.8 N/mm

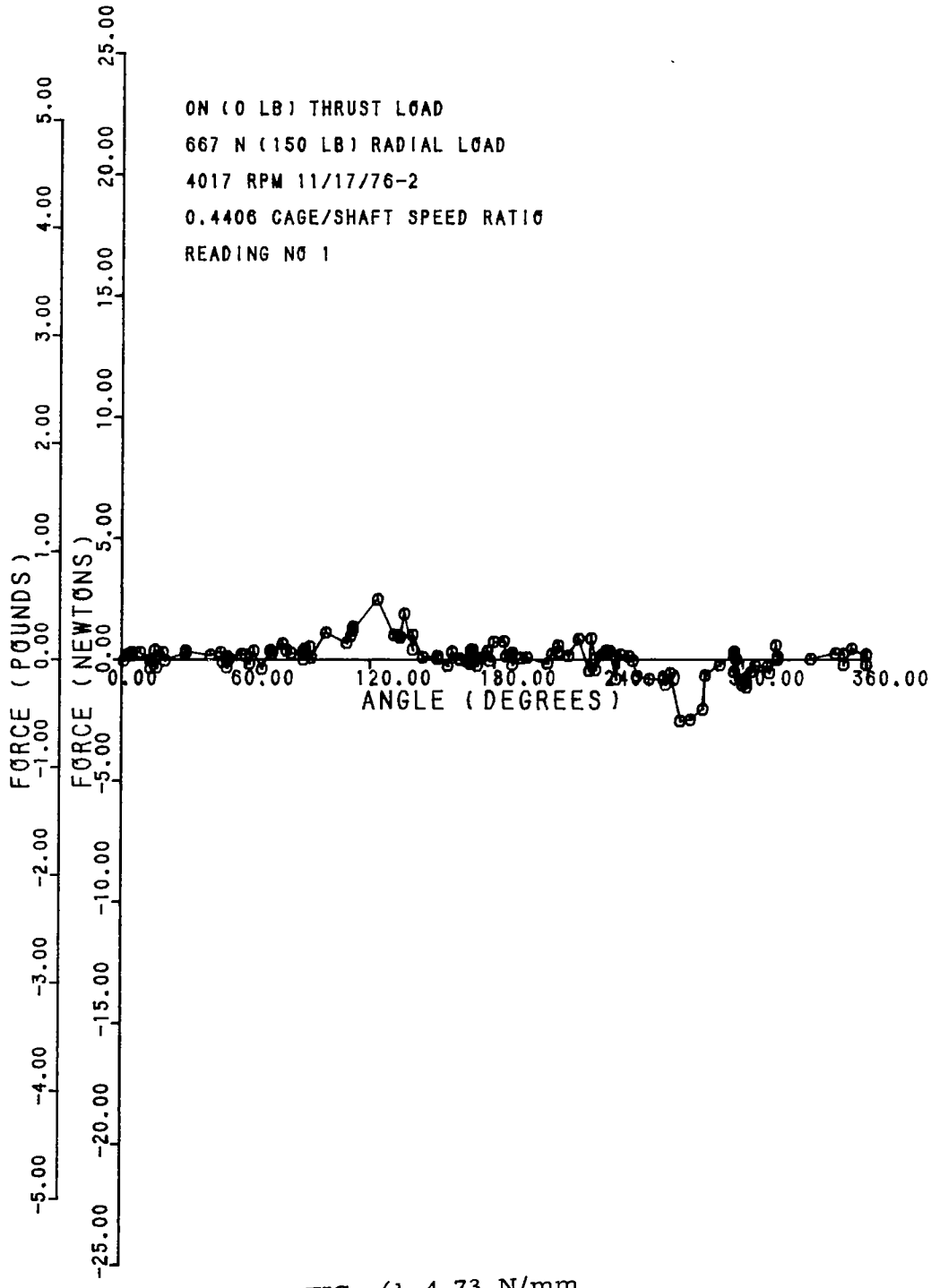

FIG. 6b-4.73 N/mm

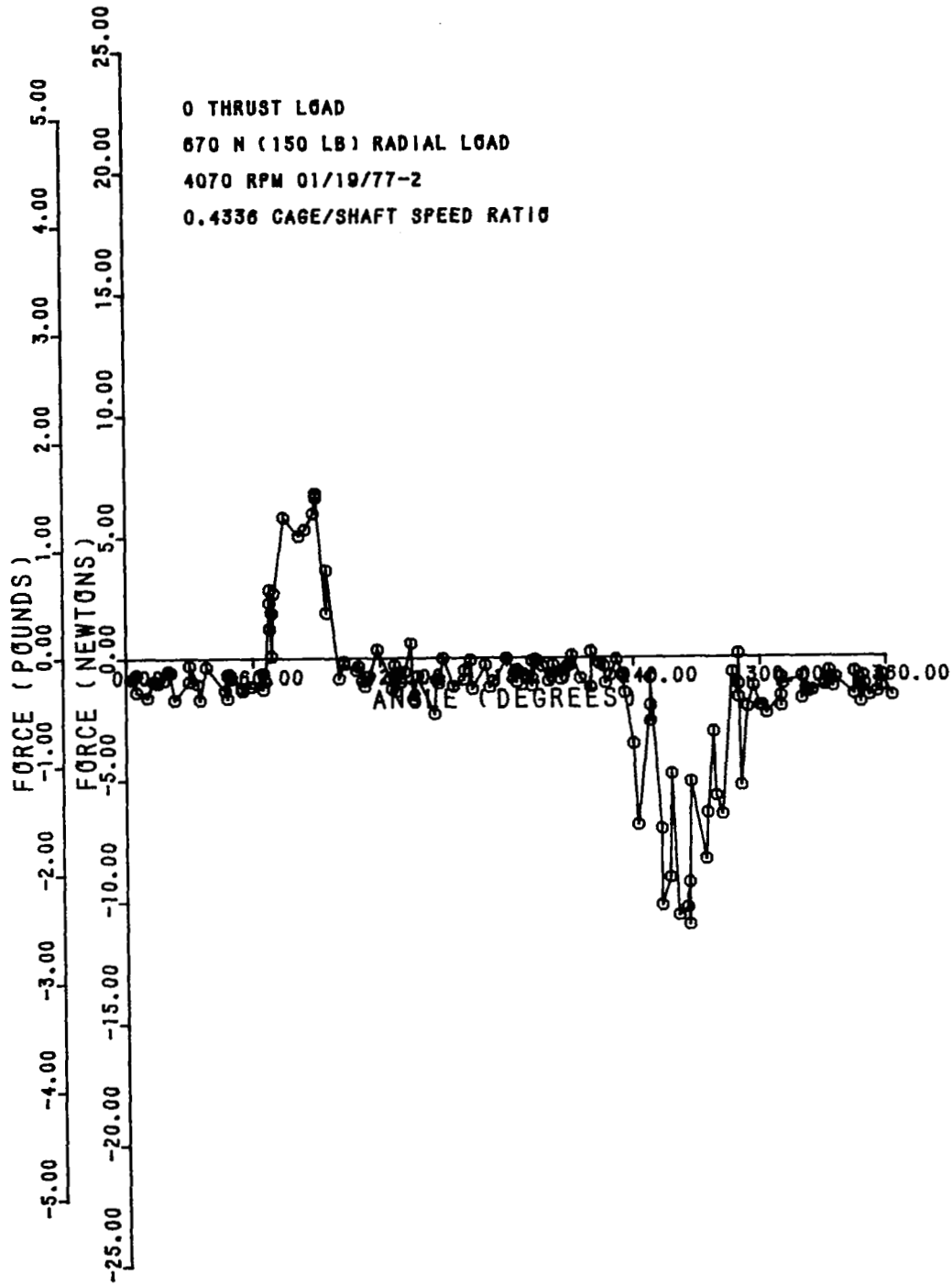

FIG. 6b-17.2 N/mm

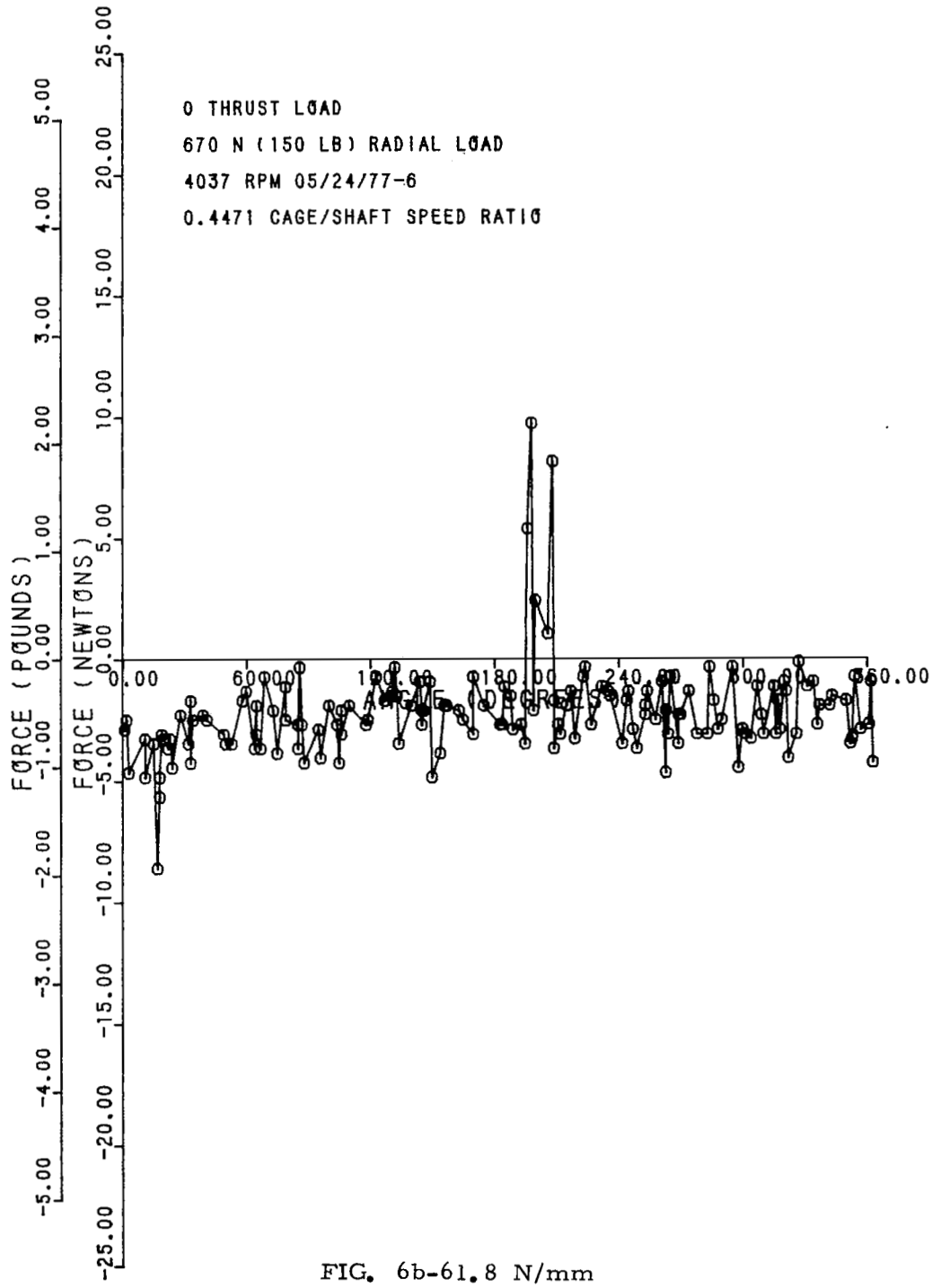

FIG. 6b-61.8 N/mm

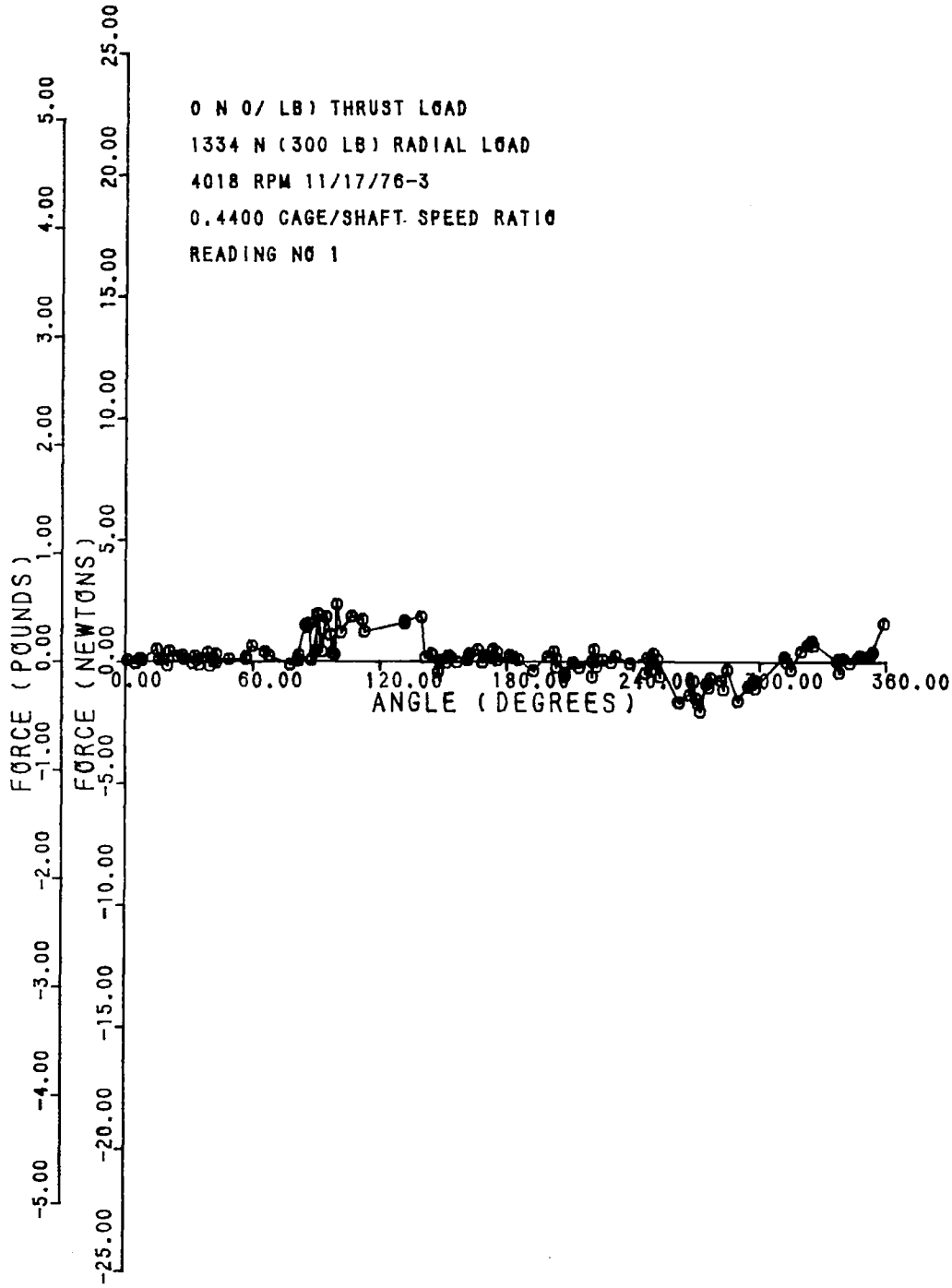

FIG. 6c-4.73 N/mm

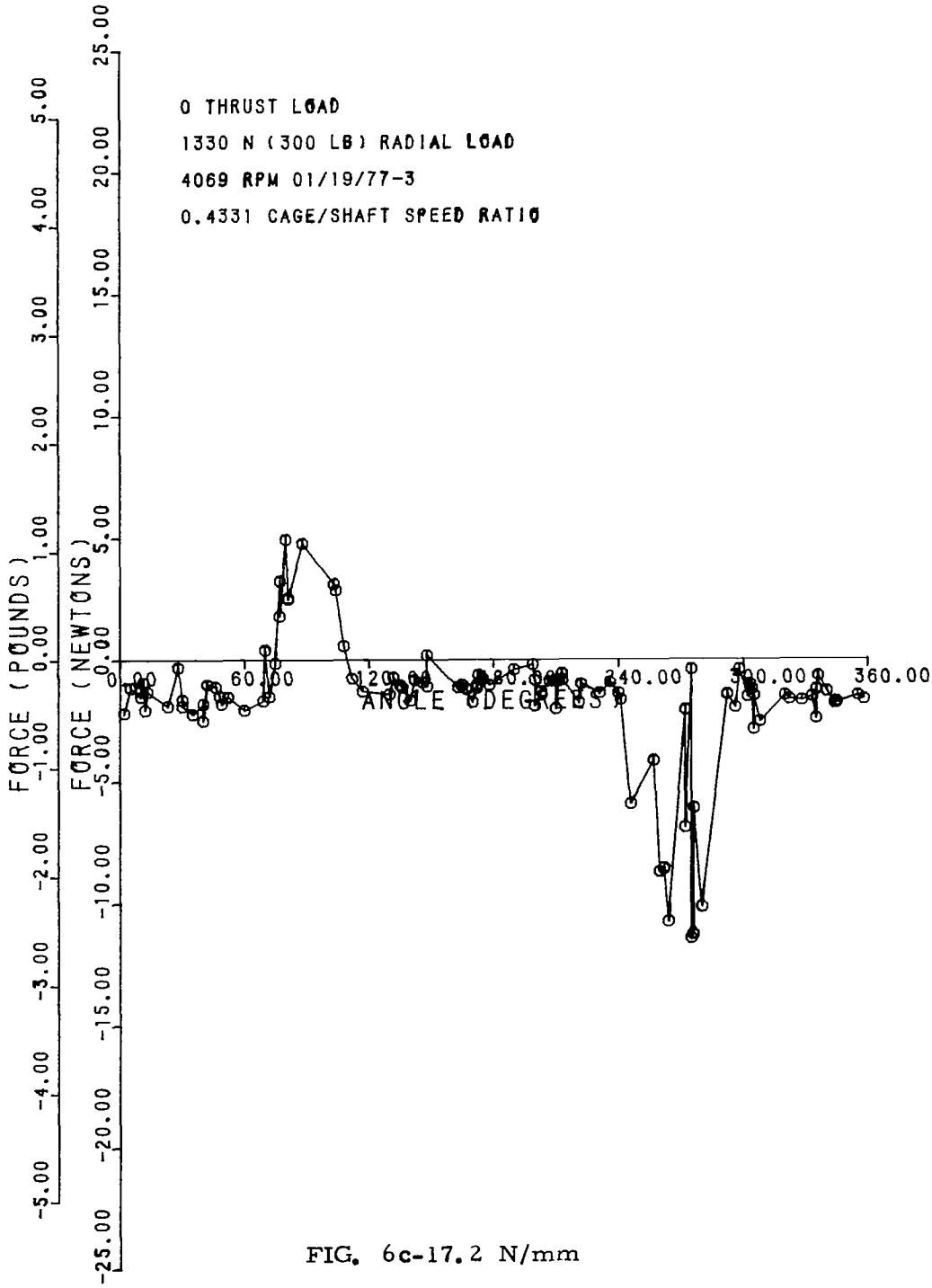

FIG. 6c-17.2 N/mm

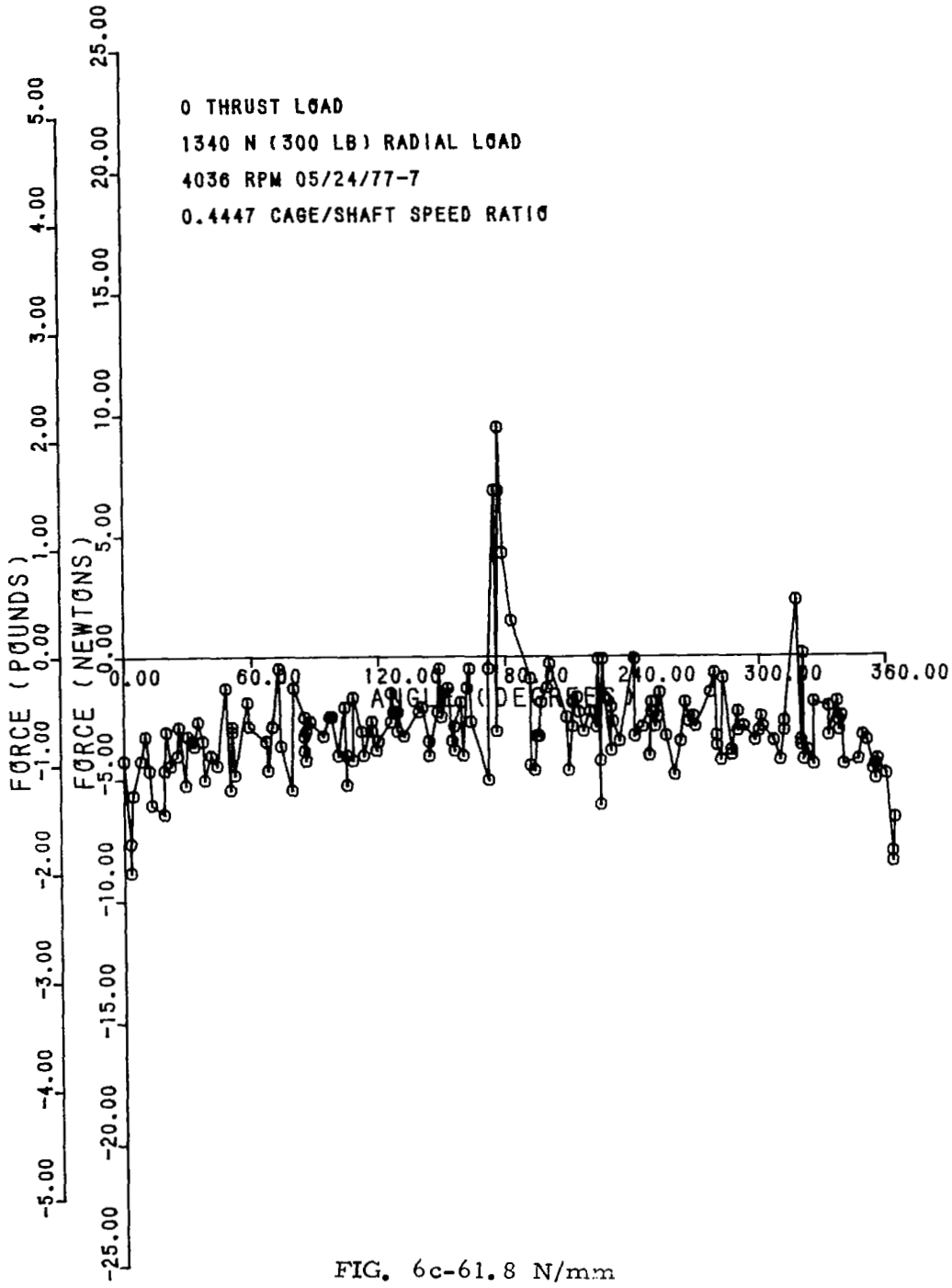

FIG. 6c-61.8 N/mm

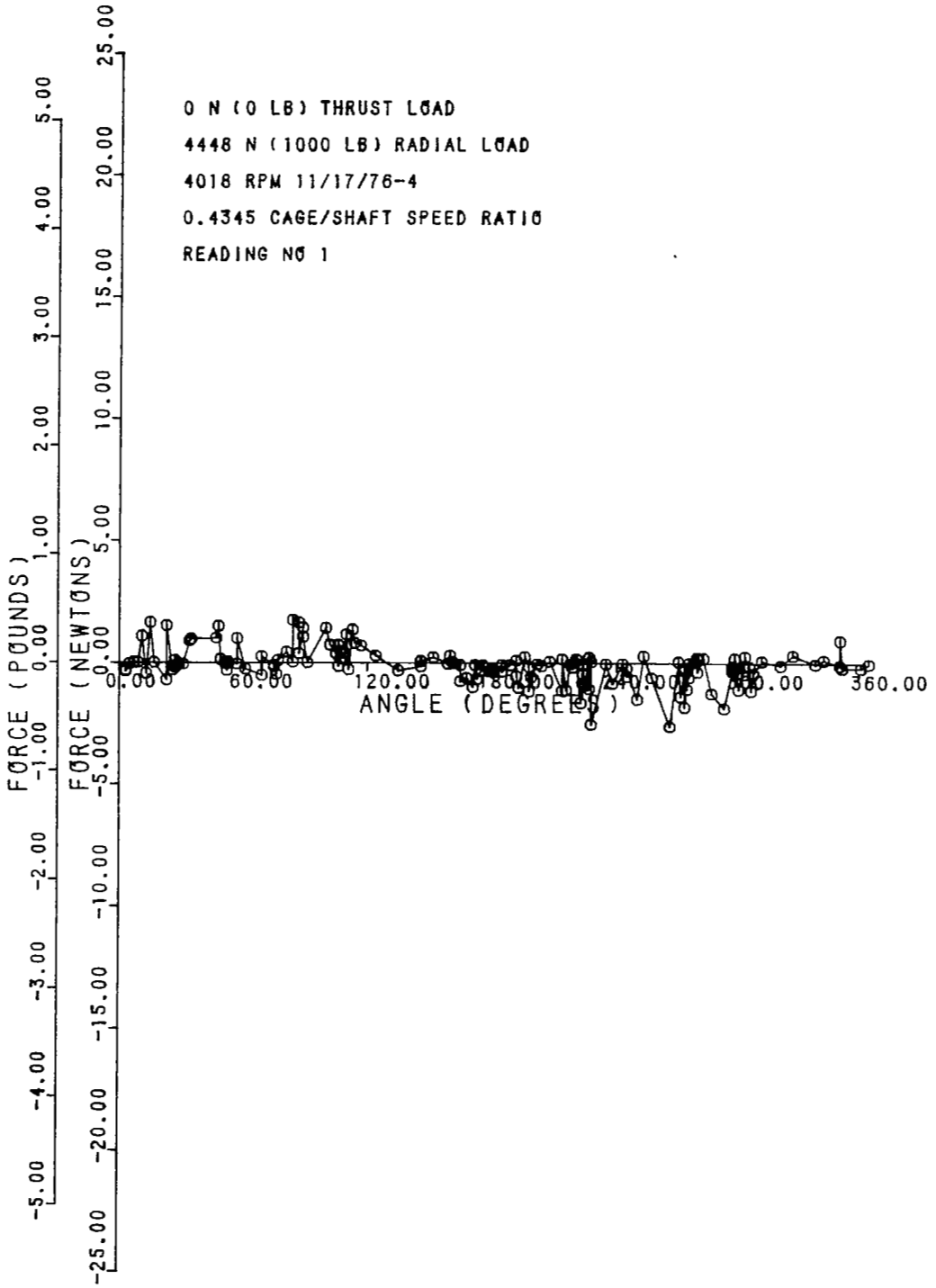

FIG. 6d-4.73 N/mm

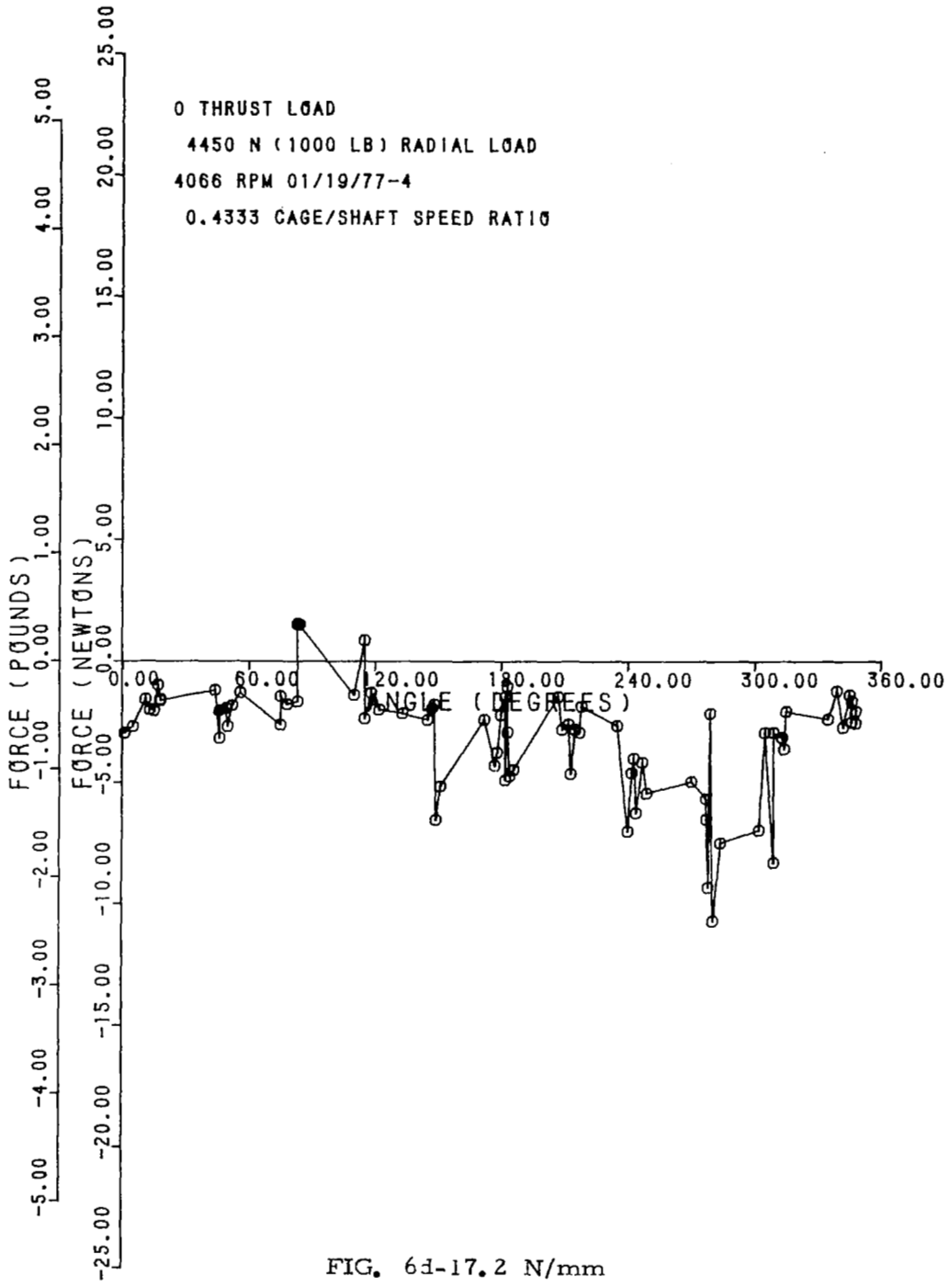

FIG. 6d-17.2 N/mm

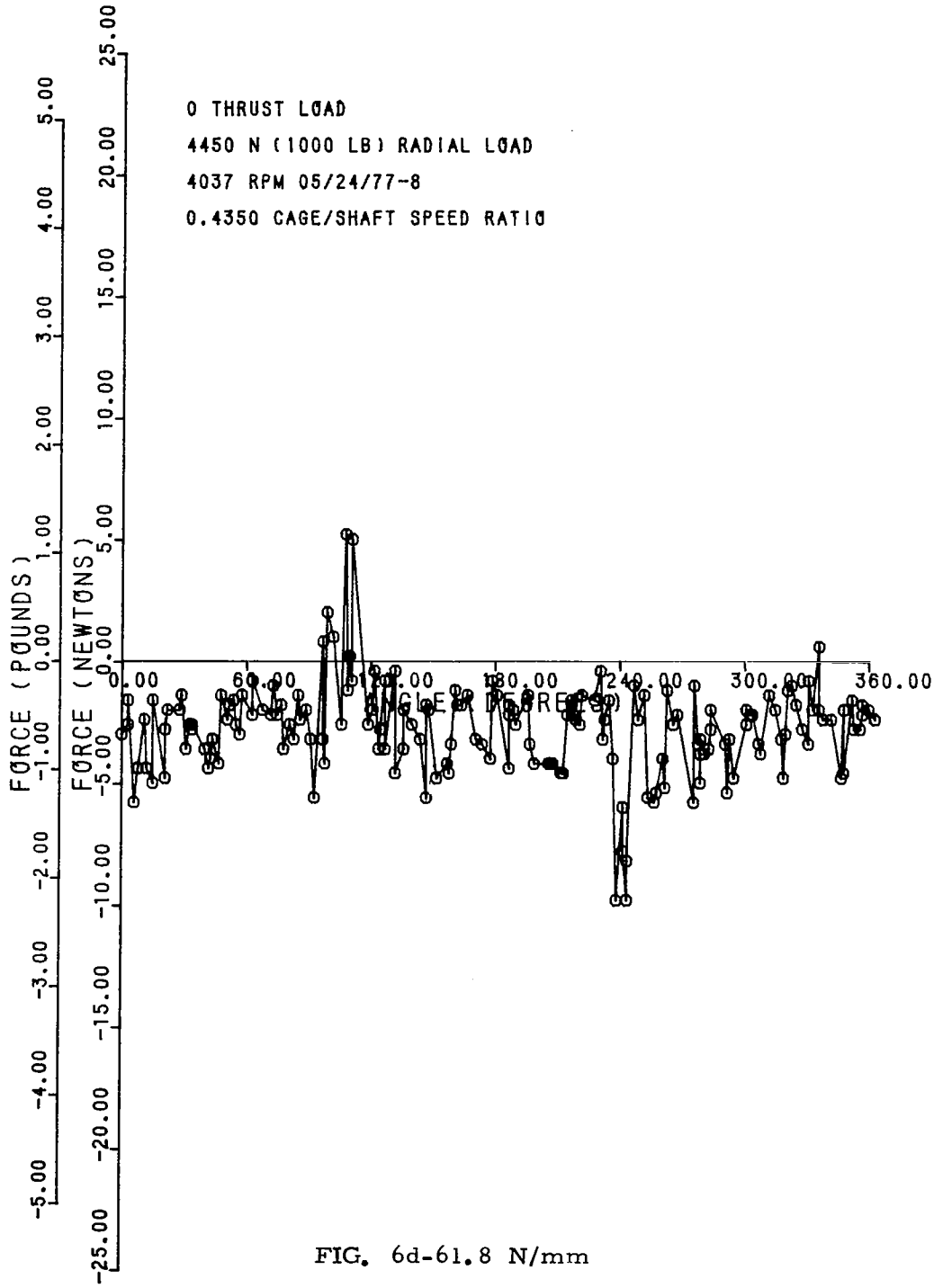

FIG. 6d-61.8 N/mm

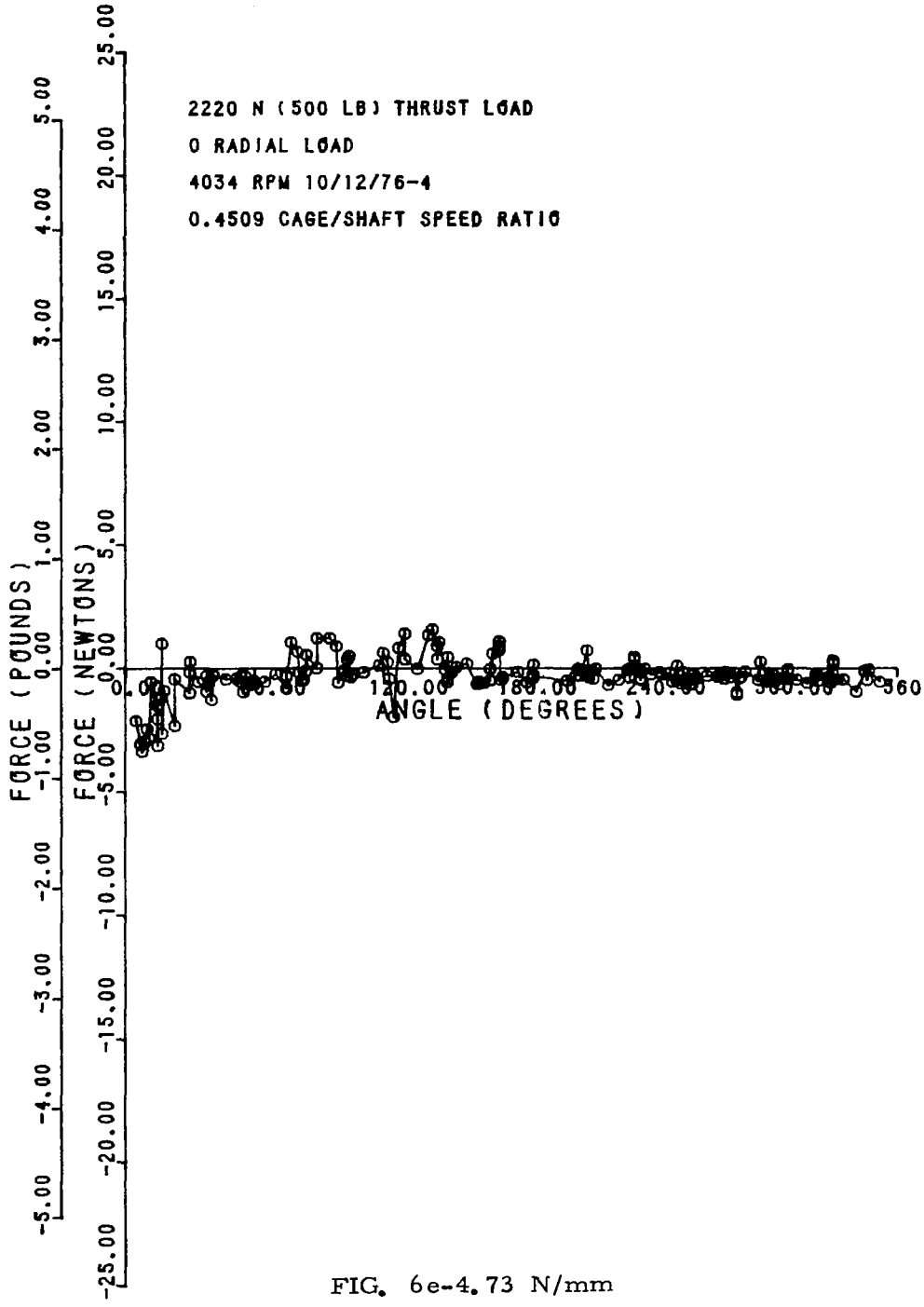

FIG. 6e-4.73 N/mm

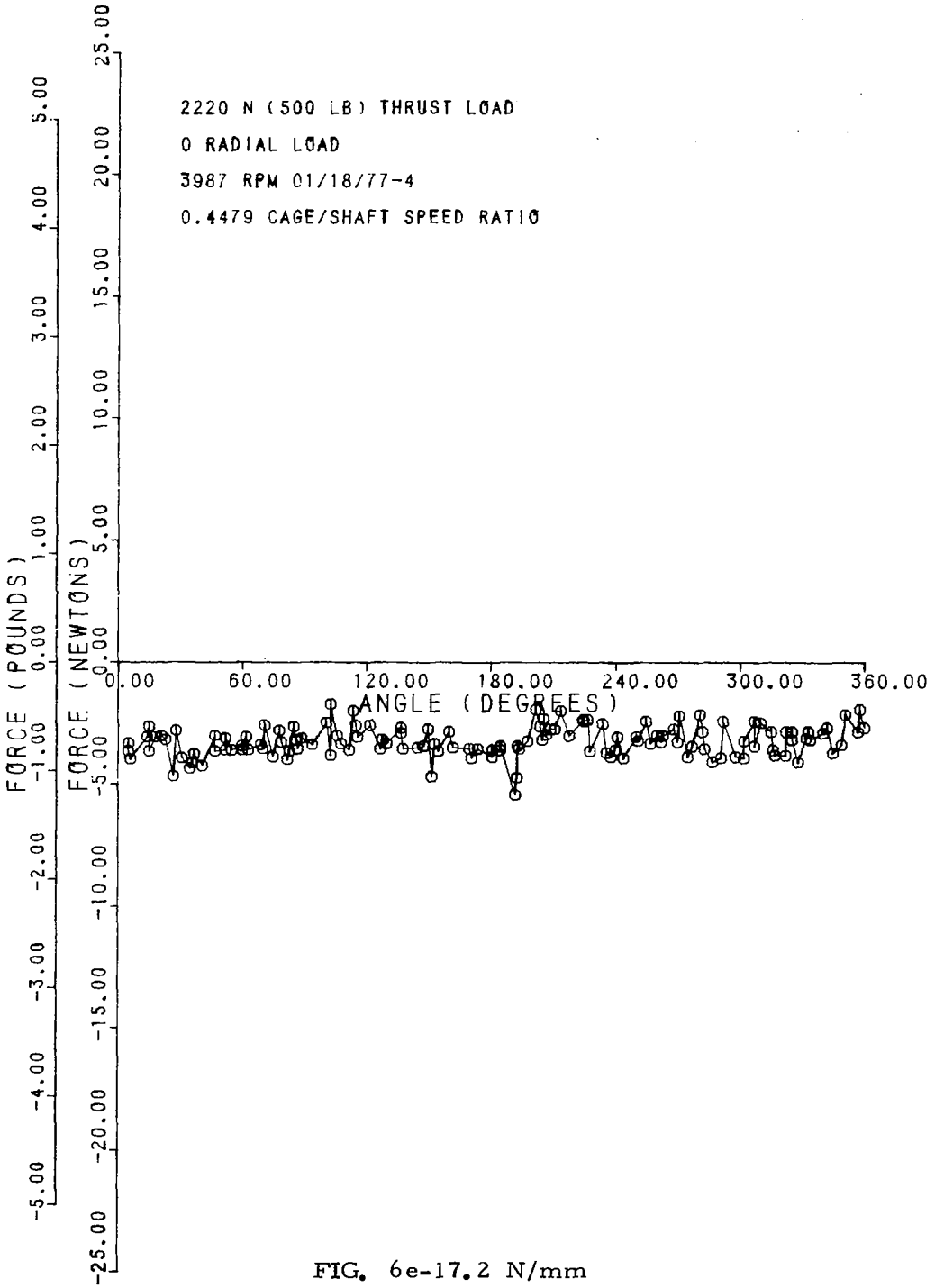

FIG. 6e-17.2 N/mm

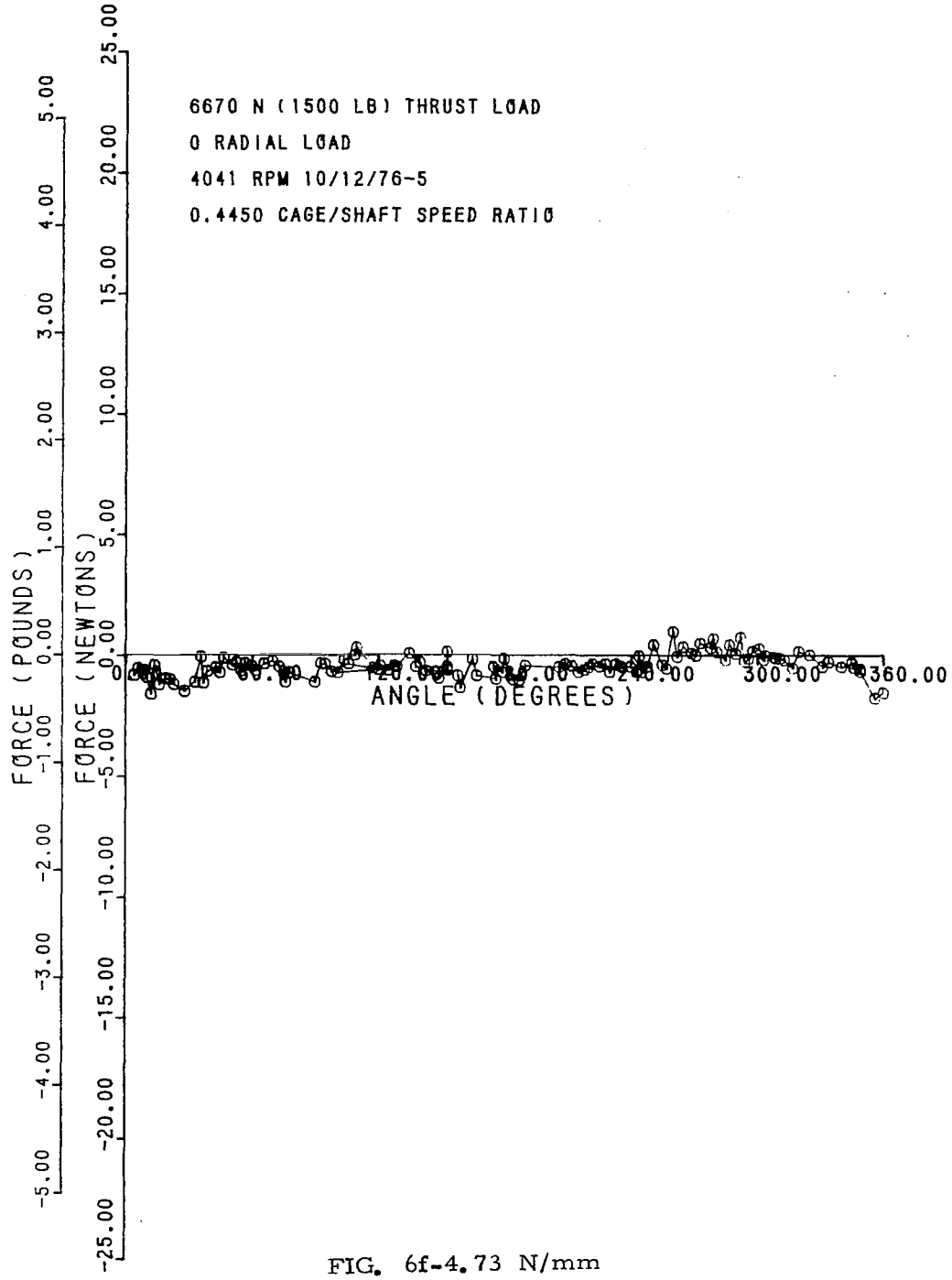

FIG. 6f-4.73 N/mm

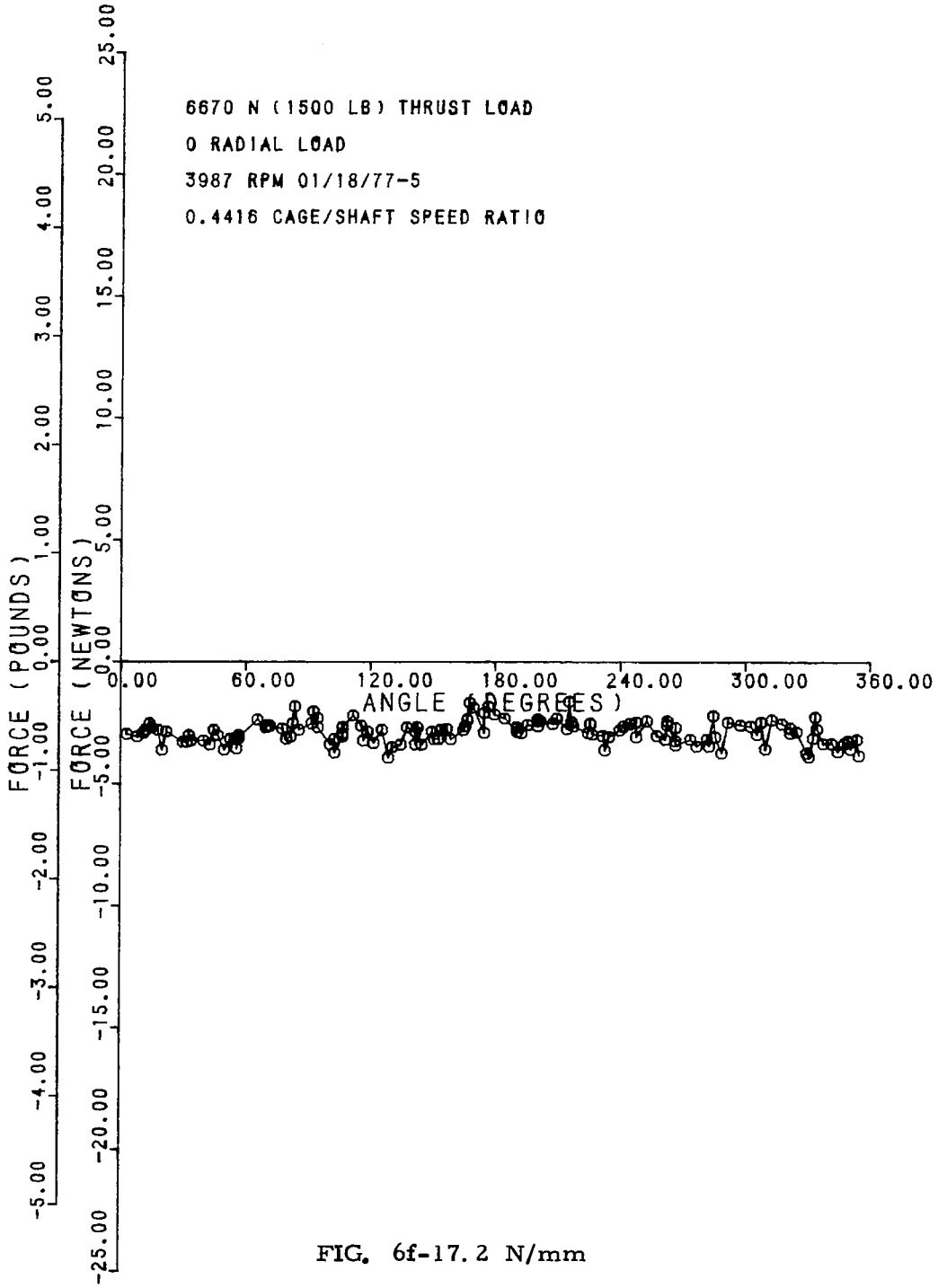

FIG. 6f-17.2 N/mm

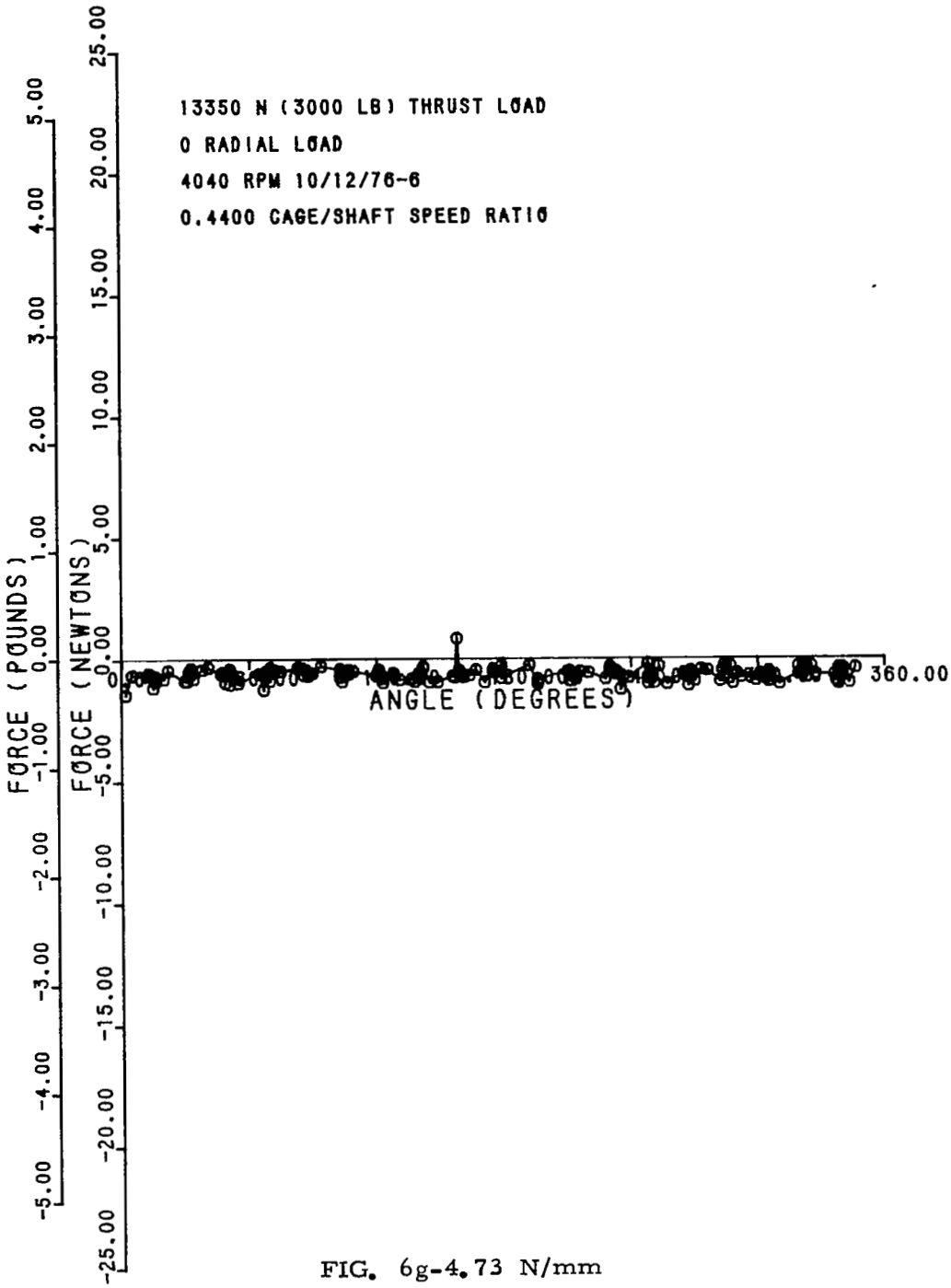

FIG. 6g-4.73 N/mm

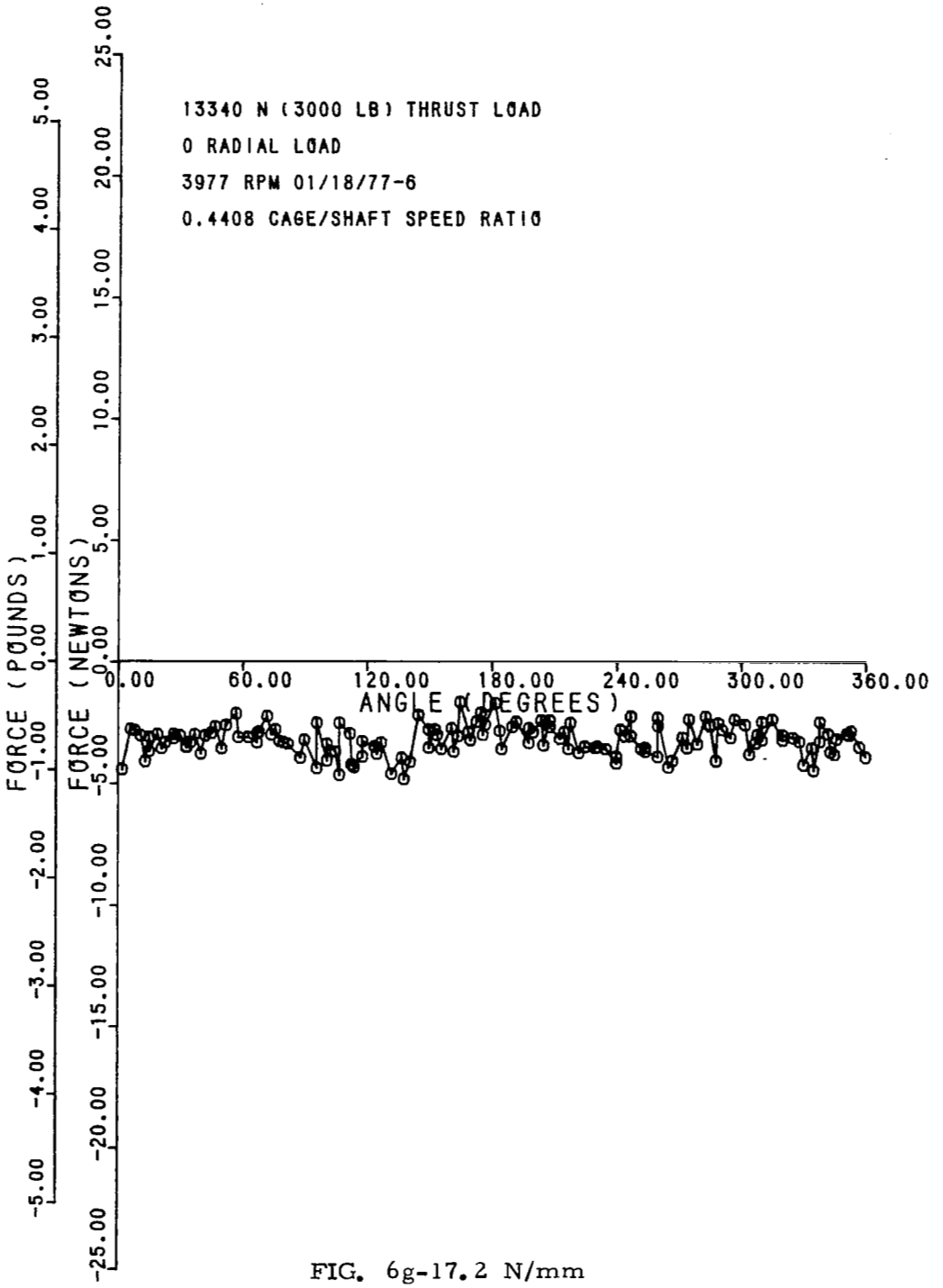

FIG. 6g-17.2 N/mm

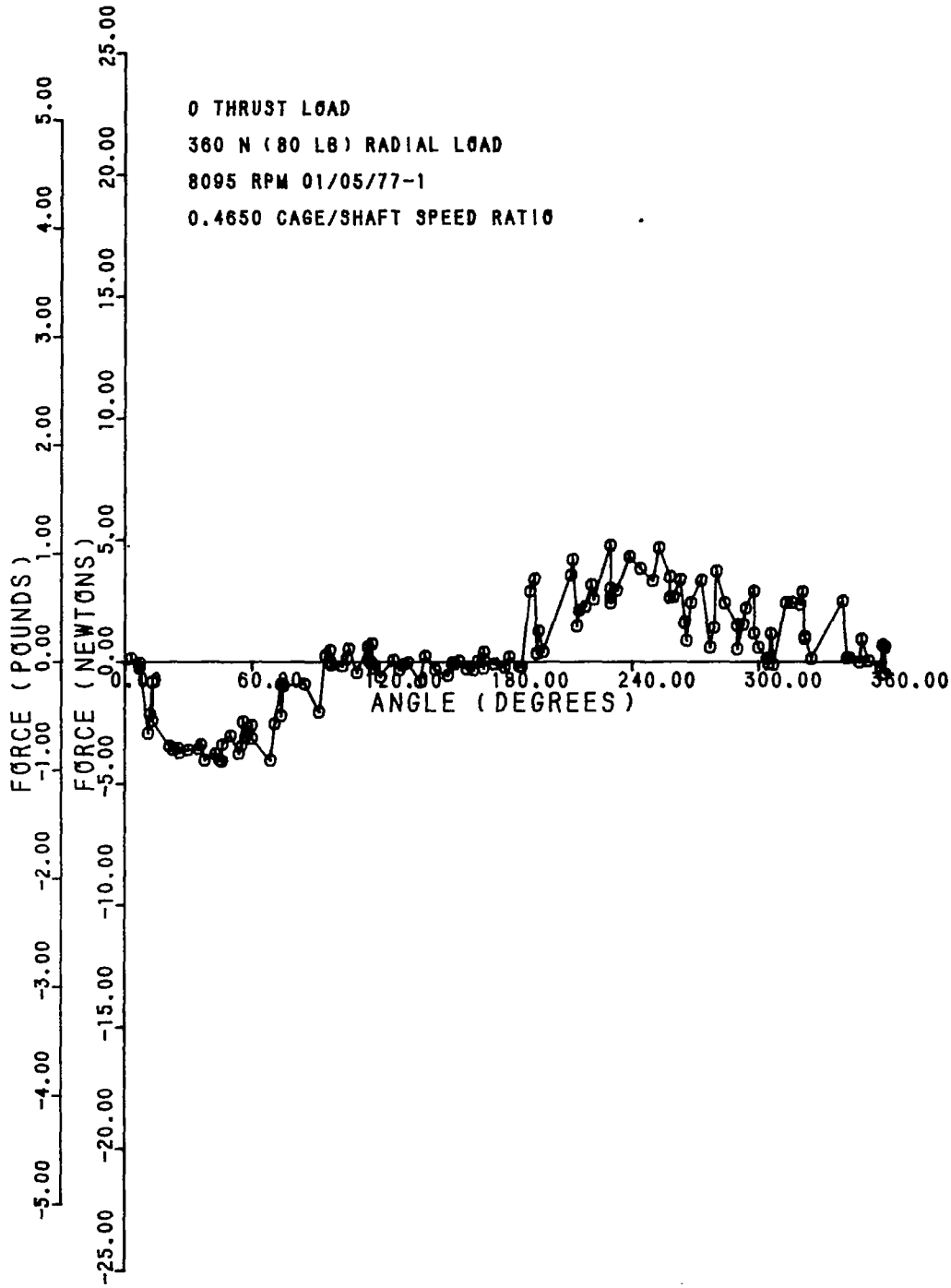

FIG. 7a-4.73 N/mm

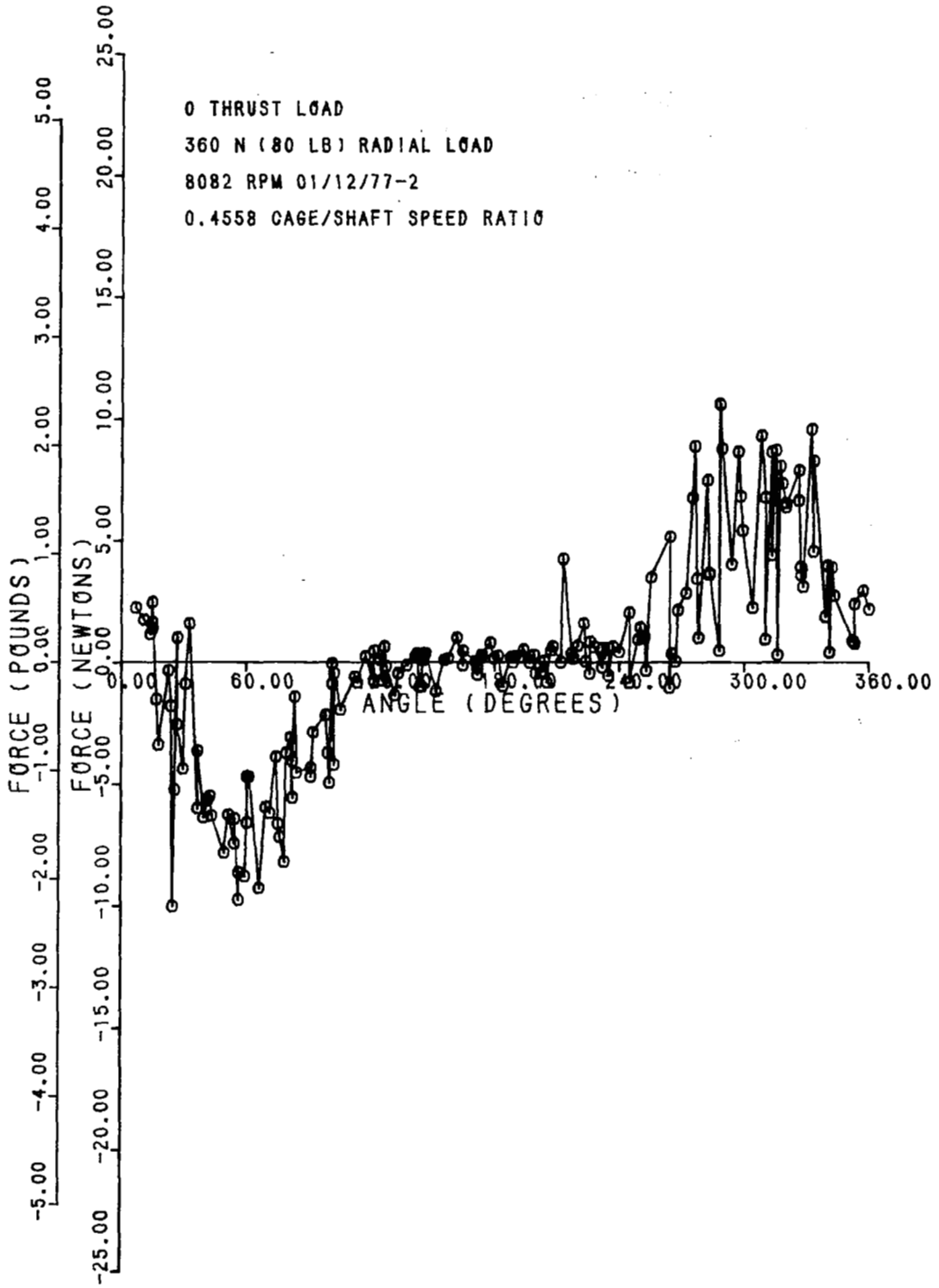

FIG. 7a-17.2 N/mm

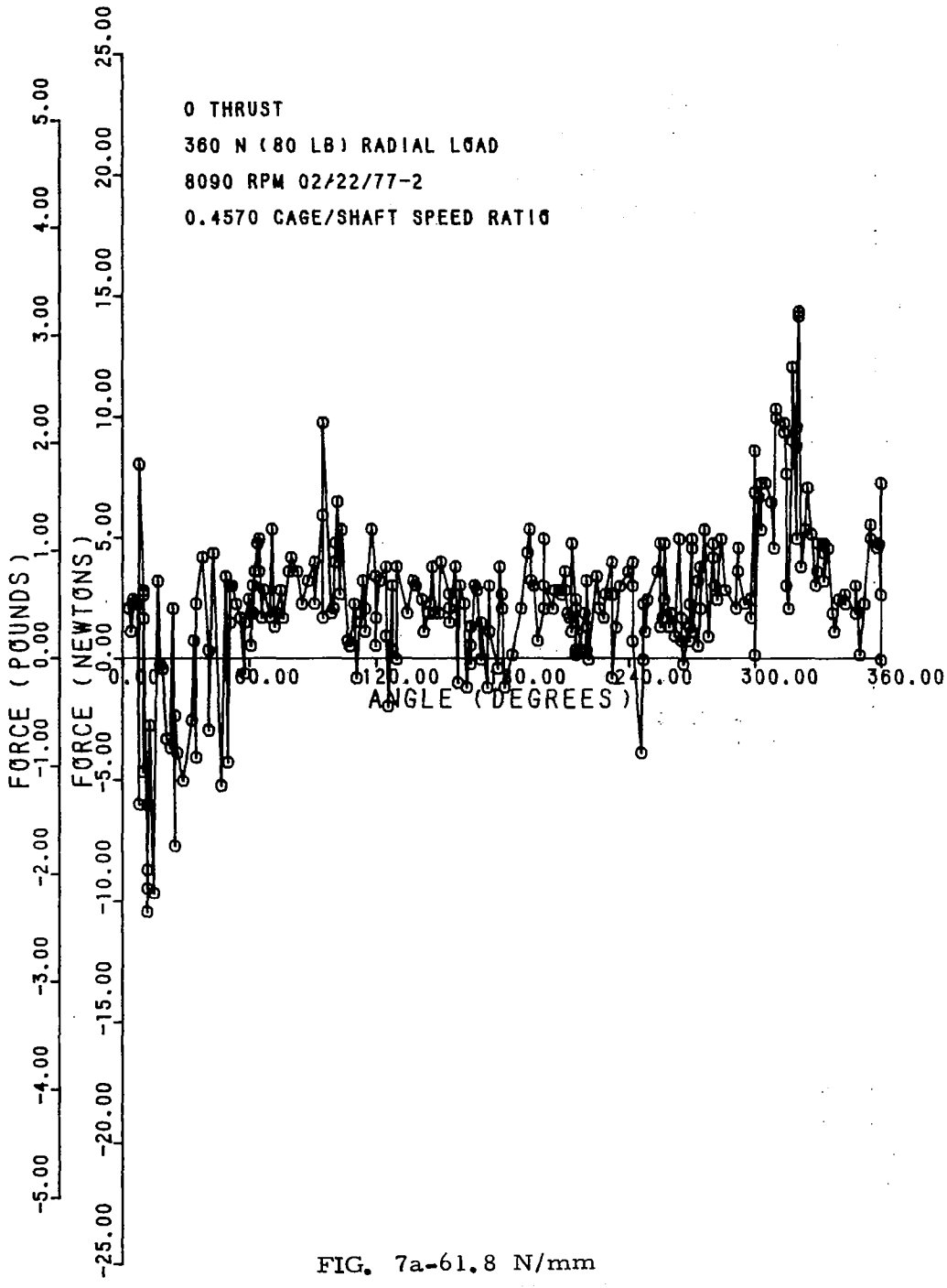

FIG. 7a-61.8 N/mm

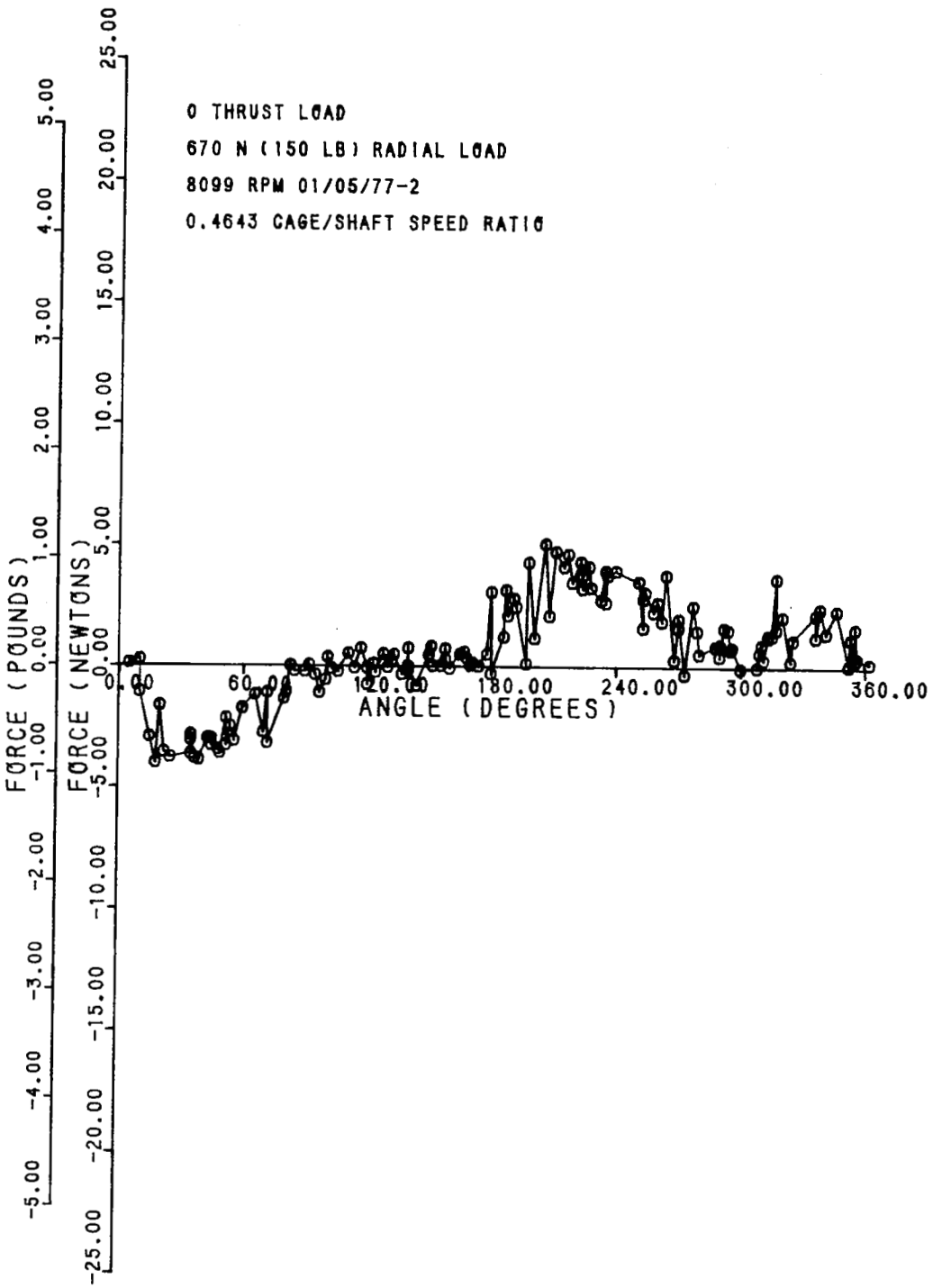

FIG. 7b-4.73 N/mm

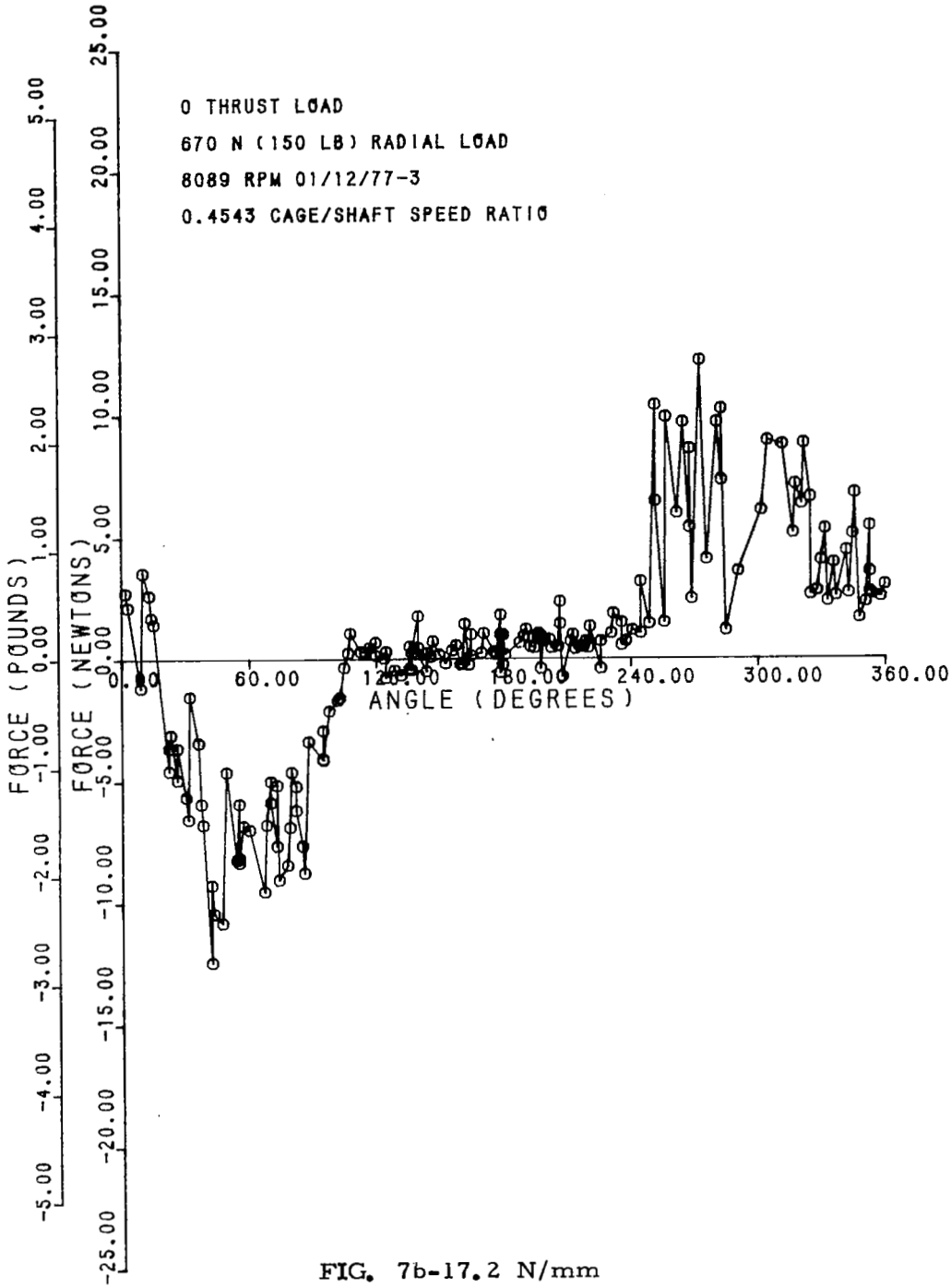

FIG. 7b-17.2 N/mm

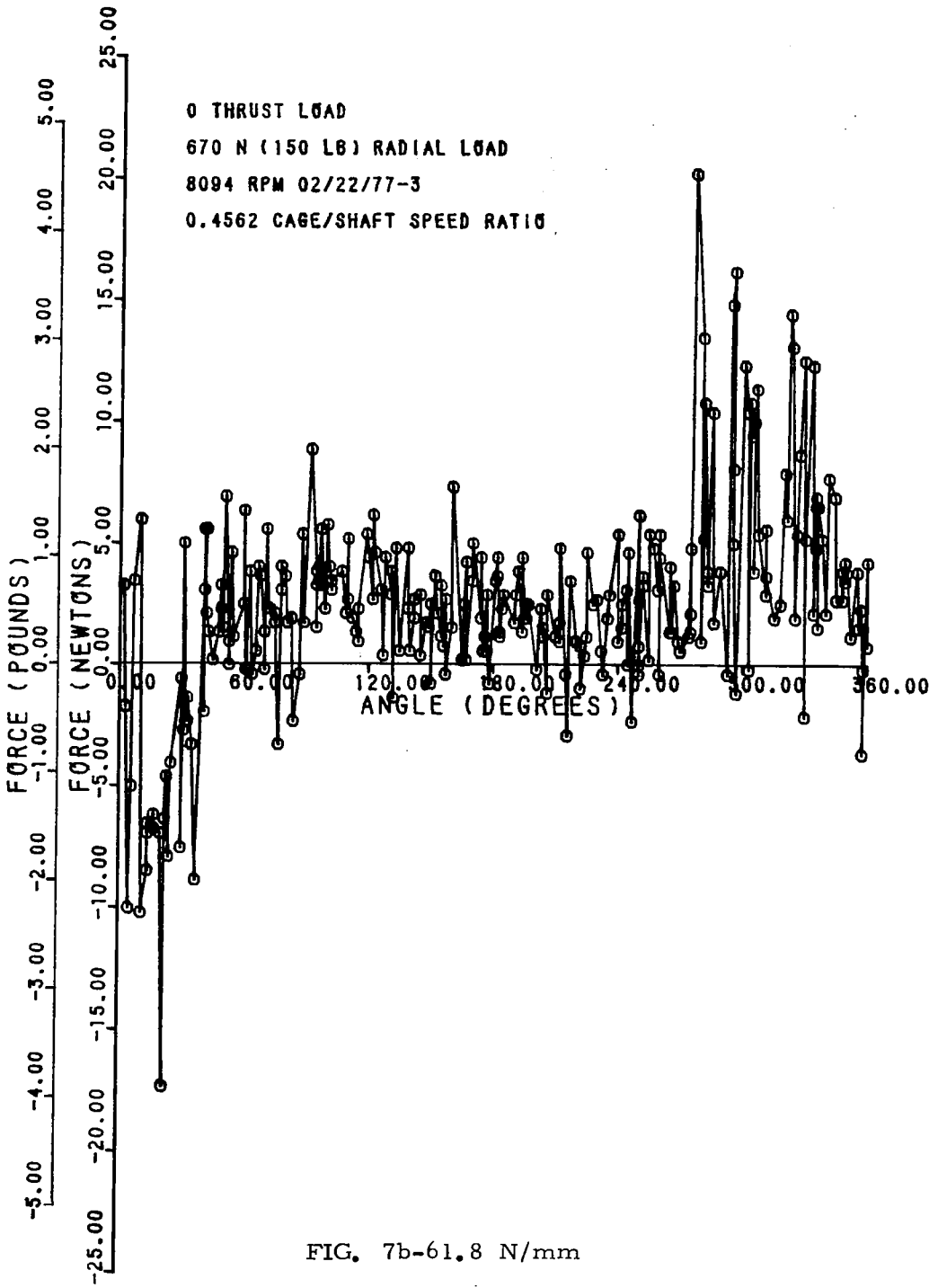

FIG. 7b-61.8 N/mm

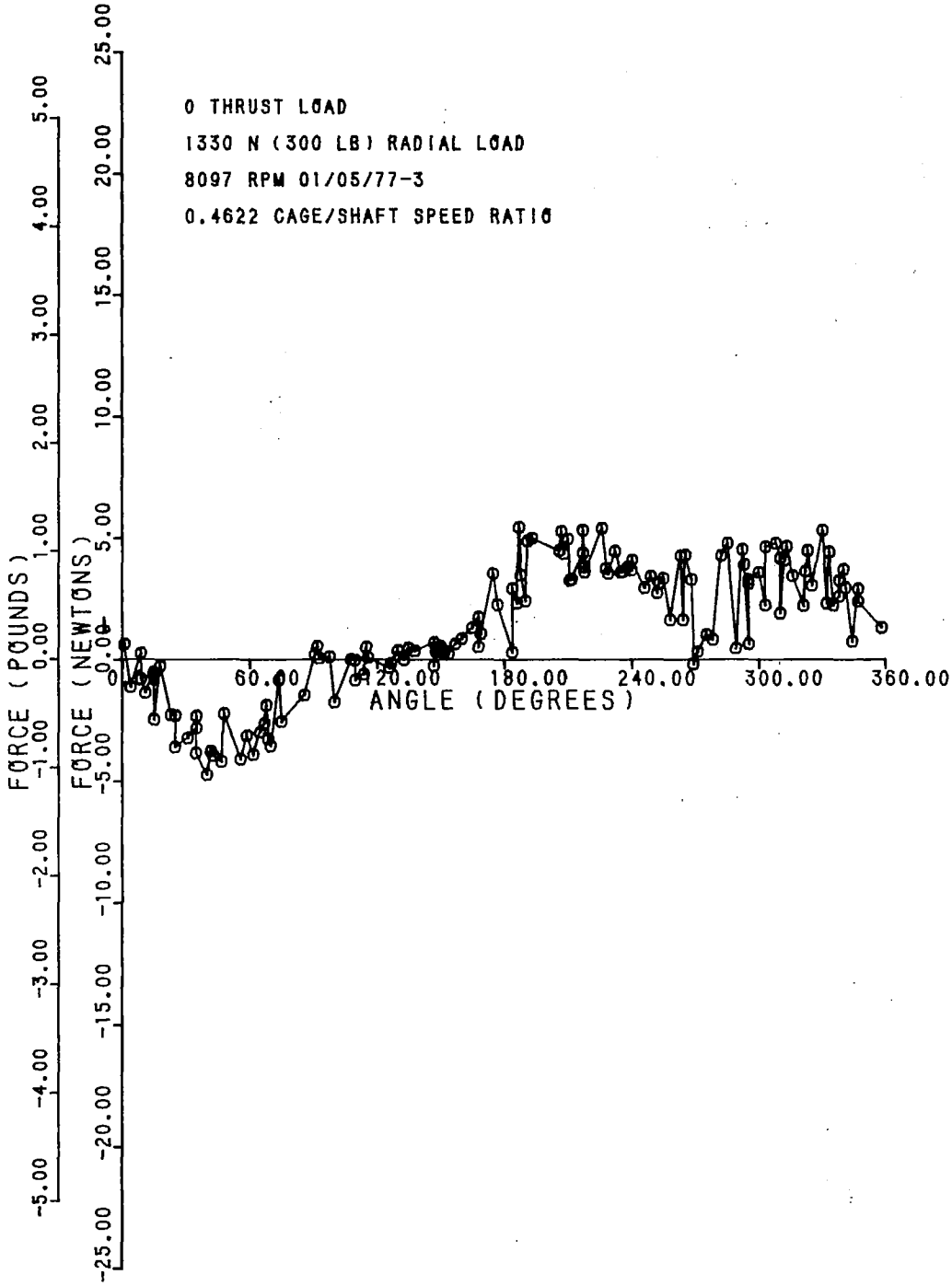

FIG. 7c-4.73 N/mm

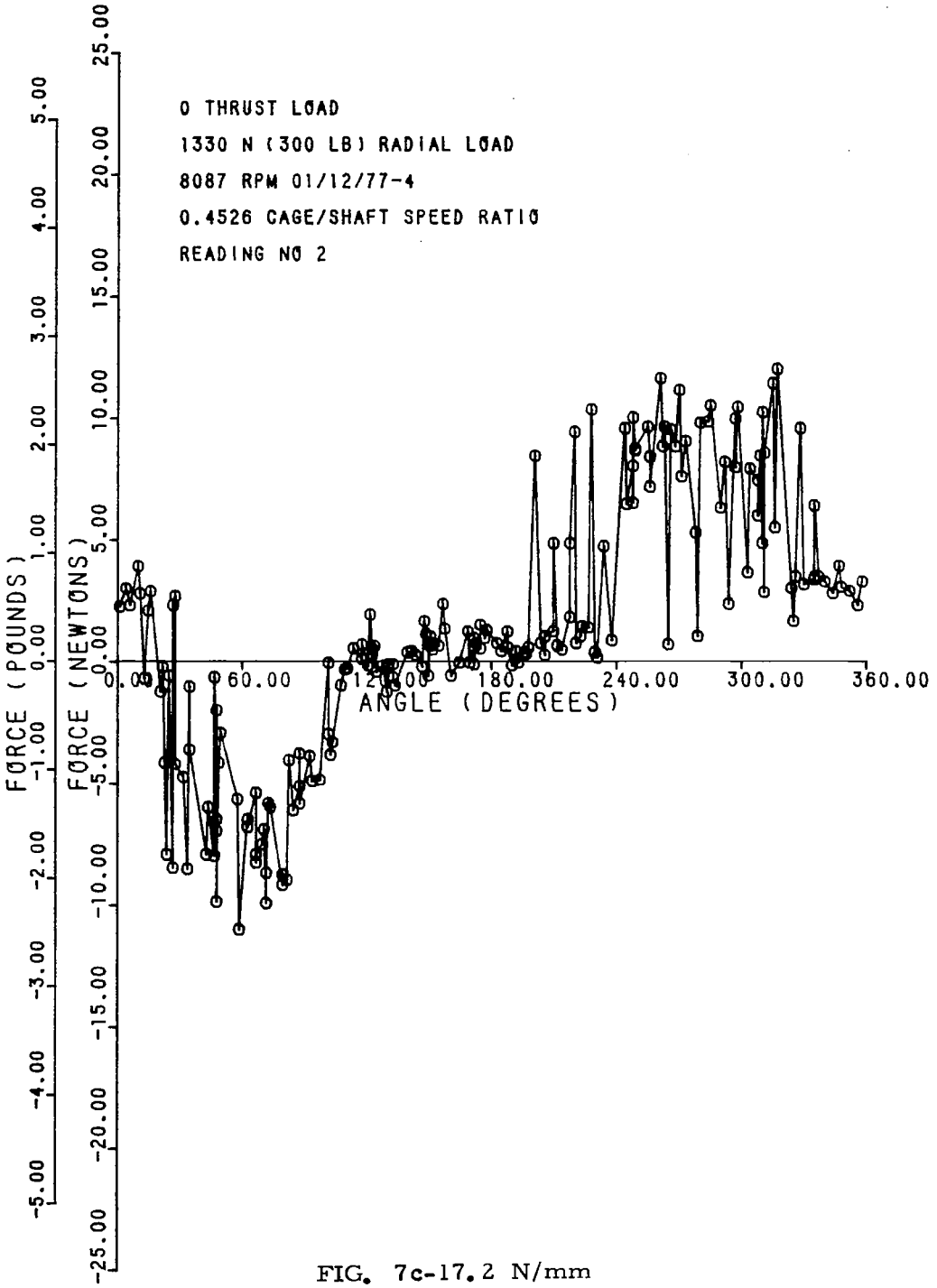

FIG. 7c-17.2 N/mm

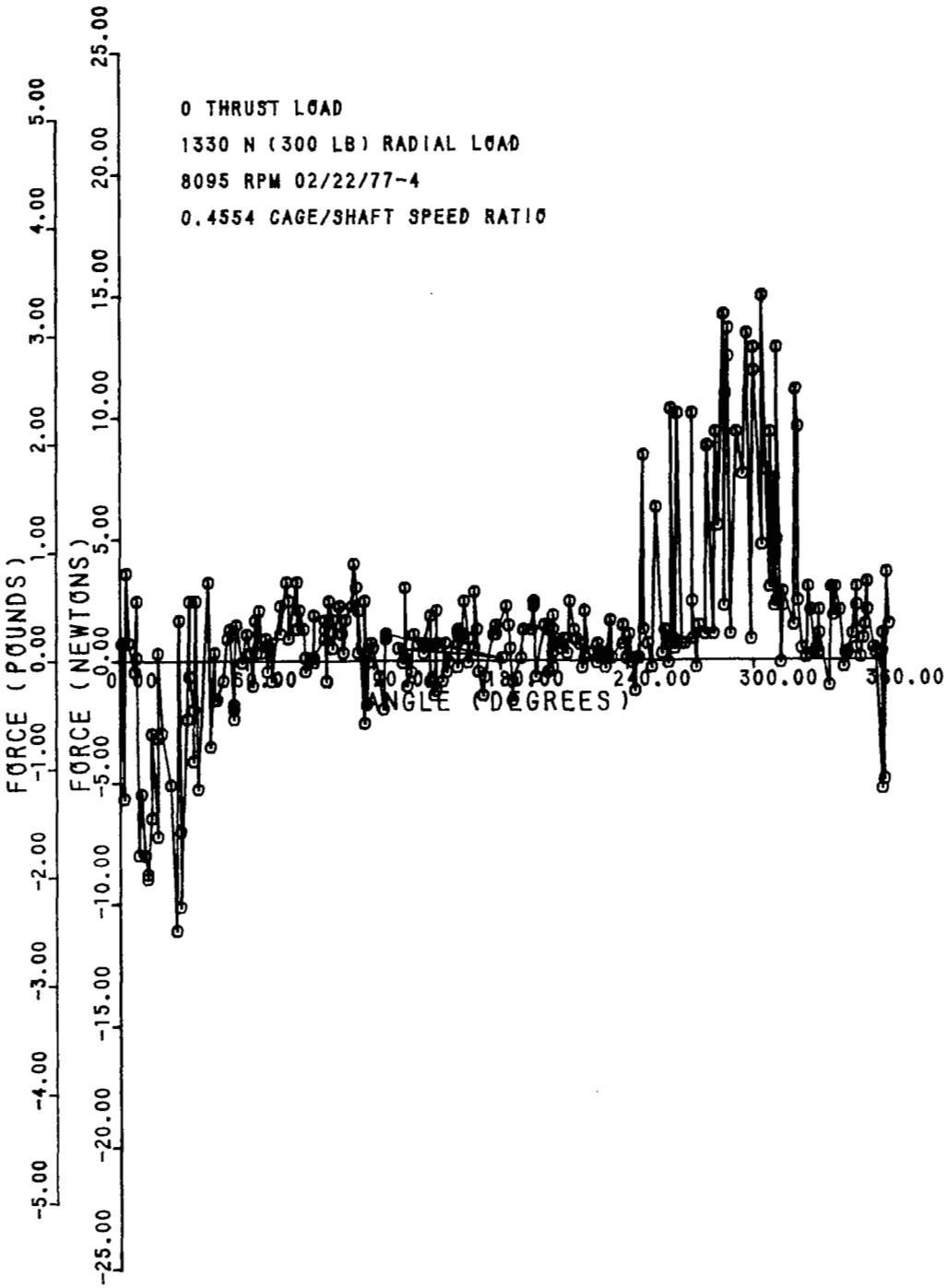

FIG. 7c-61.8 N/mm

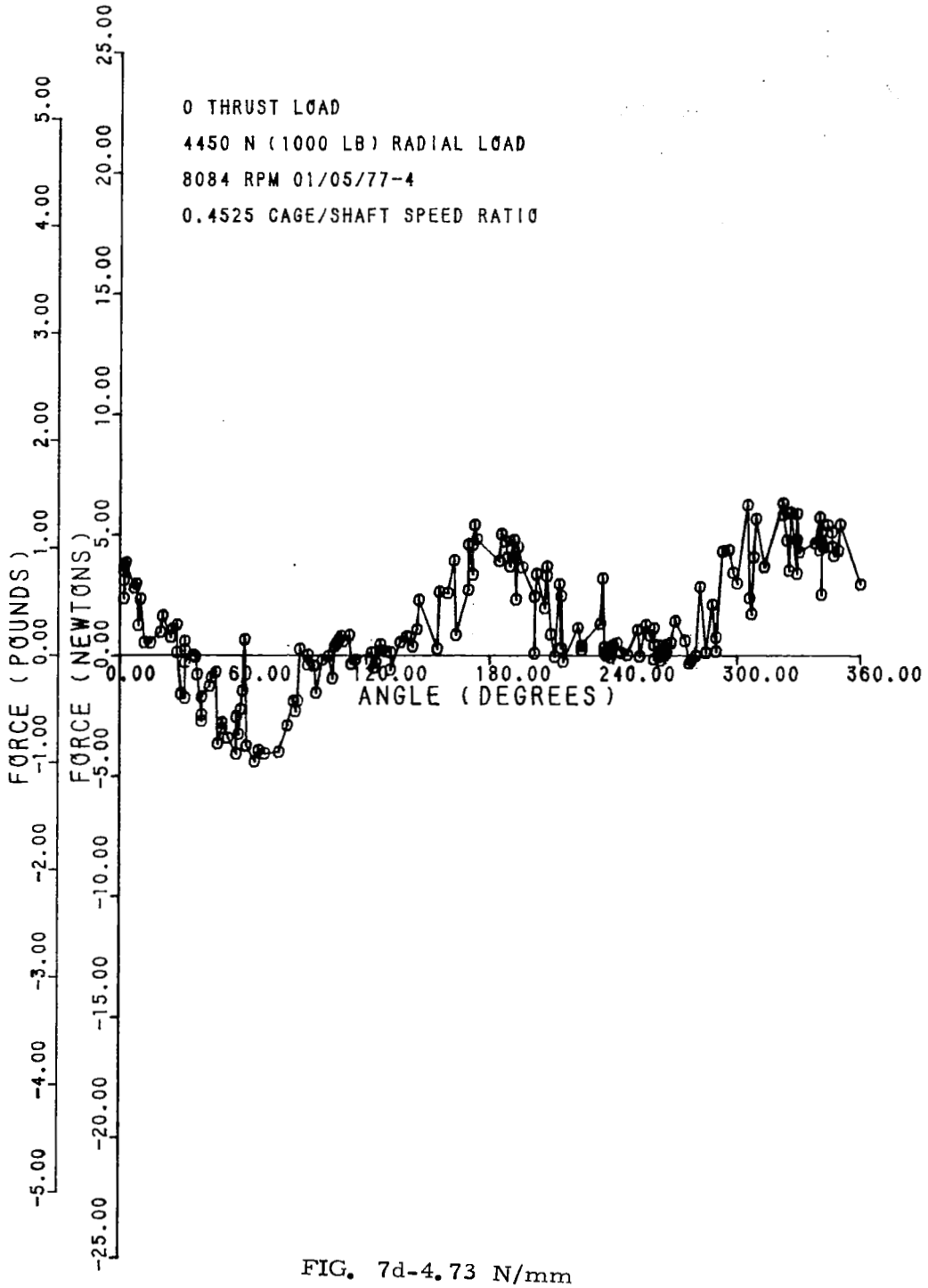

FIG. 7d-4.73 N/mm

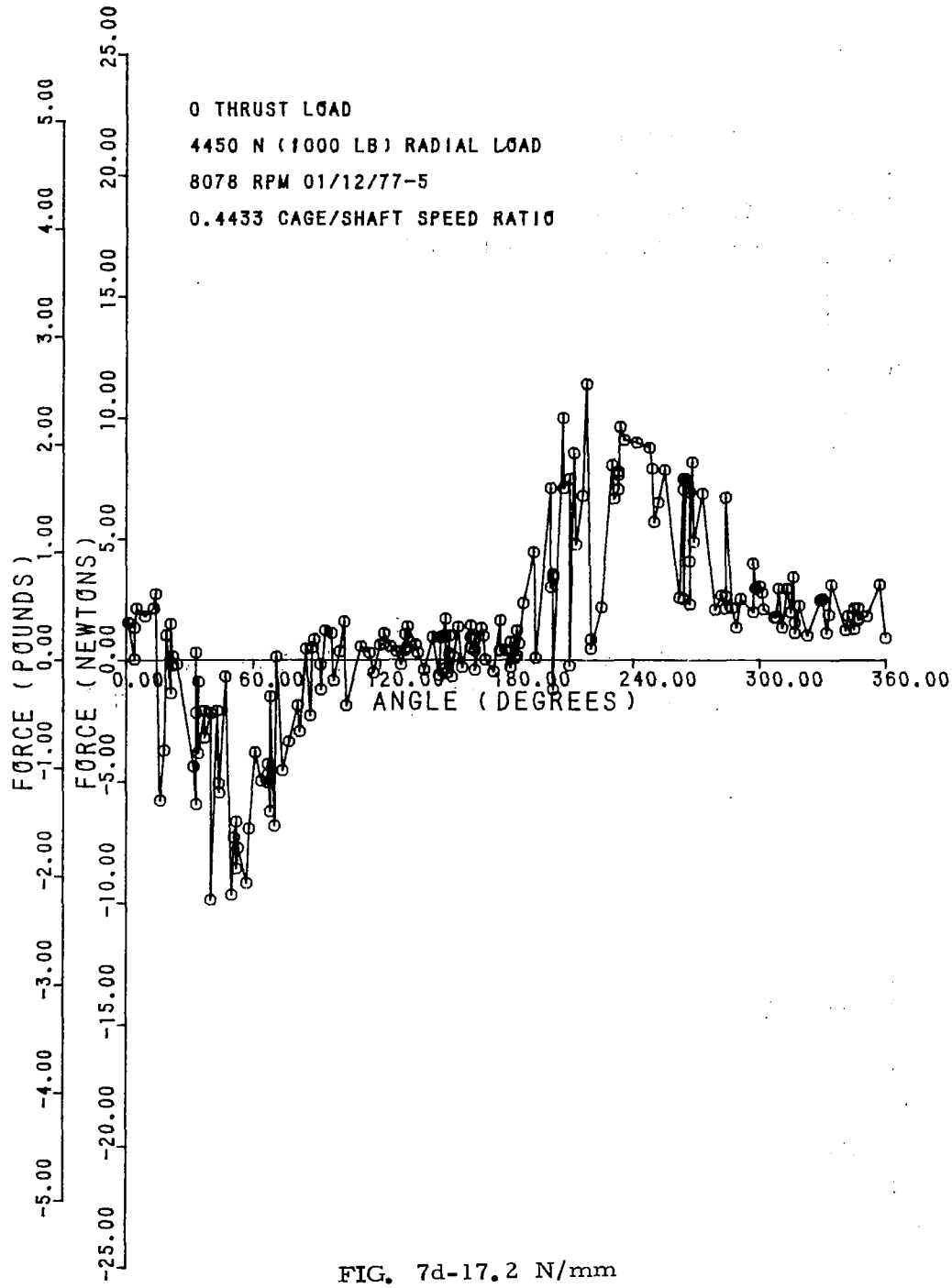

FIG. 7d-17.2 N/mm

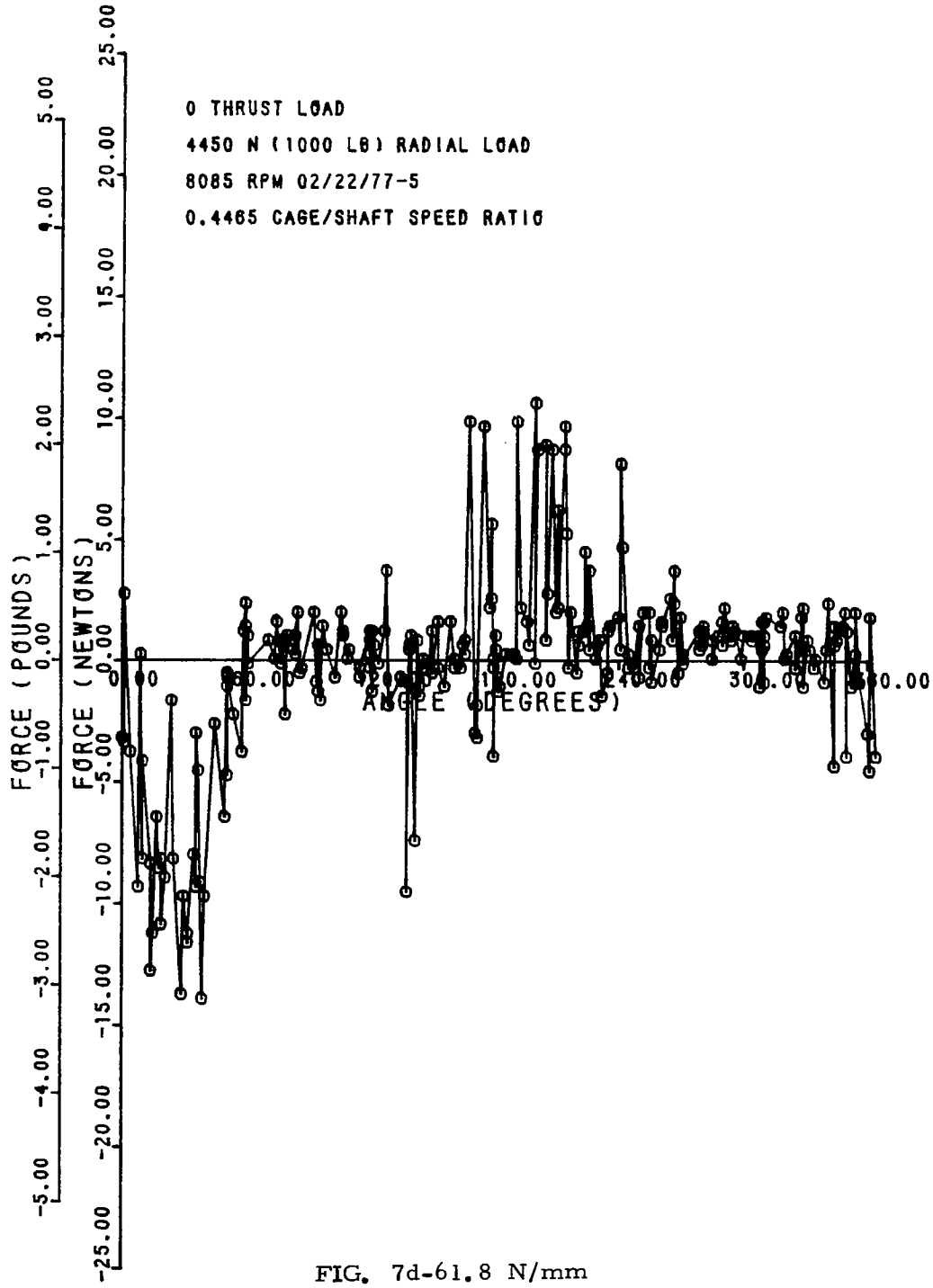

FIG. 7d-61.8 N/mm

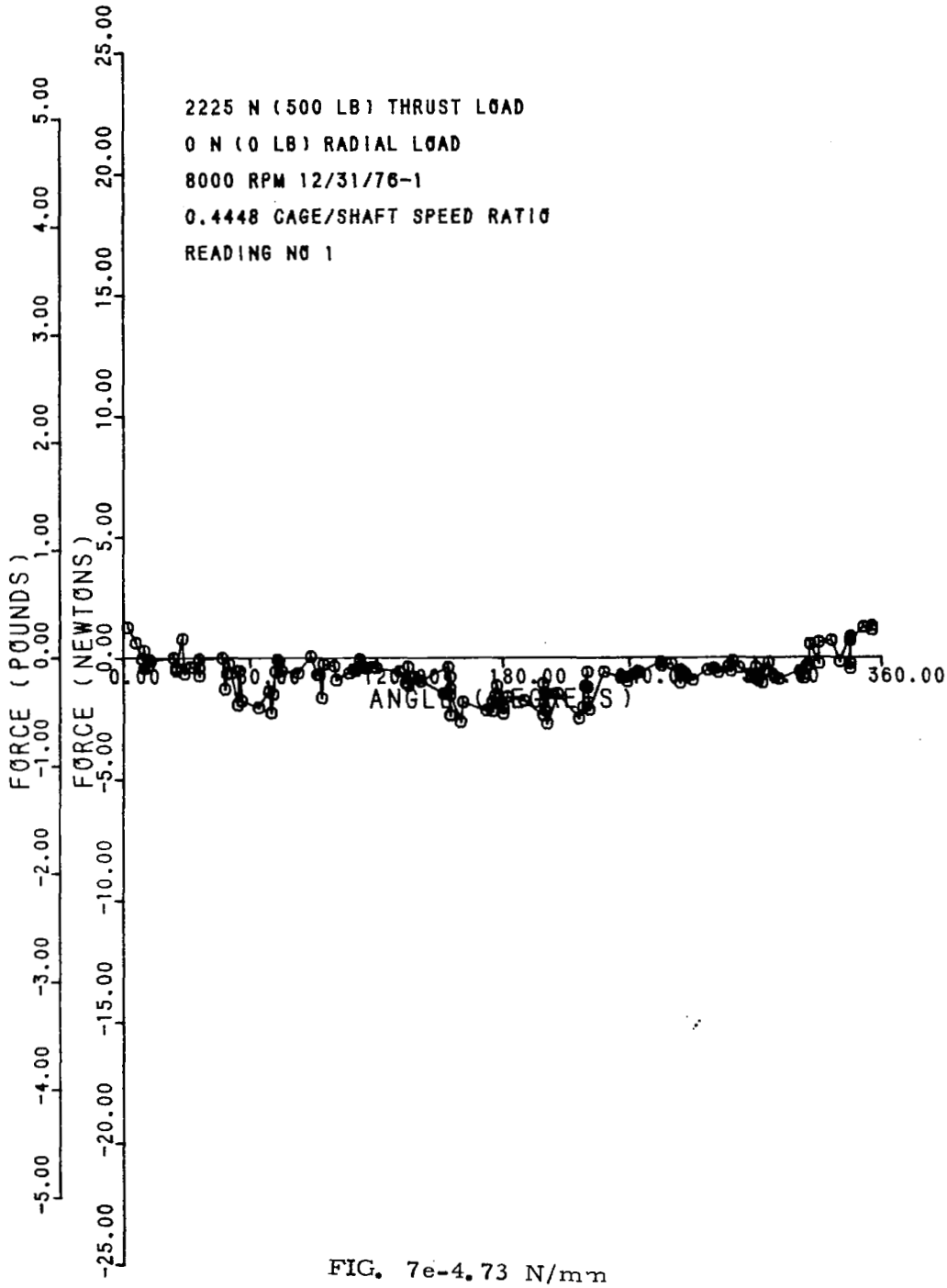

FIG. 7e-4.73 N/mm

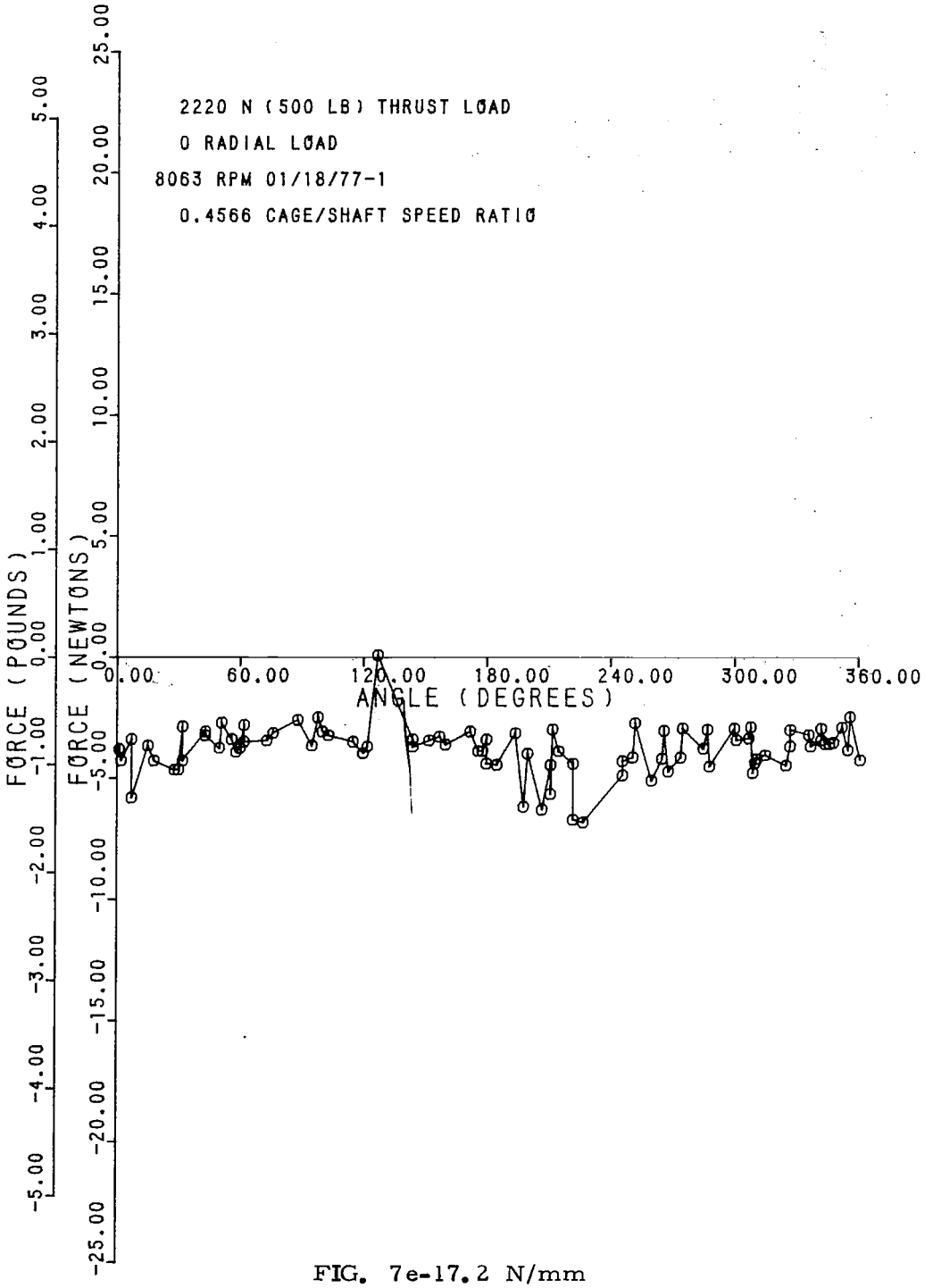

FIG. 7e-17.2 N/mm

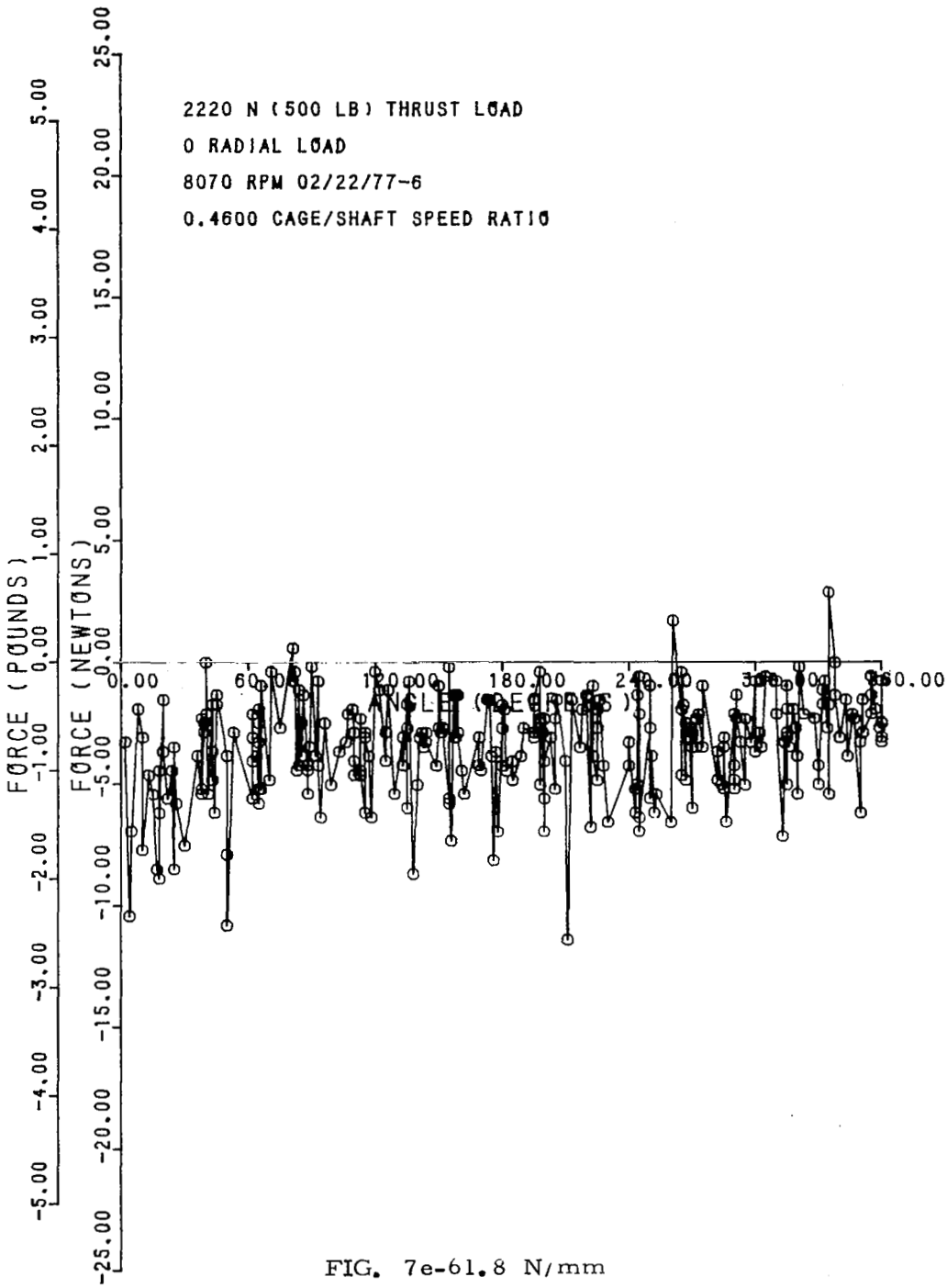

FIG. 7e-61.8 N/mm

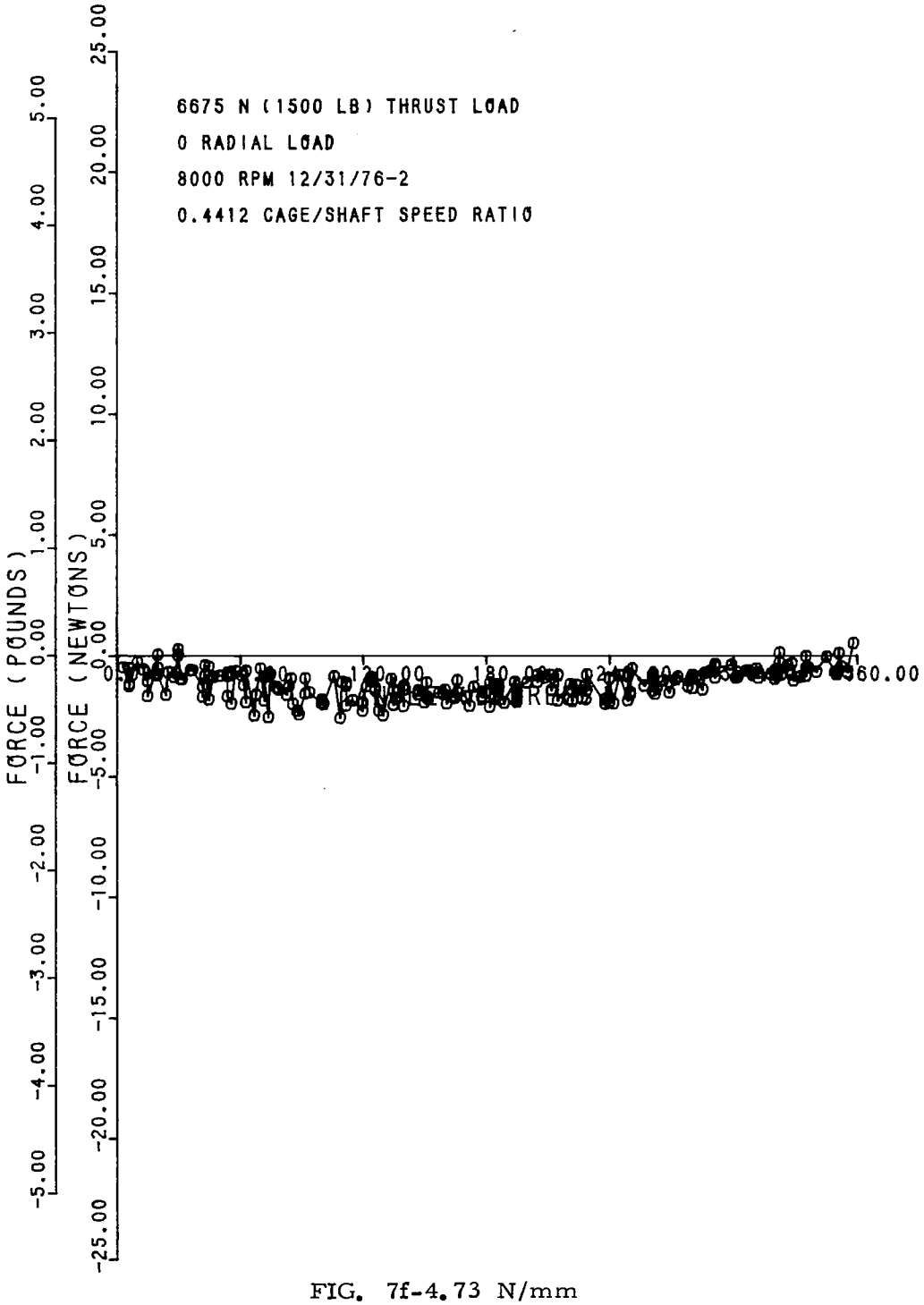

FIG. 7f-4.73 N/mm

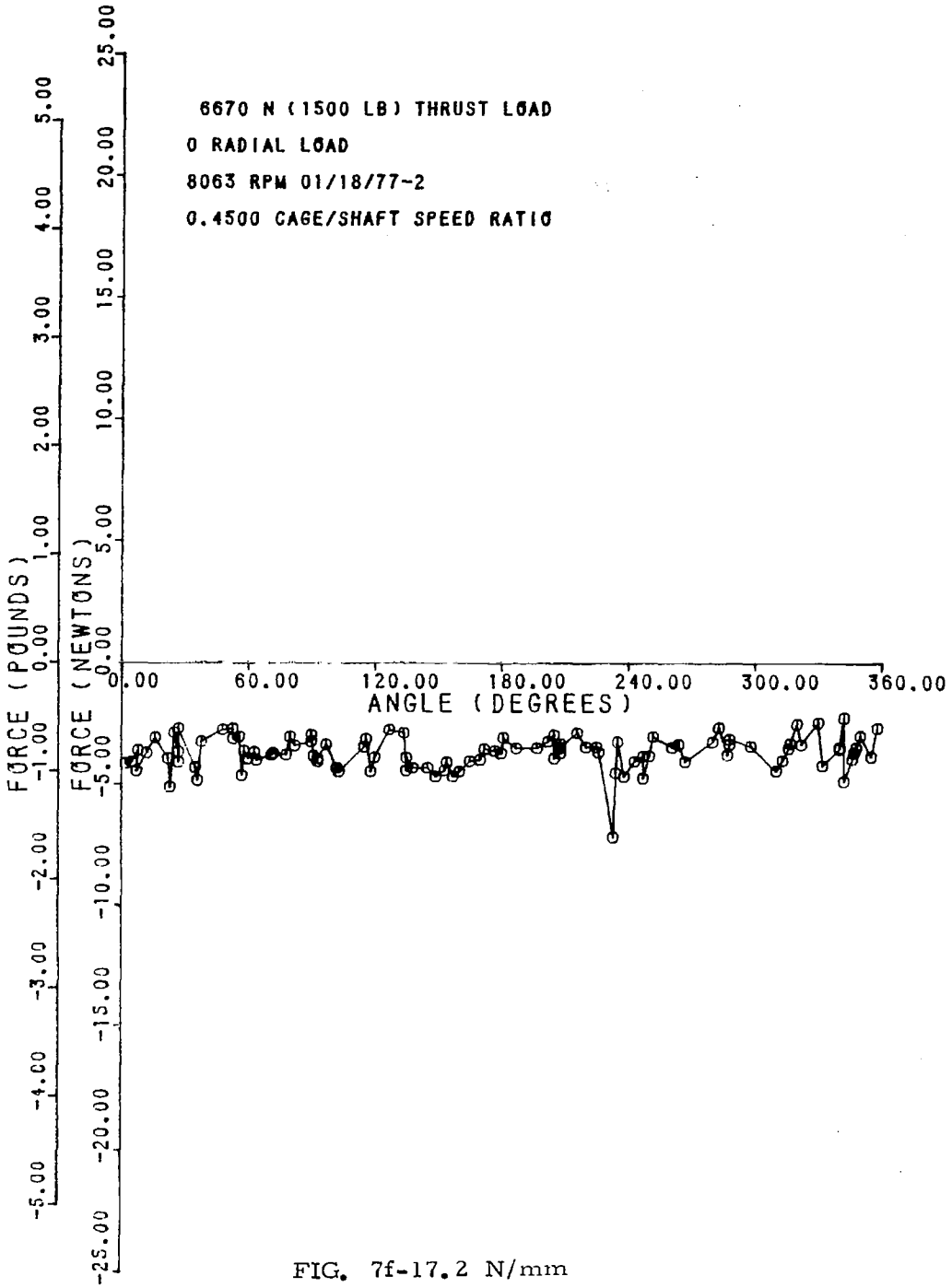

FIG. 7f-17.2 N/mm

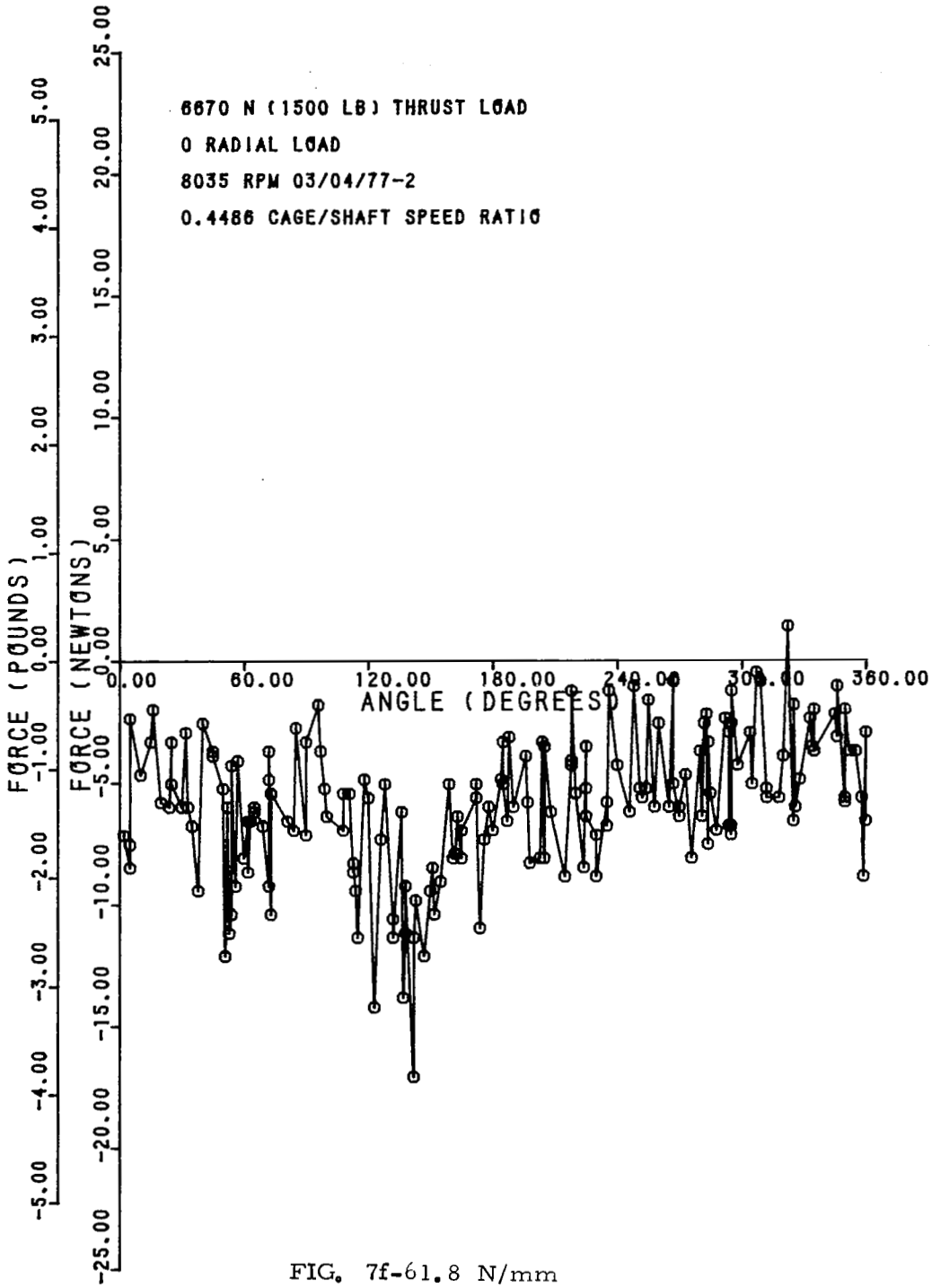

FIG. 7f-61.8 N/mm

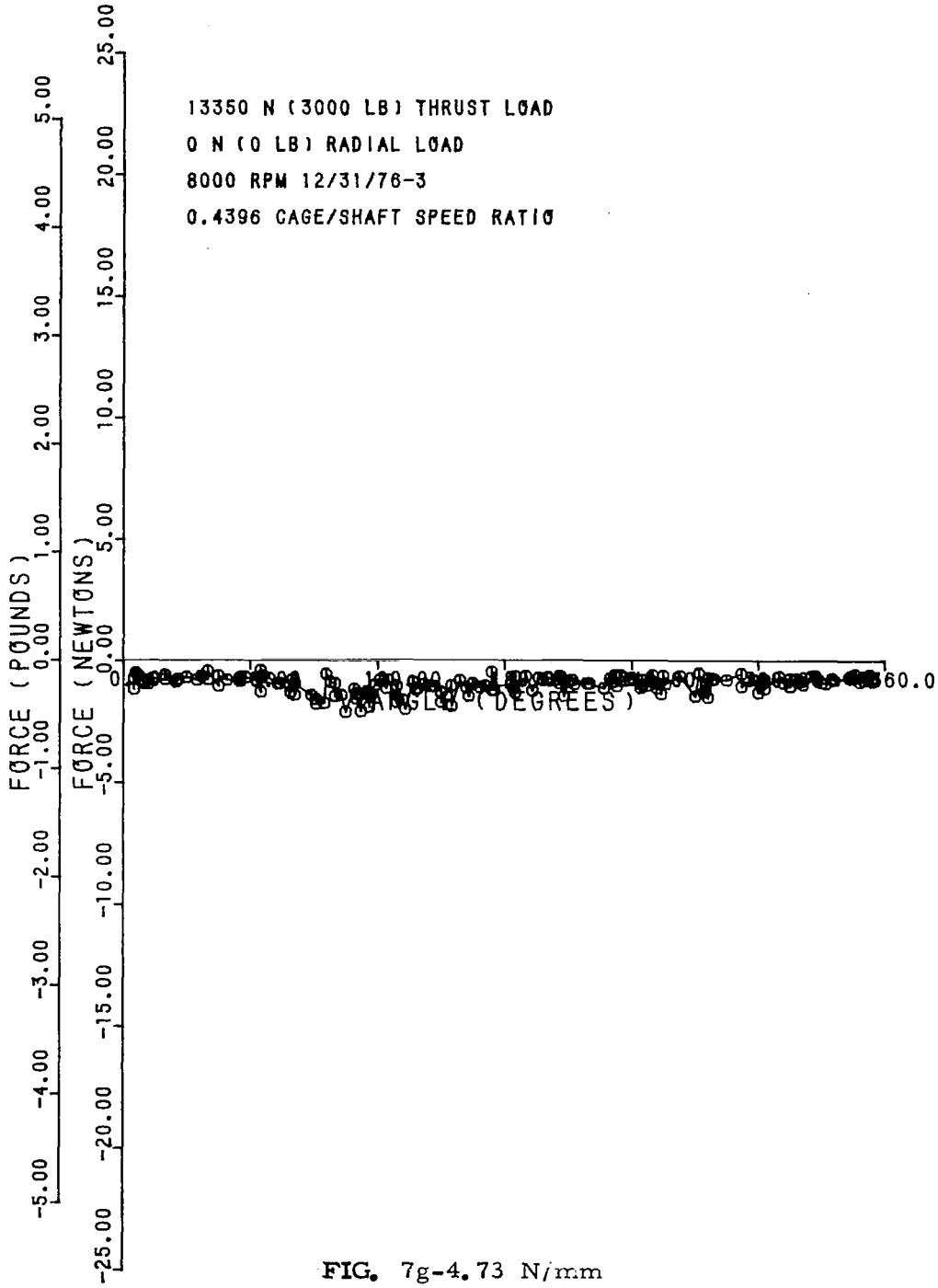

FIG. 7g-4.73 N/mm

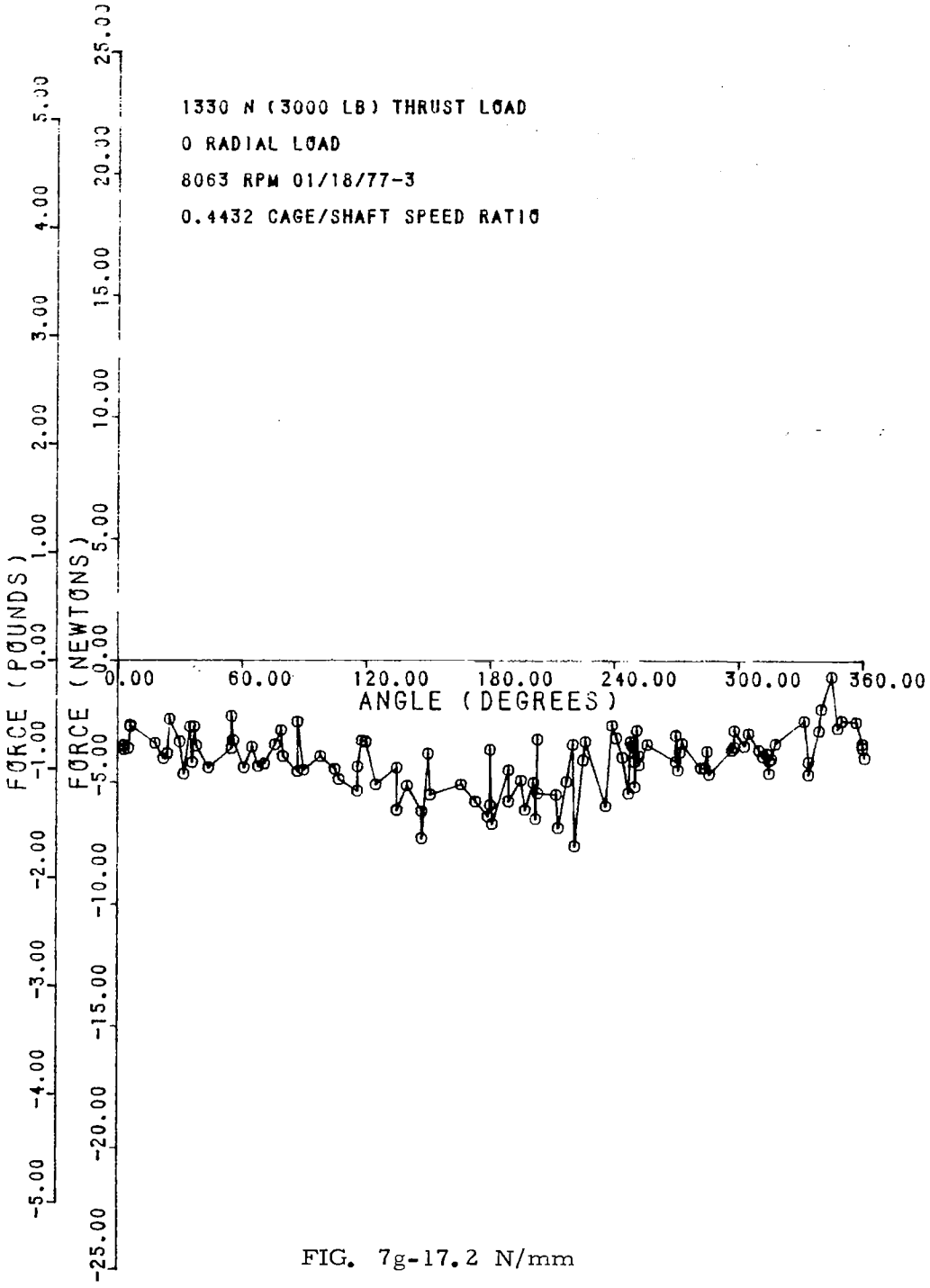

FIG. 7g-17.2 N/mm

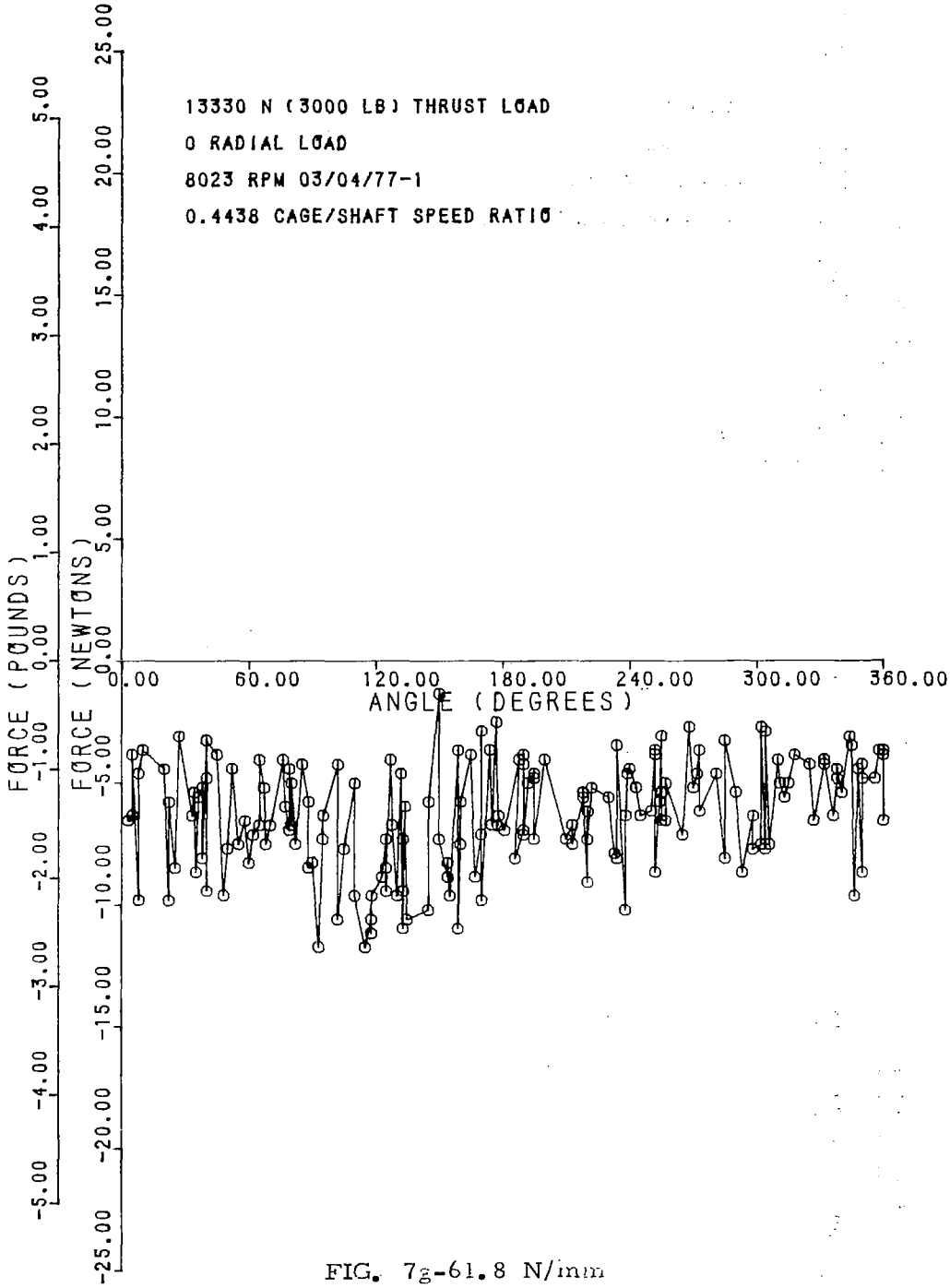

FIG. 7g-61.8 N/mm

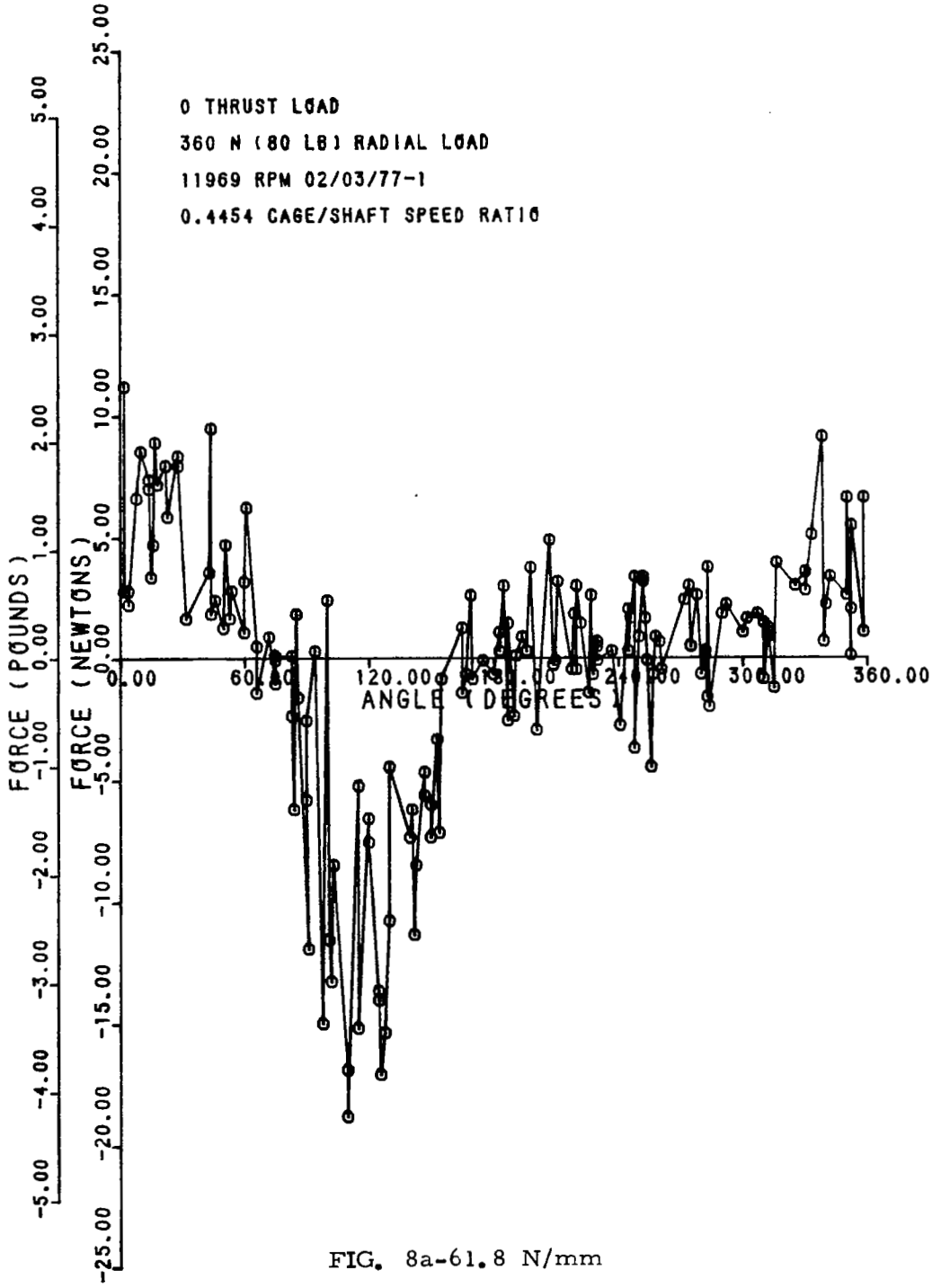

FIG. 8a-61.8 N/mm

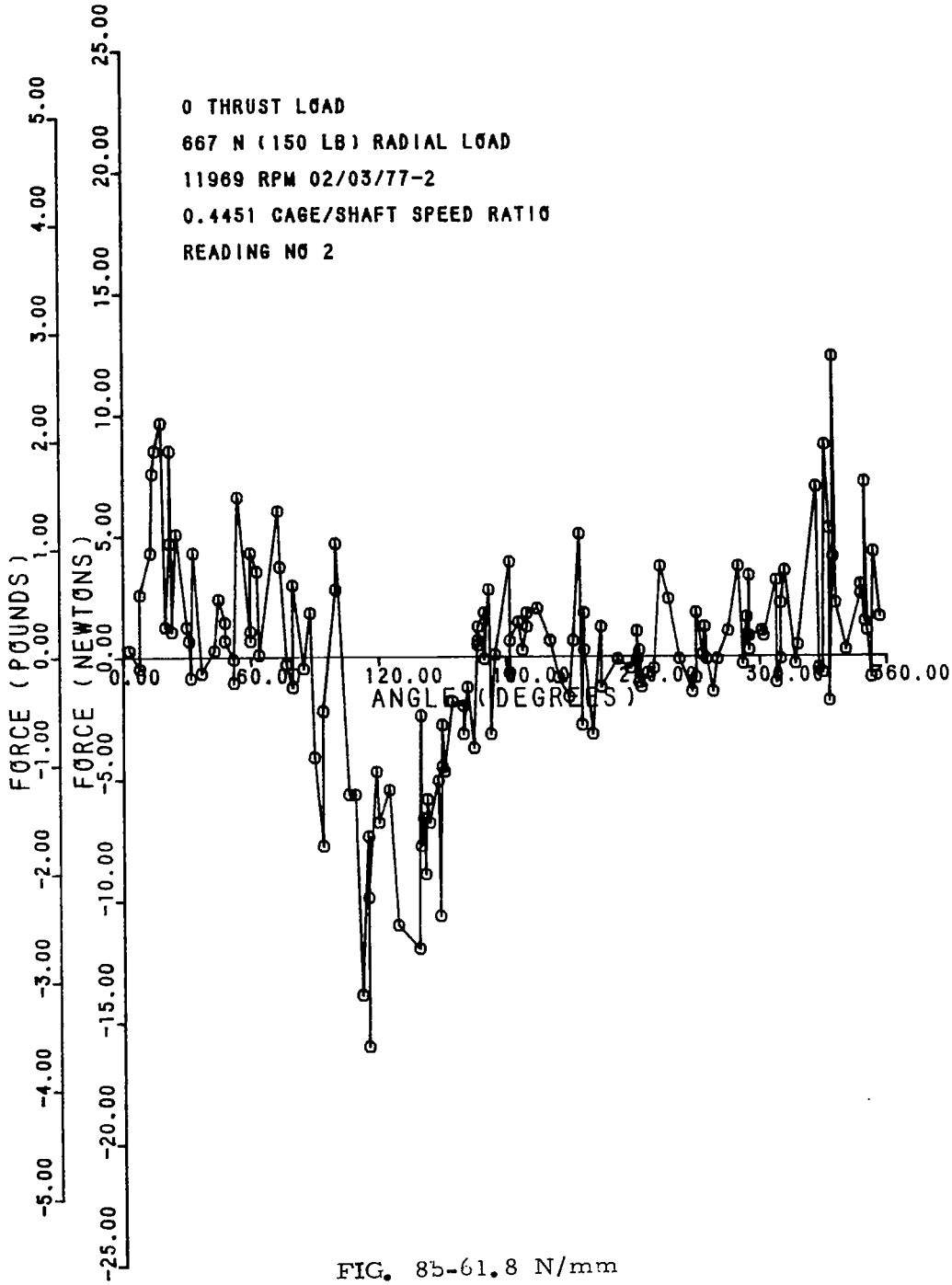

FIG. 85-61.8 N/mm

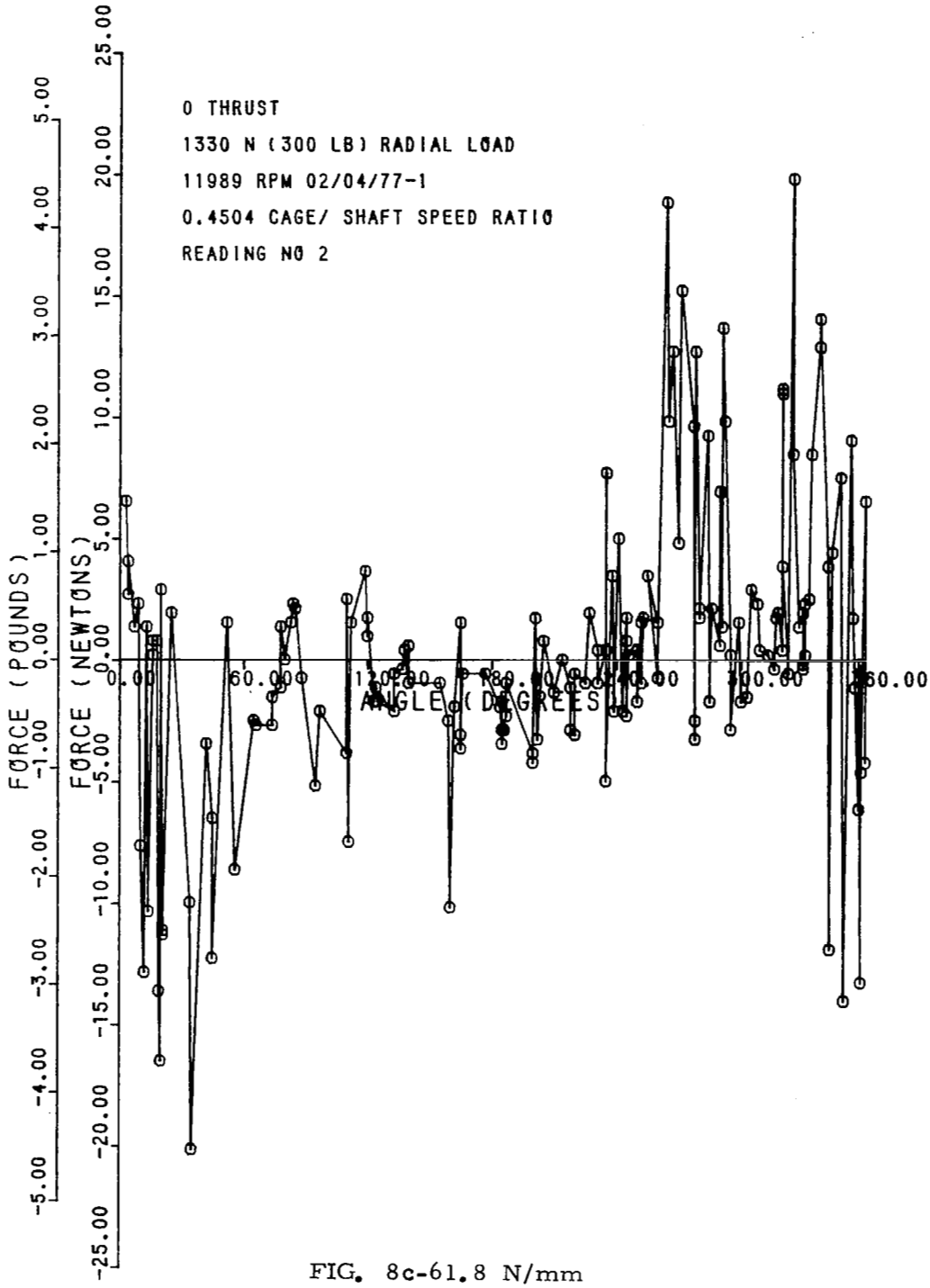

FIG. 8c-61.8 N/mm

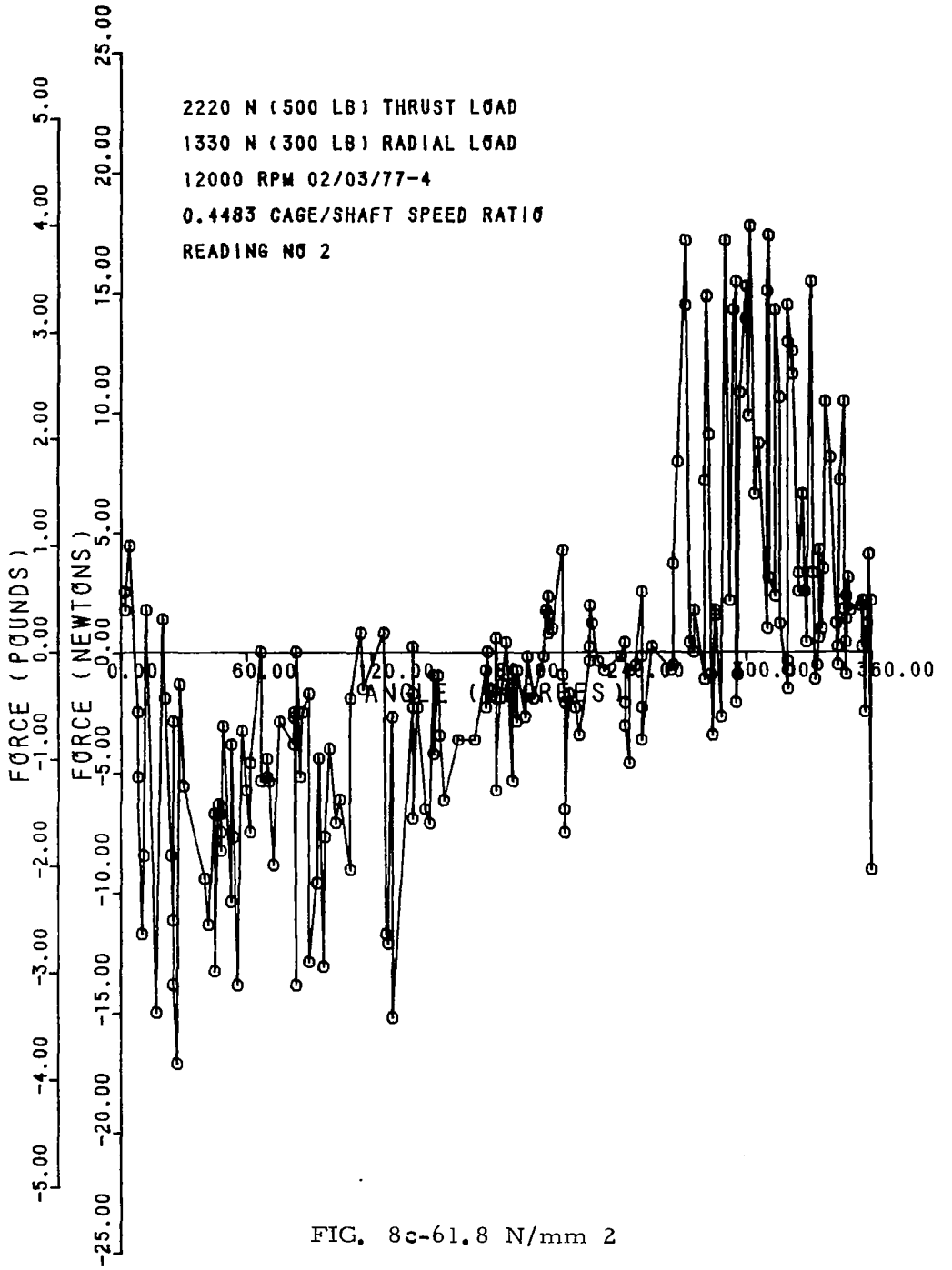

FIG. 8c-61.8 N/mm 2

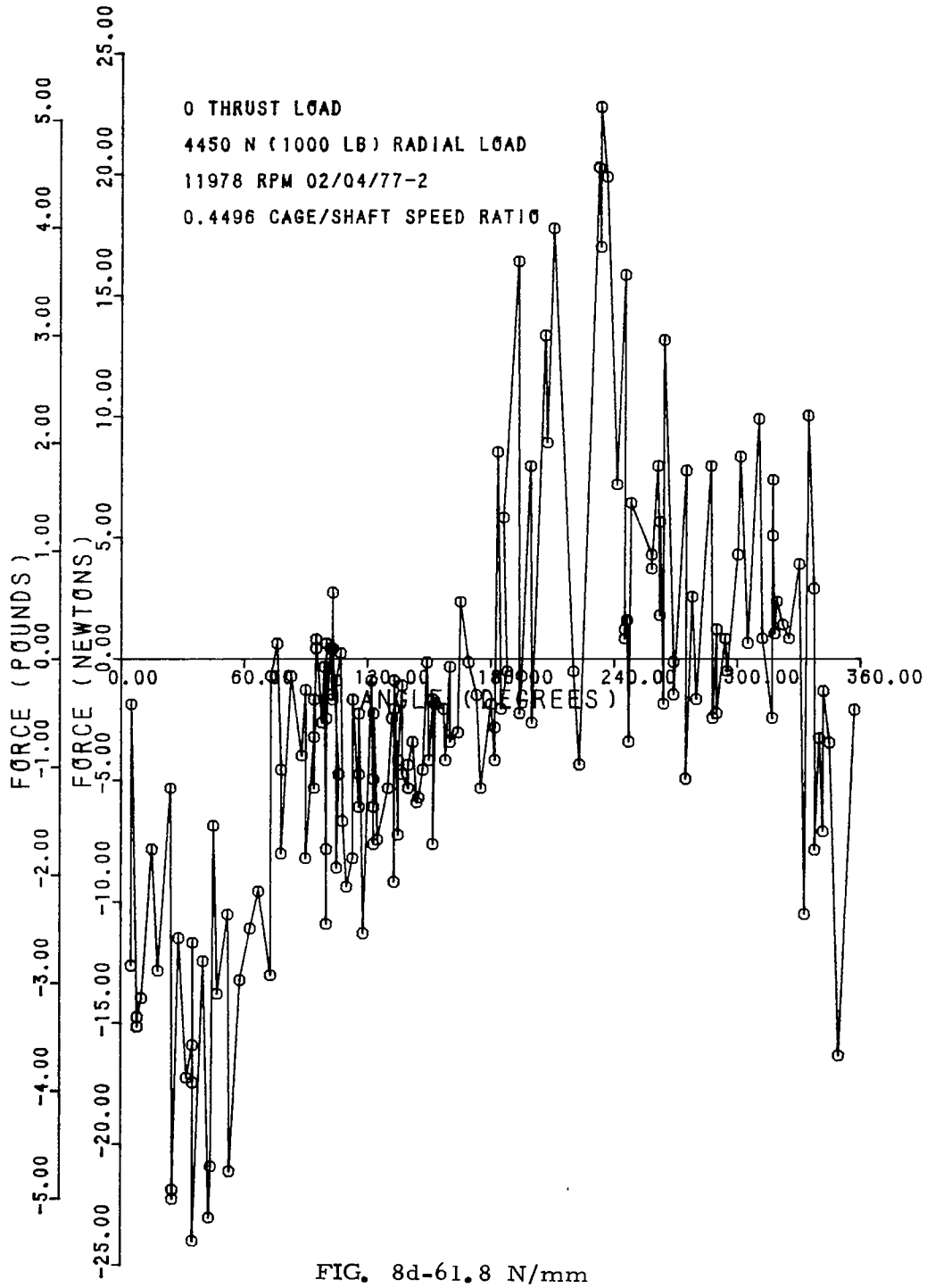

FIG. 8d-61.8 N/mm

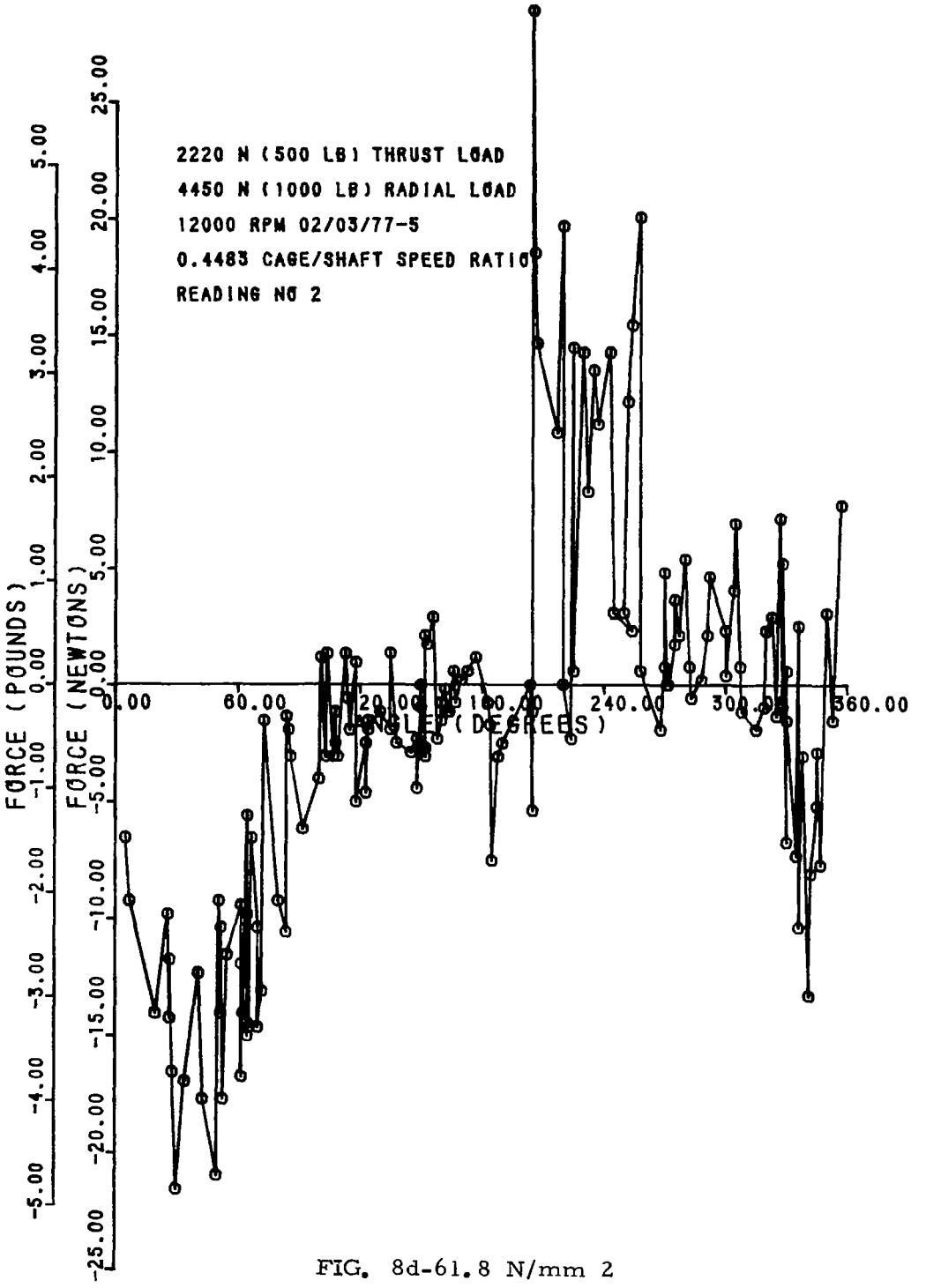

FIG. 8d-61.8 N/mm 2

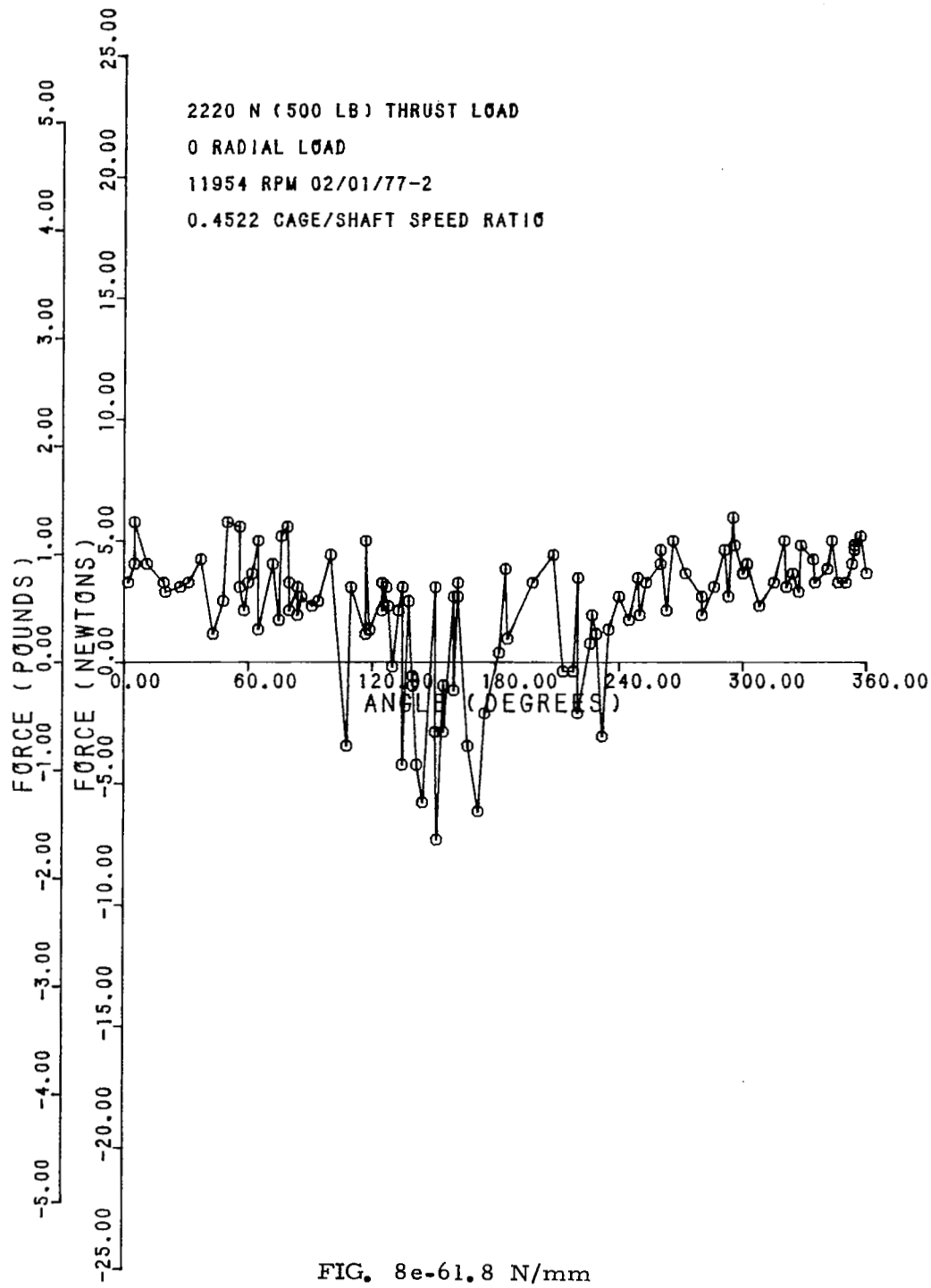

FIG. 8e-61.8 N/mm

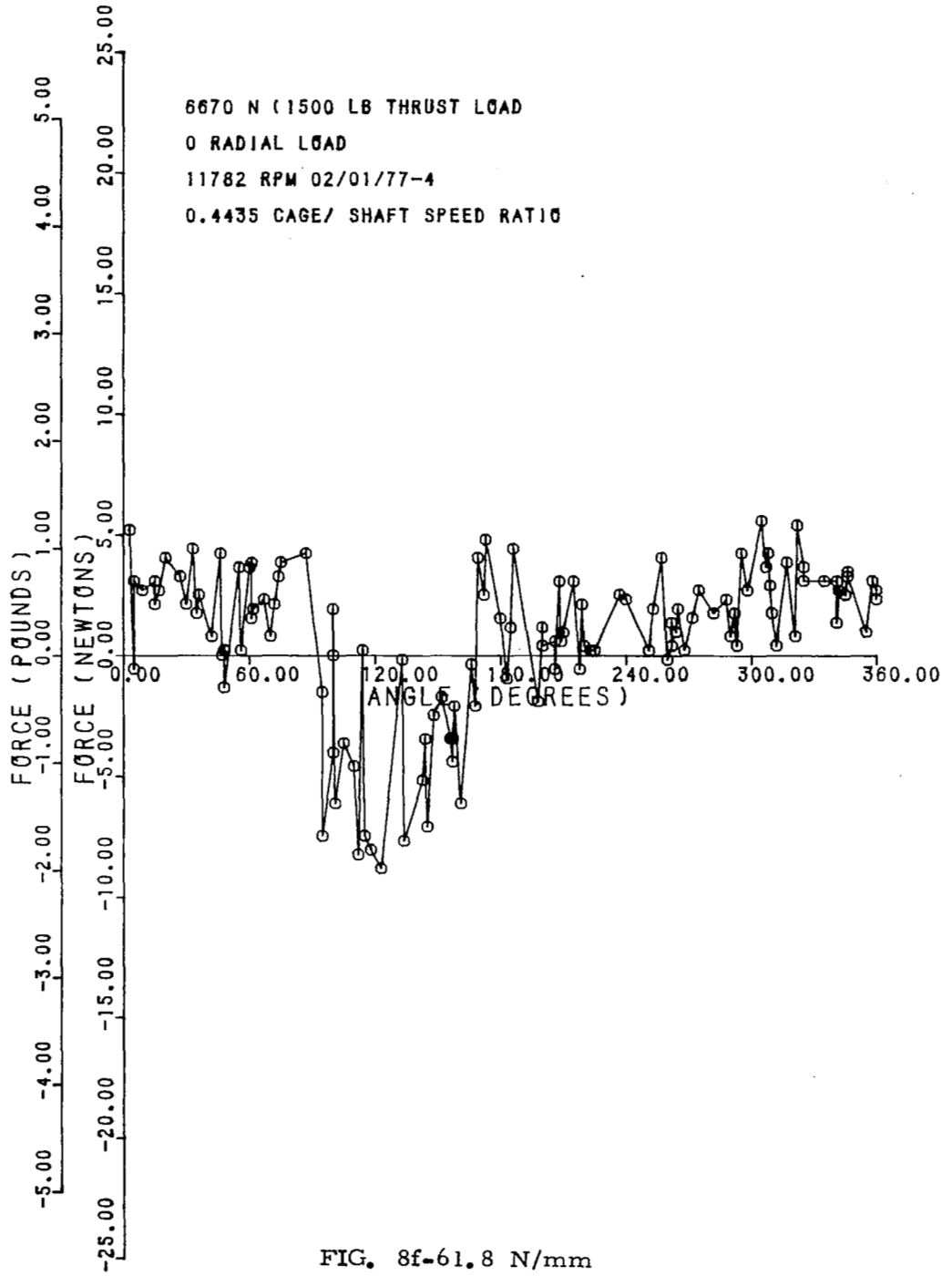

FIG. 8f-61.8 N/mm

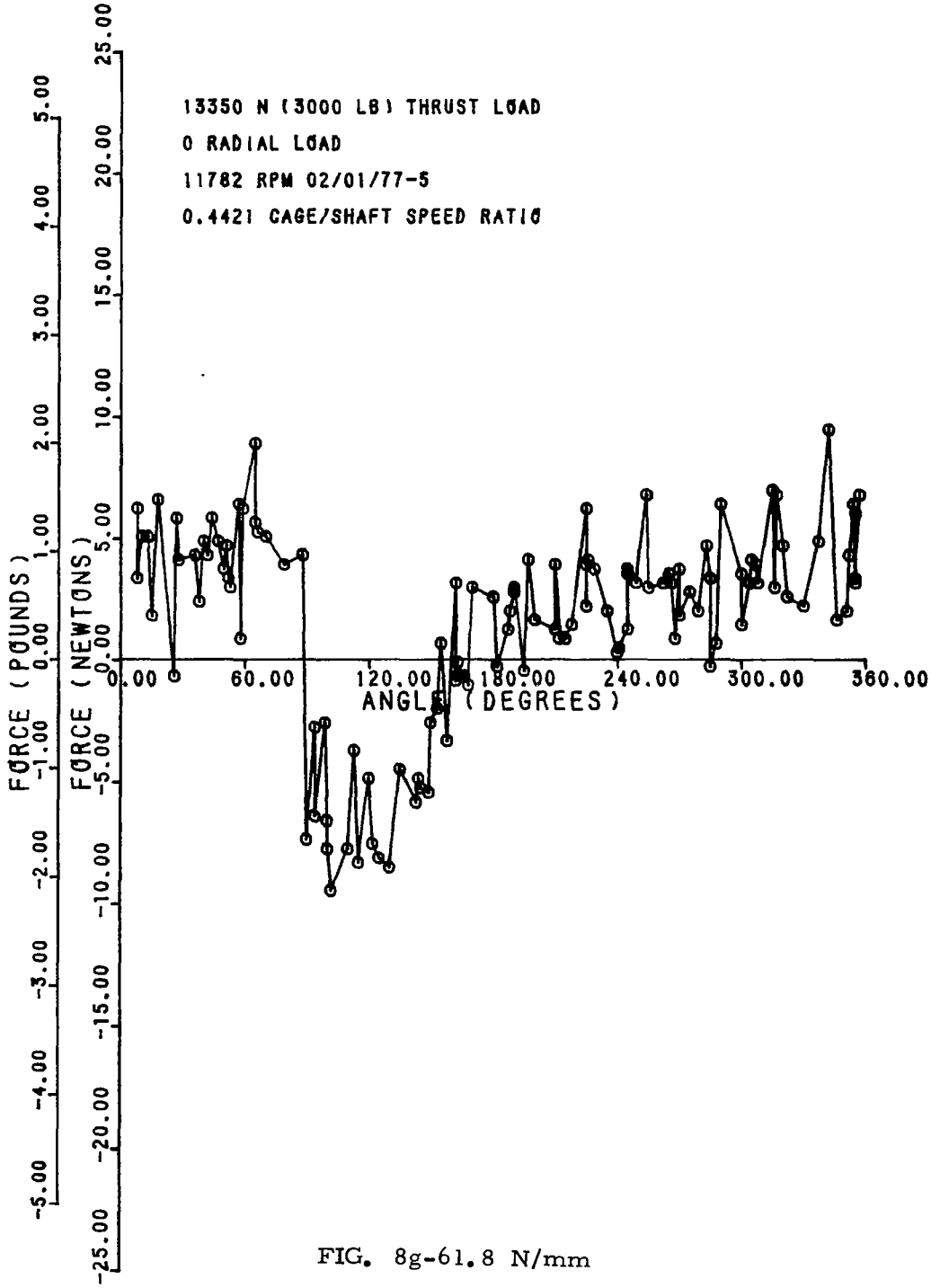

FIG. 8g-61.8 N/mm

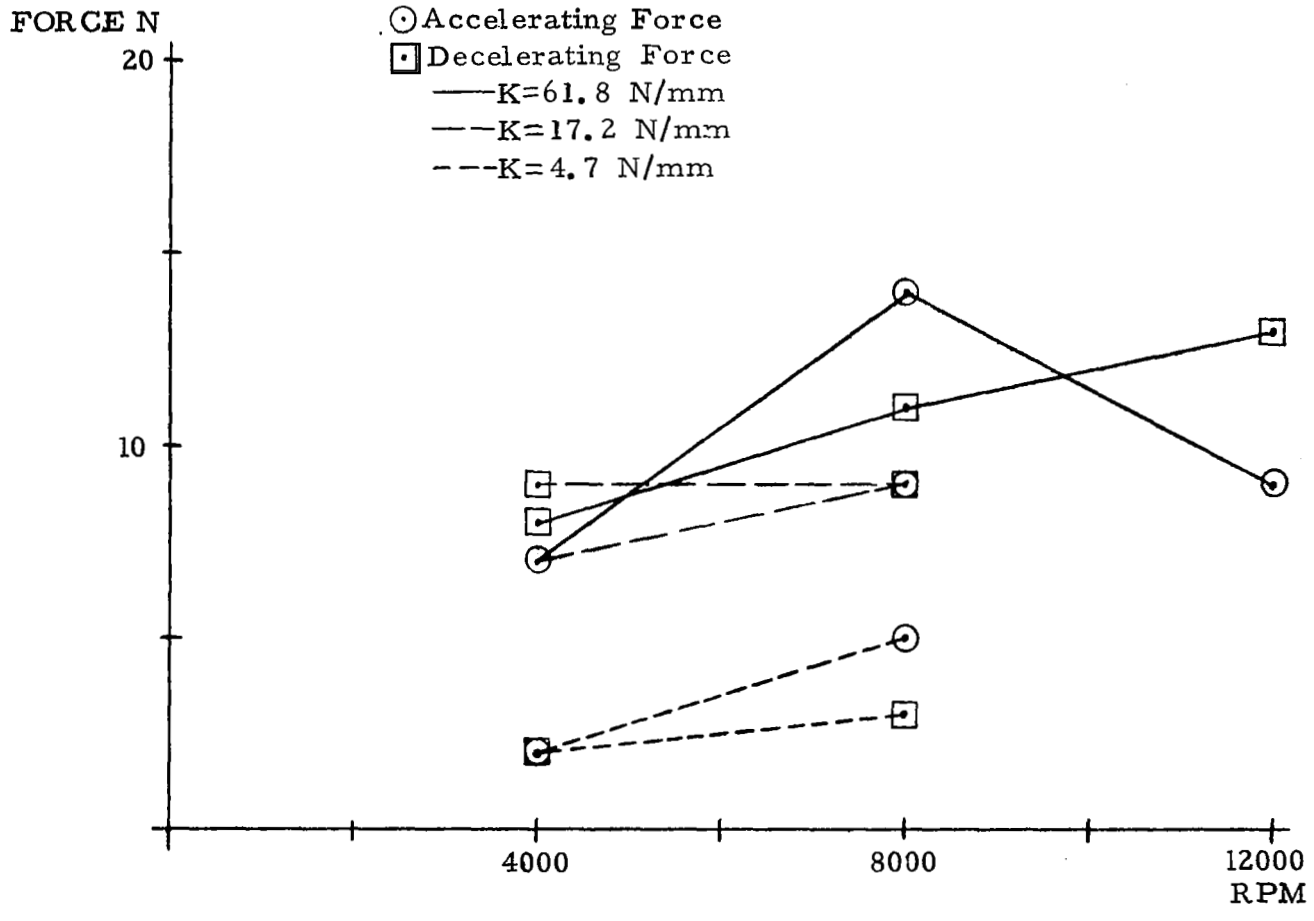

FIGURE 9a Cage Force Magnitude Versus Shaft Speed, 360 N Radial Load

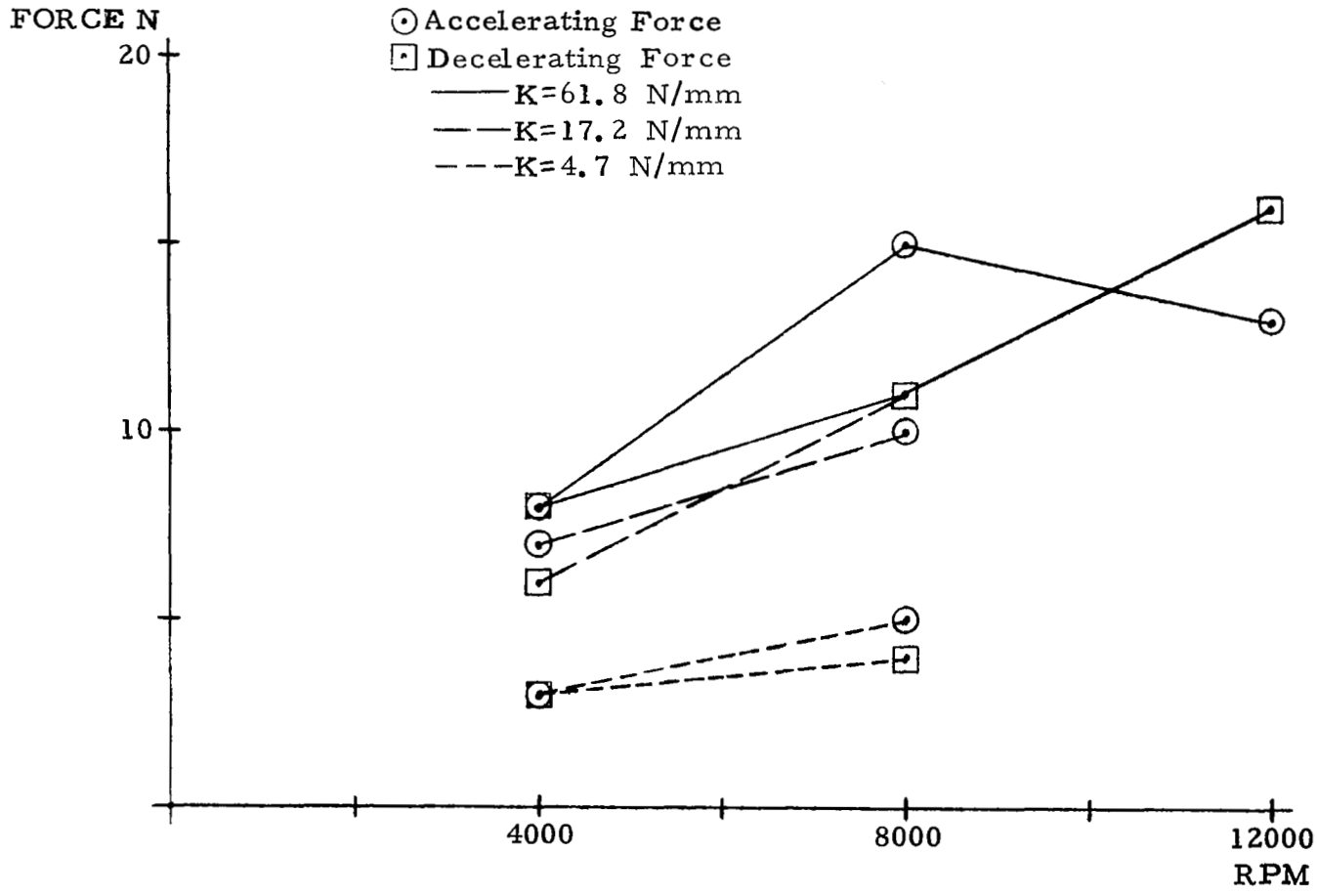

FIGURE 9b Cage Force Magnitude Versus Shaft Speed, 670 N Radial Load

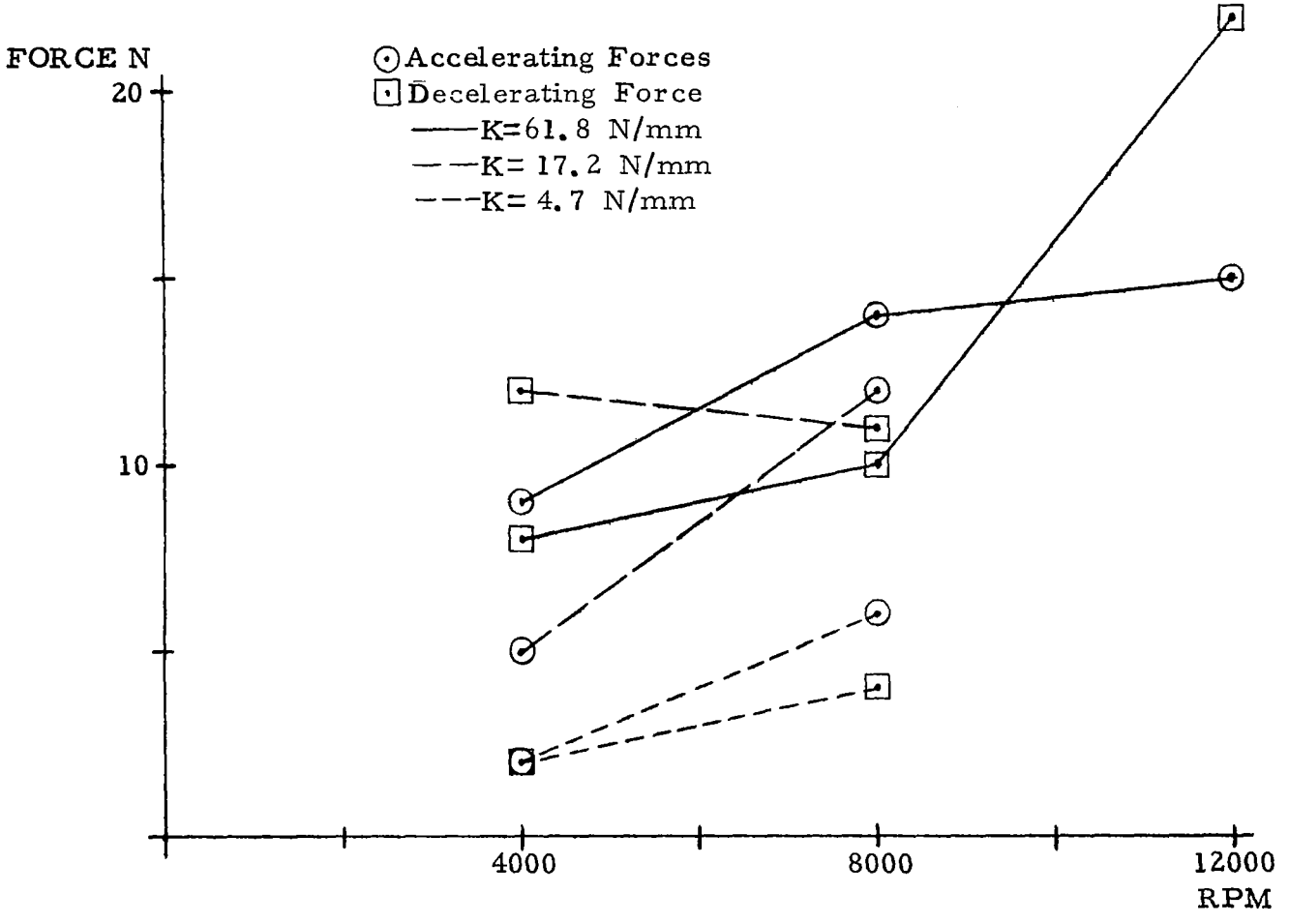

FIGURE 9c Cage Force Magnitude Versus Shaft Speed, 1330 N Radial Load

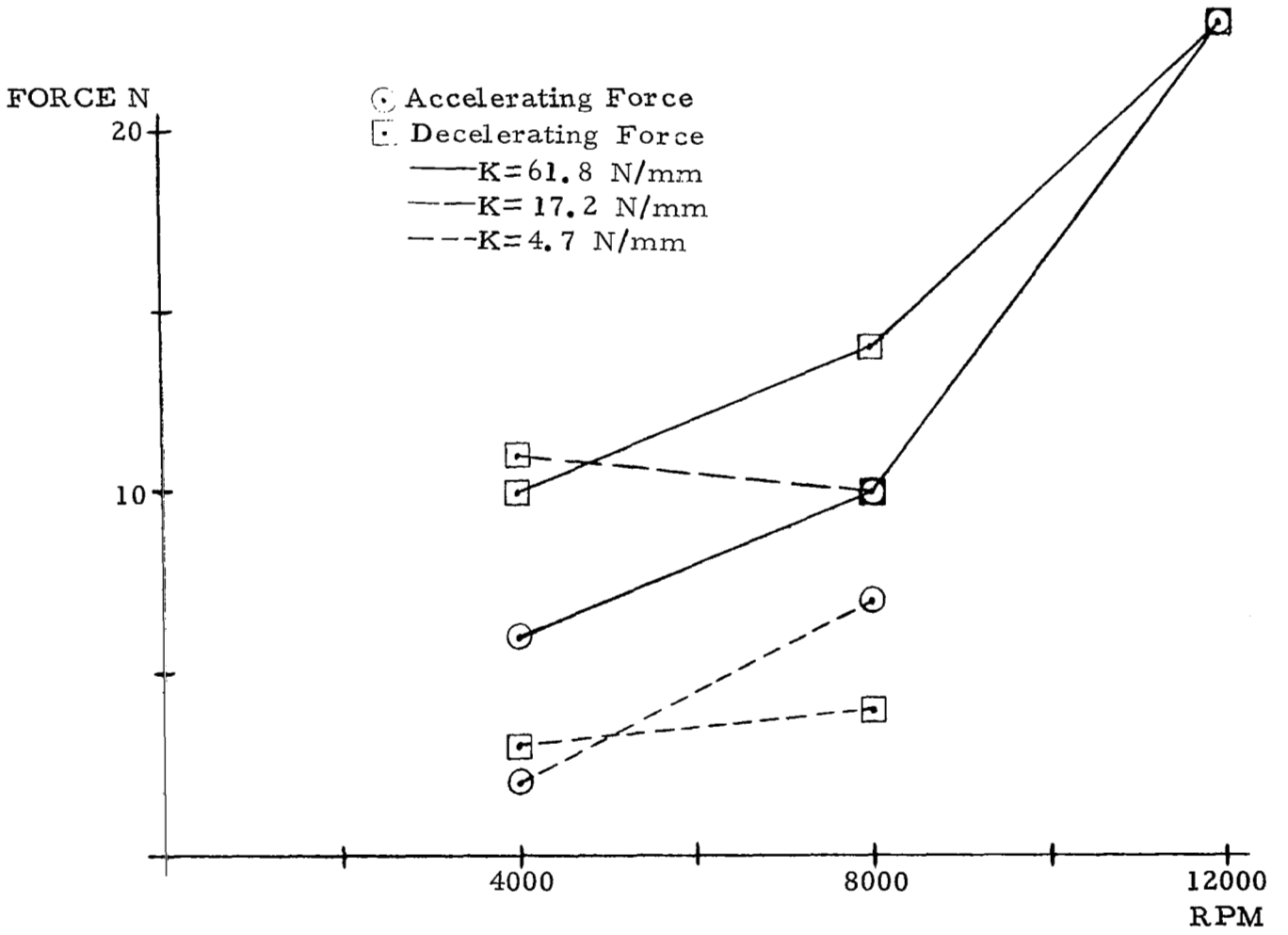

FIGURE 9d Cage Force Magnitude Versus Shaft Speed, 4450 N Radial Load

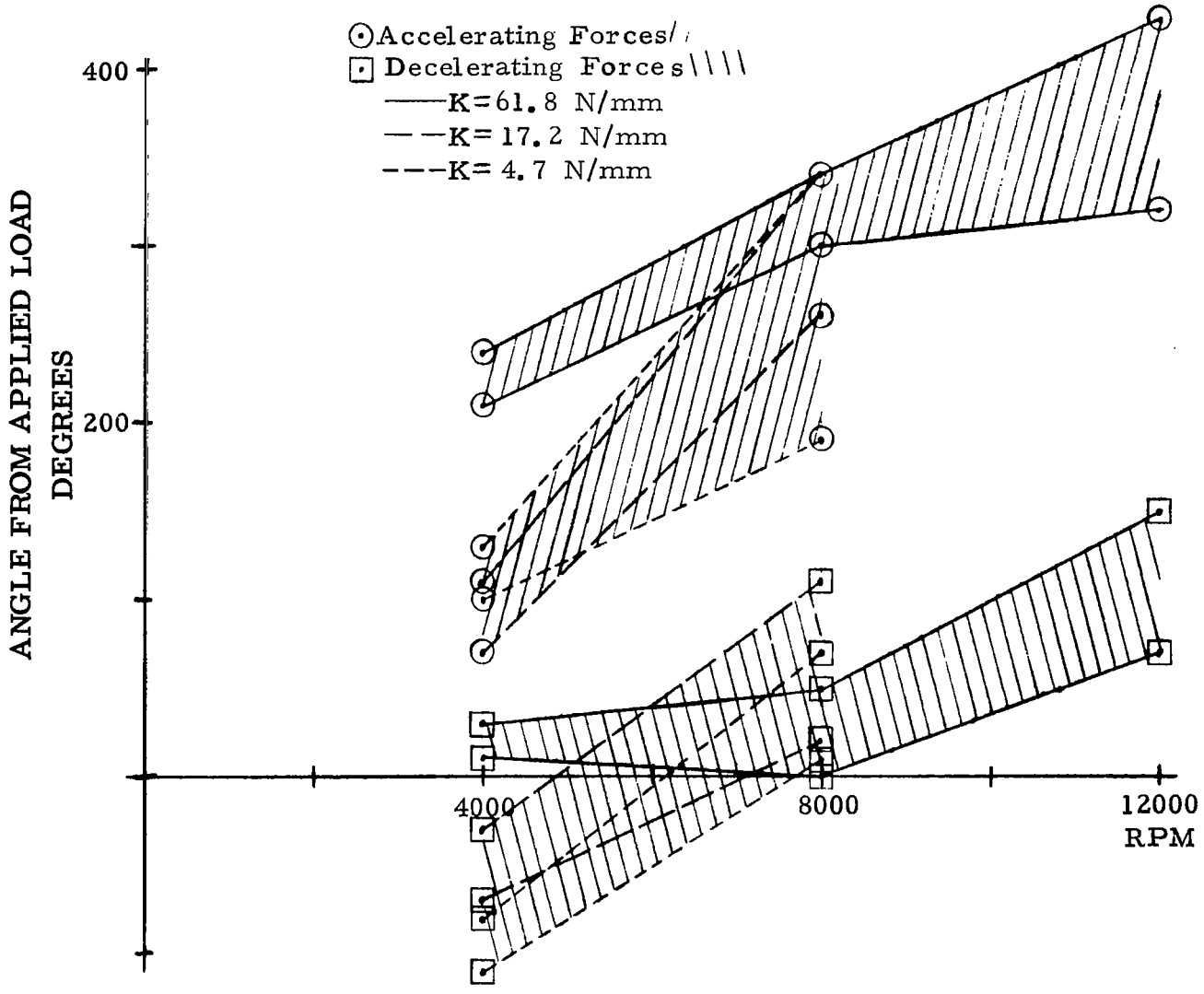

FIGURE 10a Locations of Accelerating and Decelerating Cage Forces as a Function of Shaft Speed, 360 N Radial Load

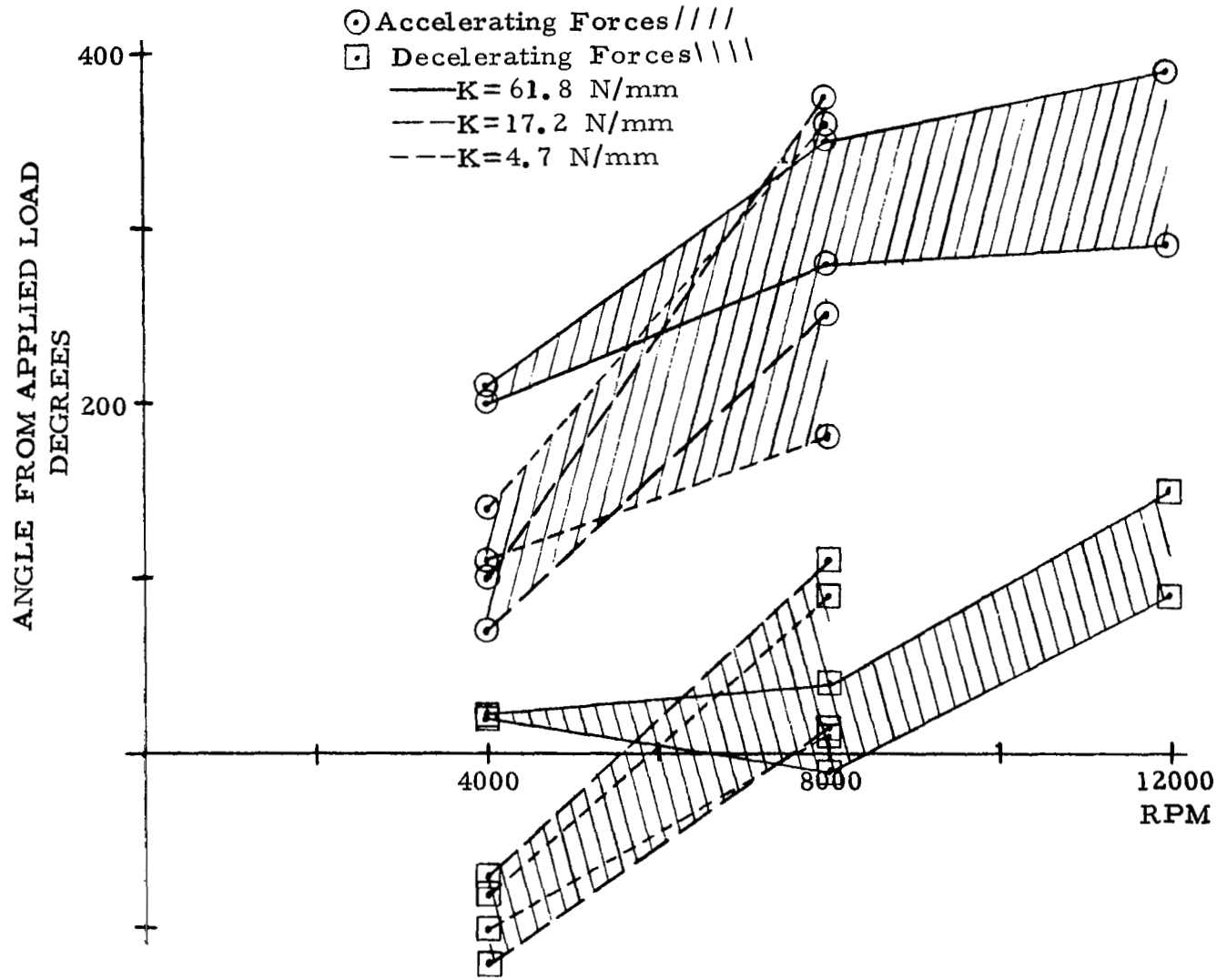

FIGURE 10b Locations of Accelerating and Deccelerating Cage Forces as a Function of Shaft Speed, 670 N Radial Load

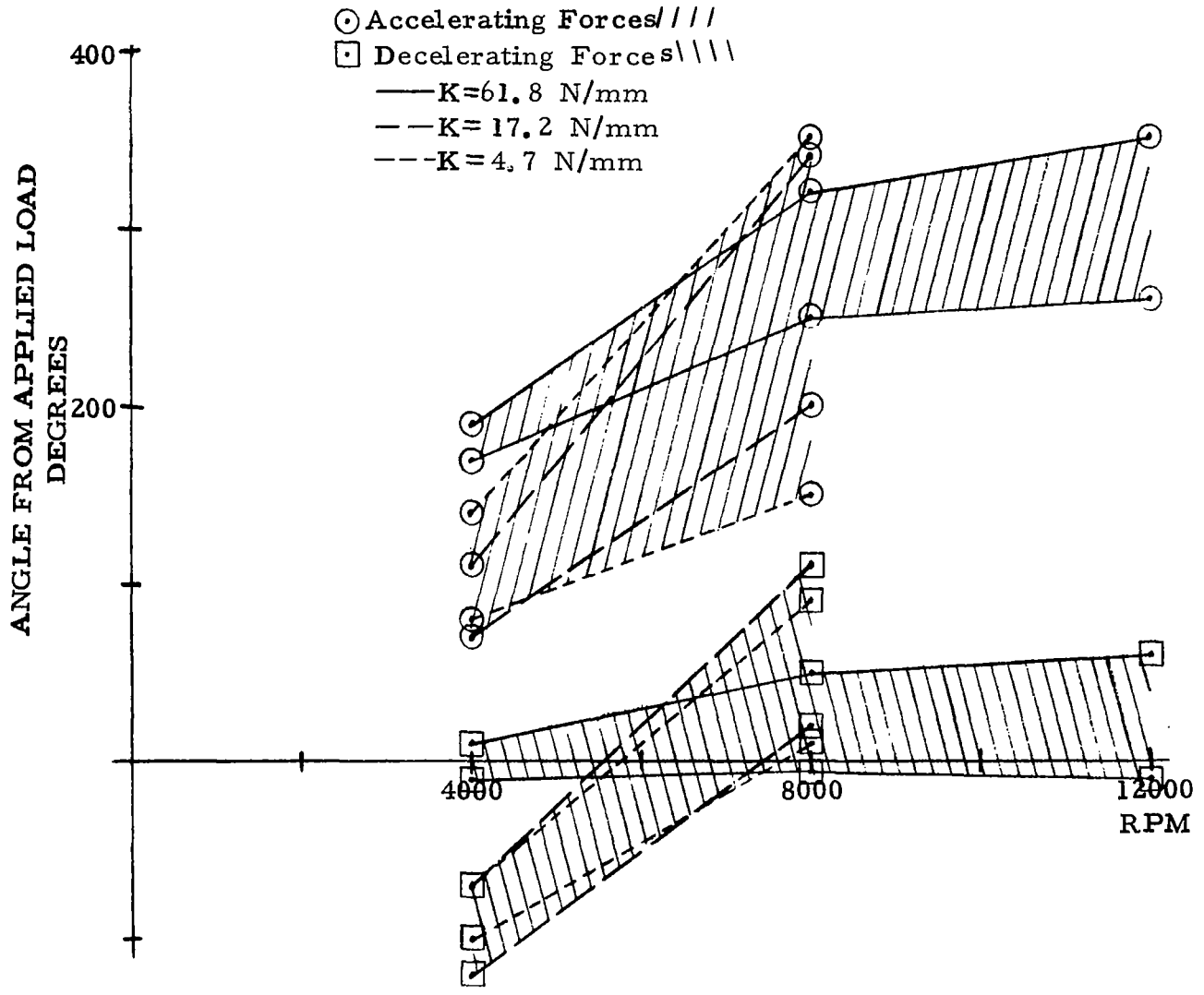

FIGURE 10c Locations of Accelerating and Deccelerating Forces as a Function of Shaft Speed, 1330 N Radial Load

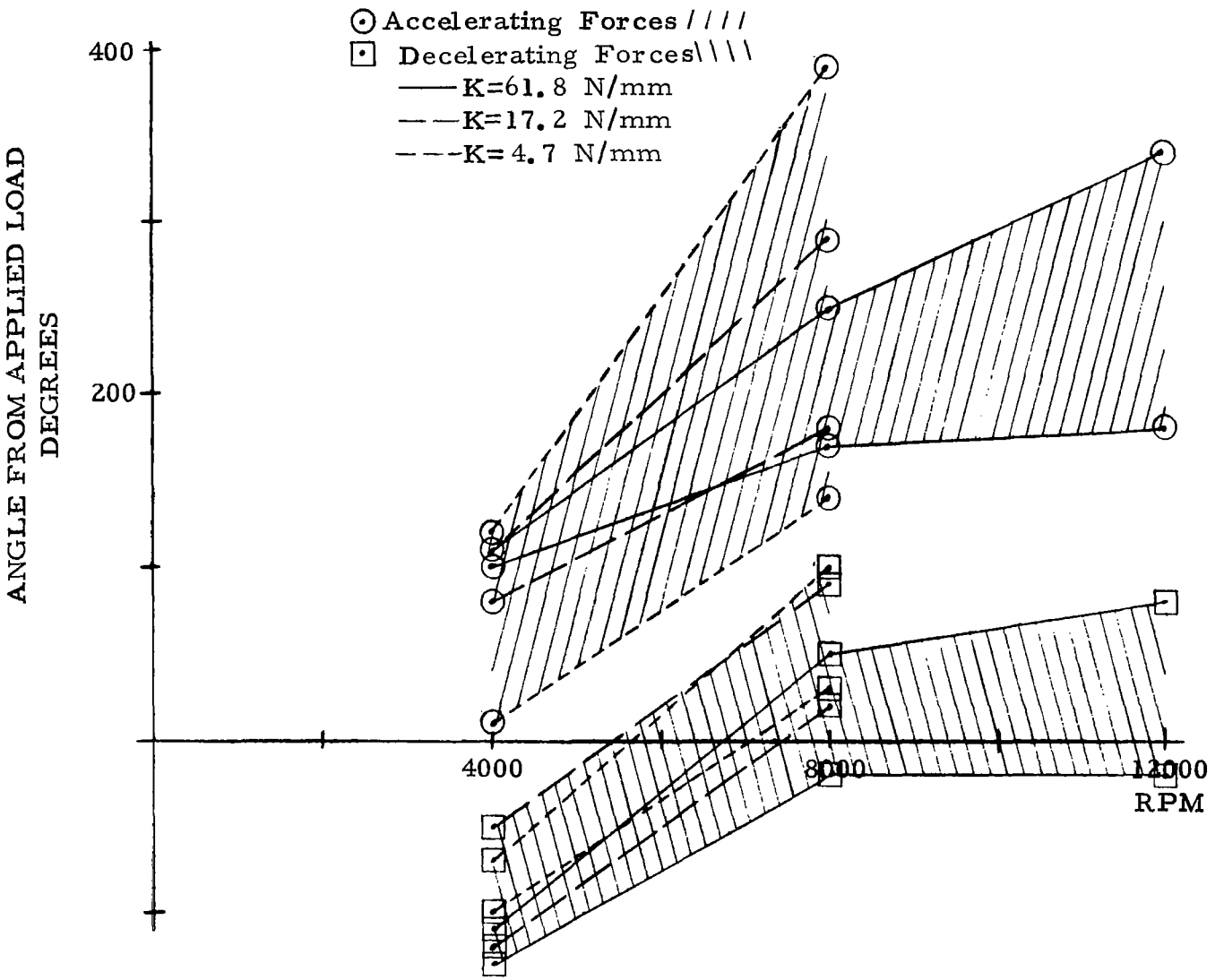

FIGURE 10d Locations of Accelerating and Deccelerating Cage Forces as a Function of Shaft Speed, 4450 N Radial Load

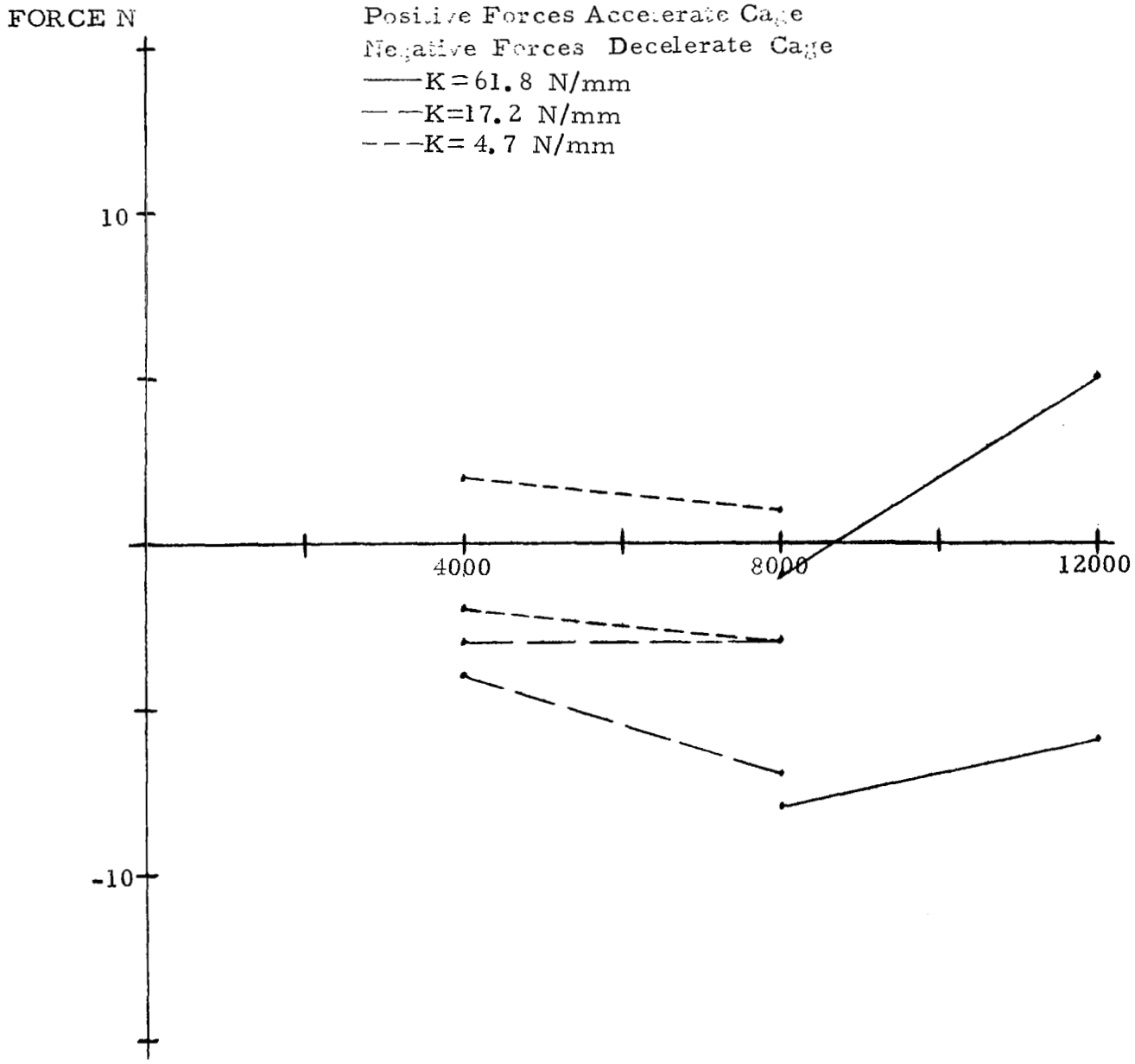

FIGURE 11a Cage Force Magnitude Range Versus Shaft Speed, 2220 N Thrust Load

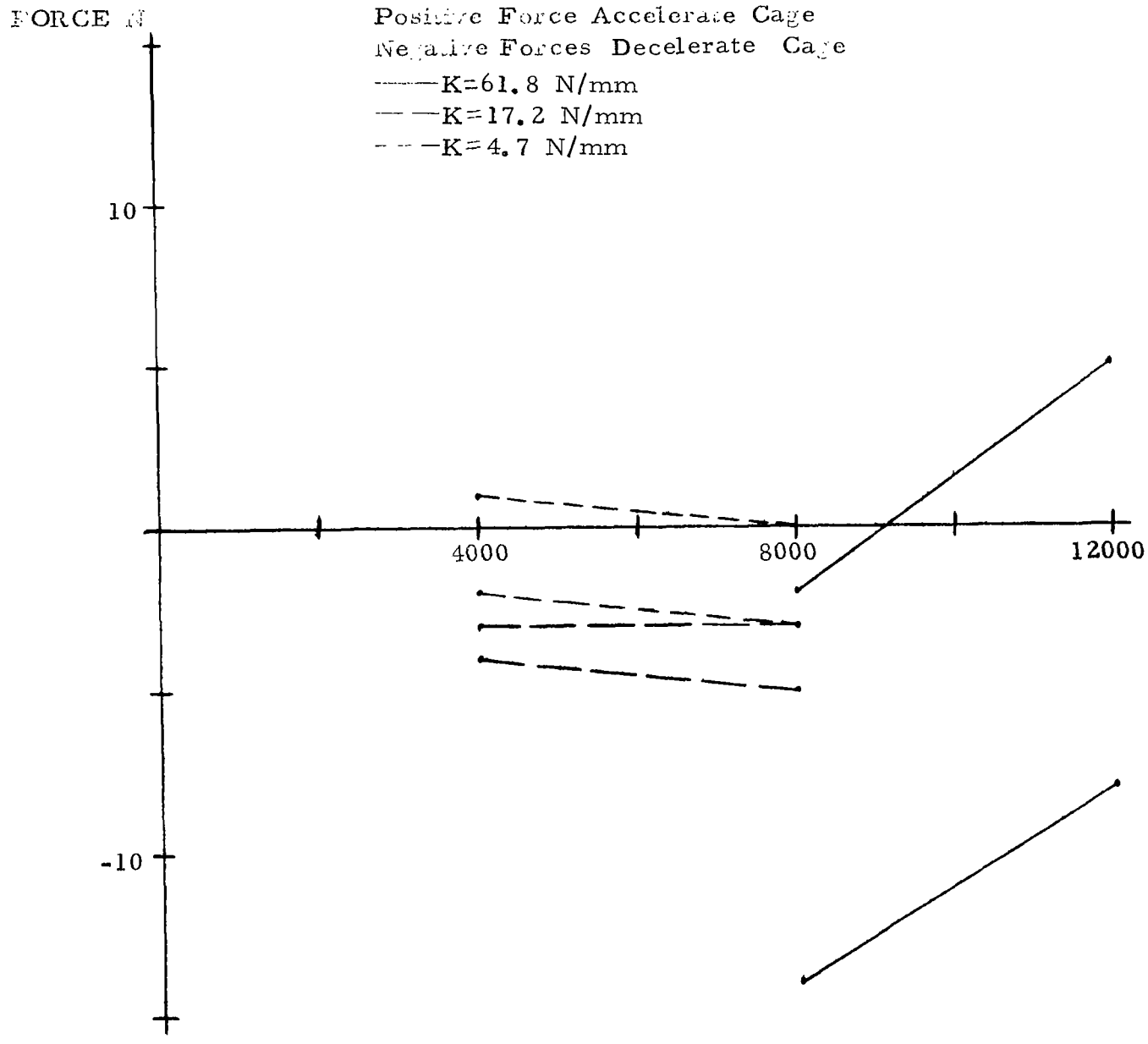

FIGURE 11b Cage Force MagnitudeRange Versus Shaft Speed, 6670 N Thrust Load

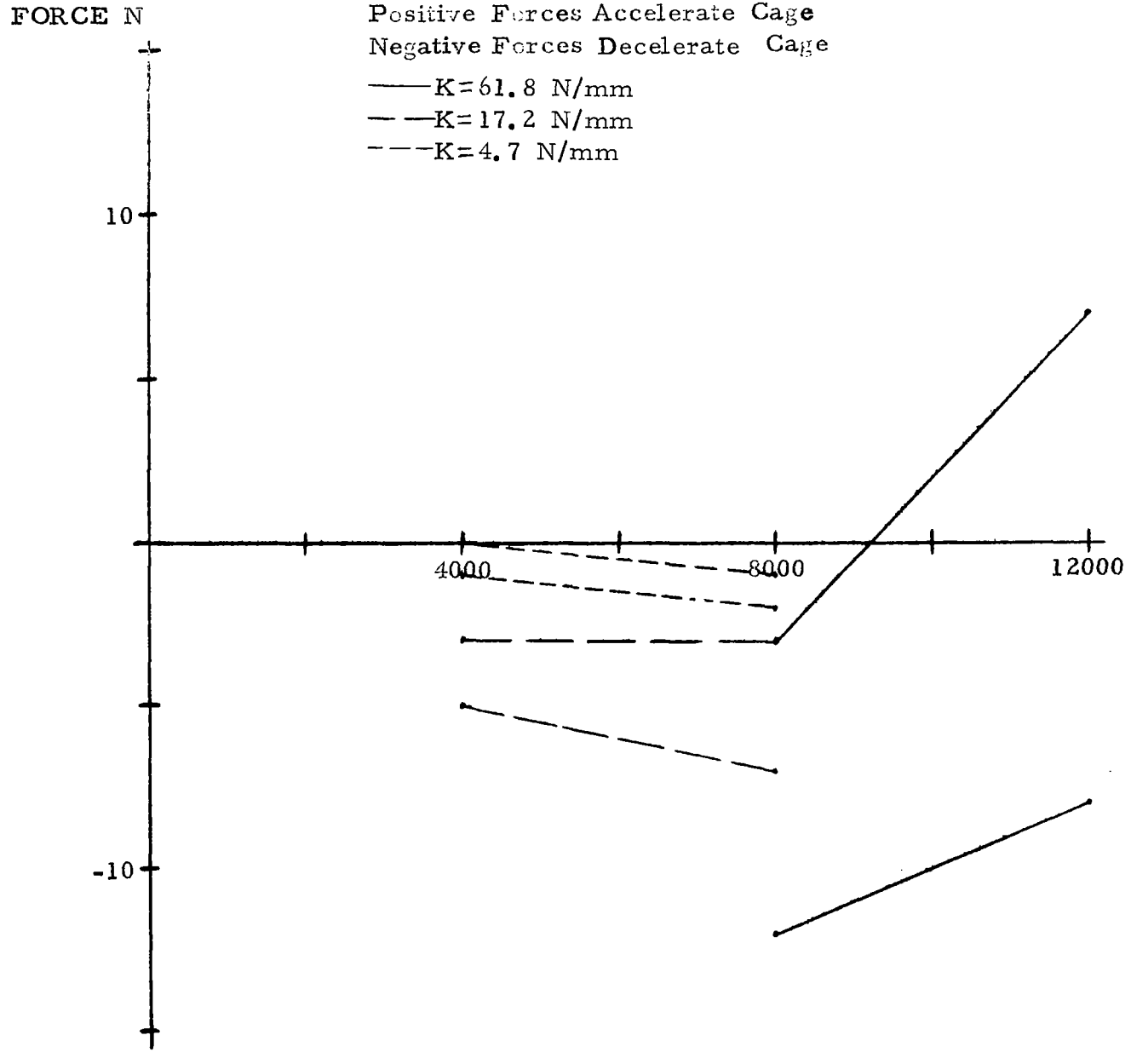

FIGURE 11c Cage Force Magnitude Range Versus Shaft Speed, 13330 N Thrust Load

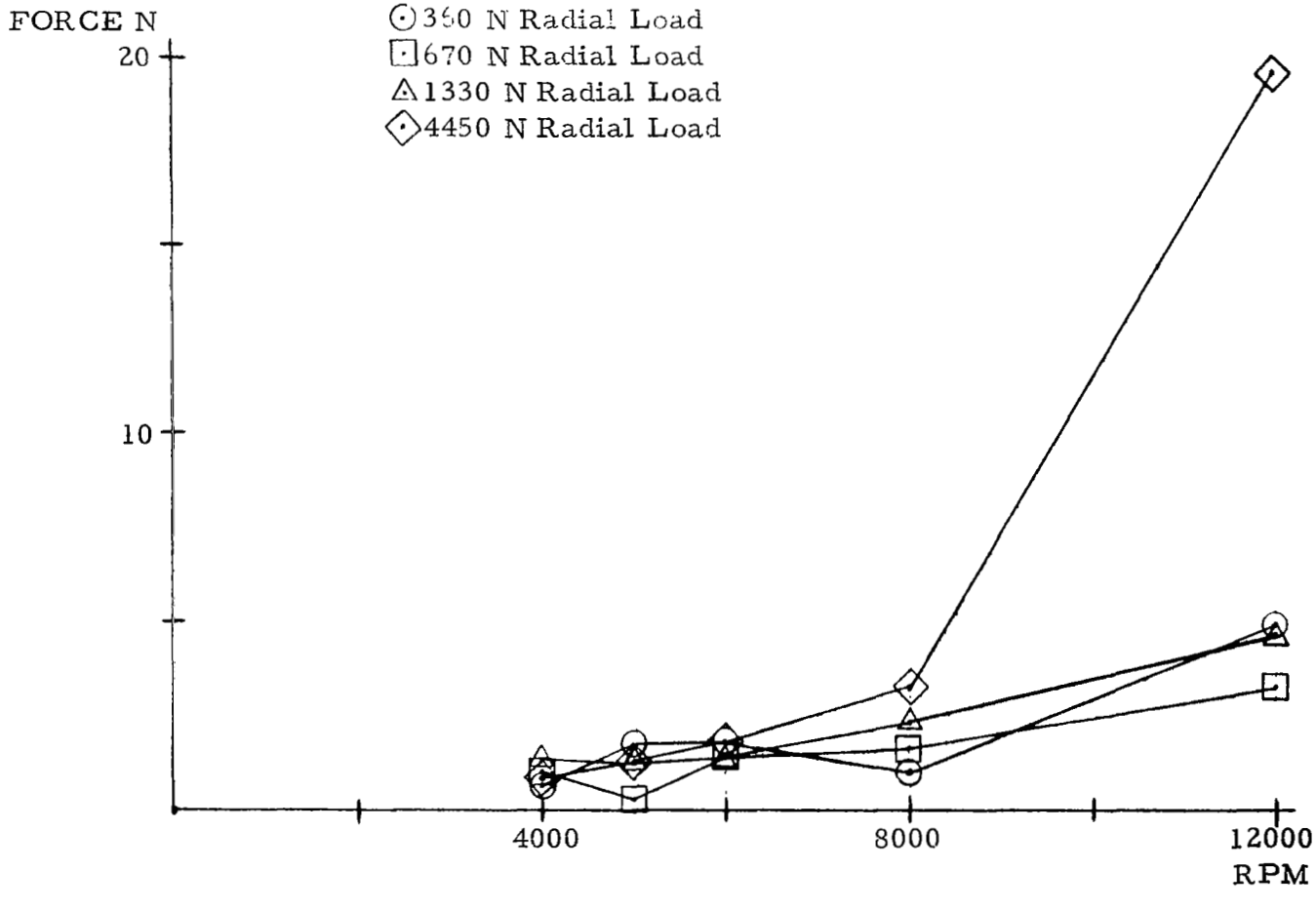

FIGURE 12a Resultant Cage Force Versus Shaft Speed

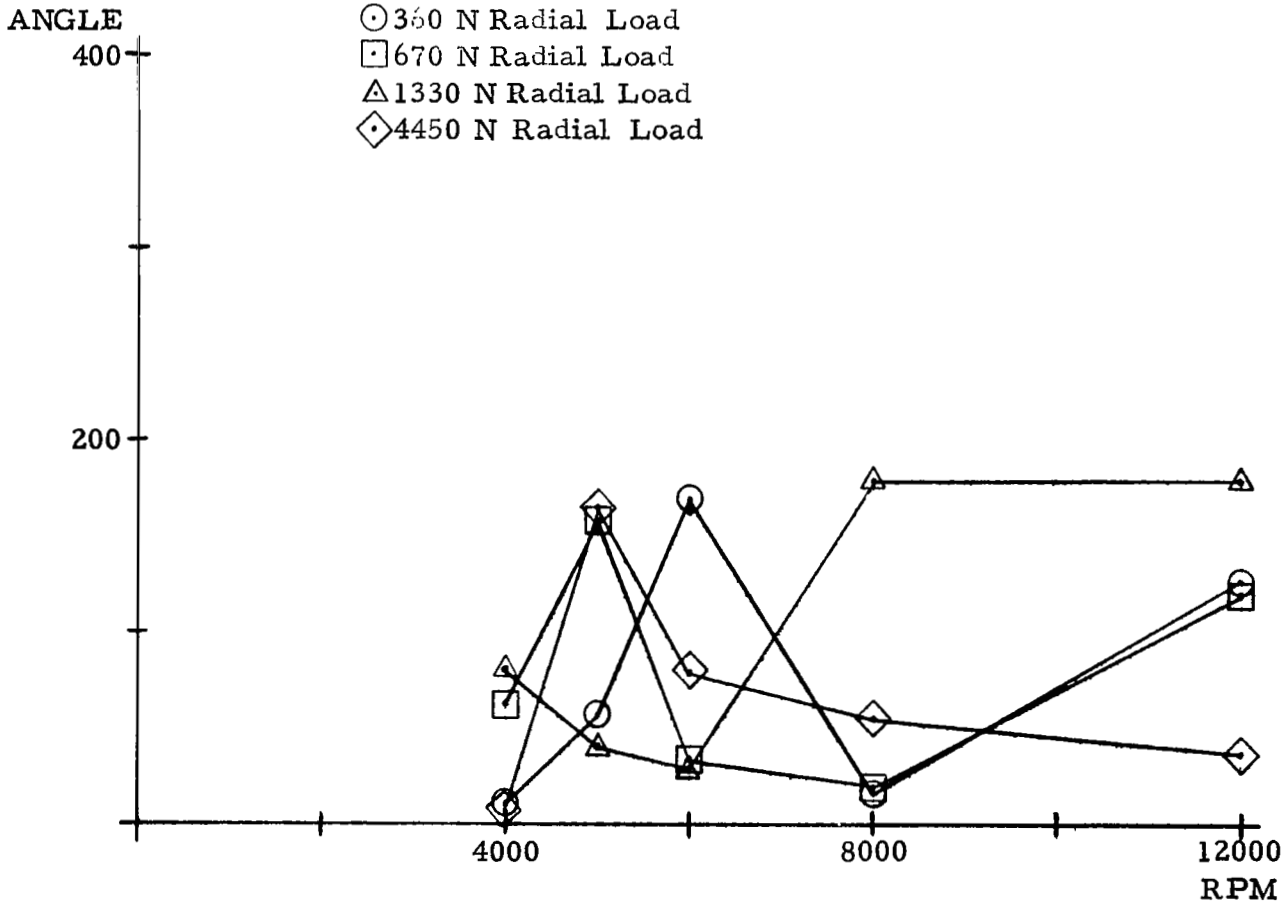

FIGURE 12b Resultant Cage Force Location Versus Shaft Speed

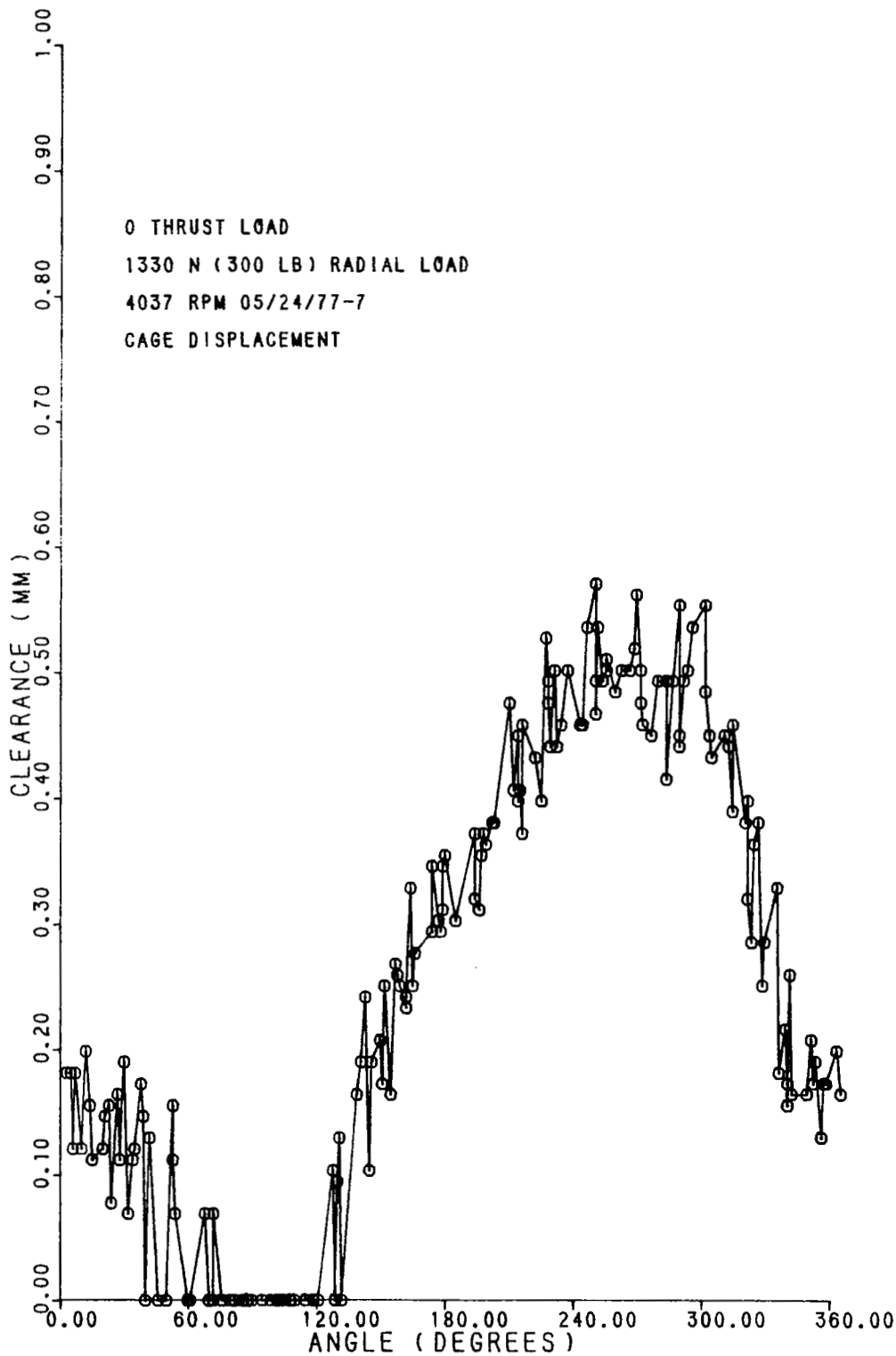
0 THRUST LOAD
1330 N (300 LB) RADIAL LOAD
4037 RPM 05/24/77-7
CAGE DISPLACEMENT
CLEARANCE (MM)
0.00
0.10
0.20
0.30
0.40
0.50
0.60
0.70
0.80
0.90
1.00
0.00
60.00
120.00
180.00
240.00
300.00
360.00
ANGLE (DEGREES)

FIG. 13a

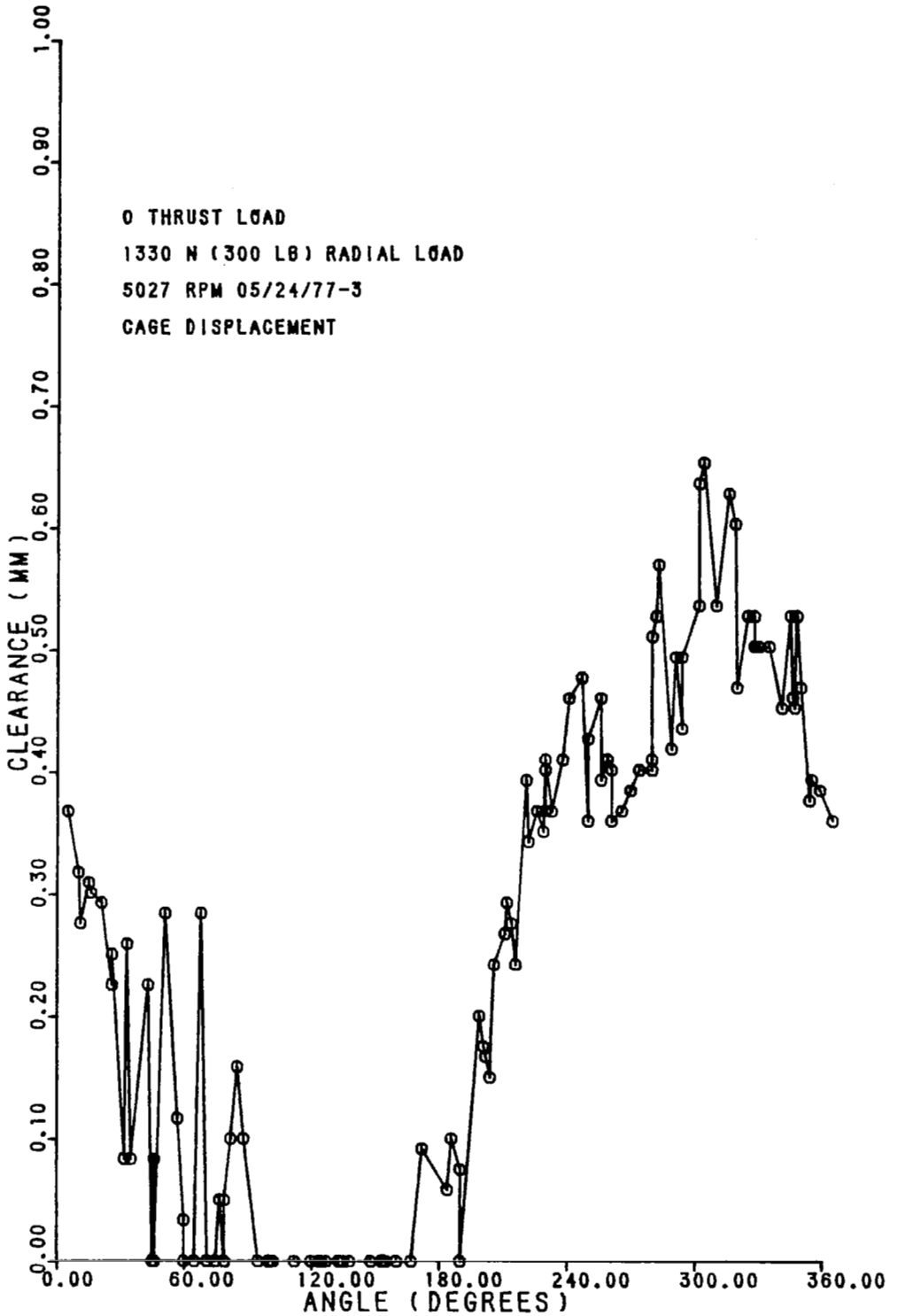
0 THRUST LOAD
1330 N (300 LB) RADIAL LOAD
5027 RPM 05/24/77-3
CAGE DISPLACEMENT
CLEARANCE (MM)
0.00
0.10
0.20
0.30
0.40
0.50
0.60
0.70
0.80
0.90
1.00
0.00
60.00
120.00
180.00
240.00
300.00
360.00
ANGLE (DEGREES)

FIG. 13b

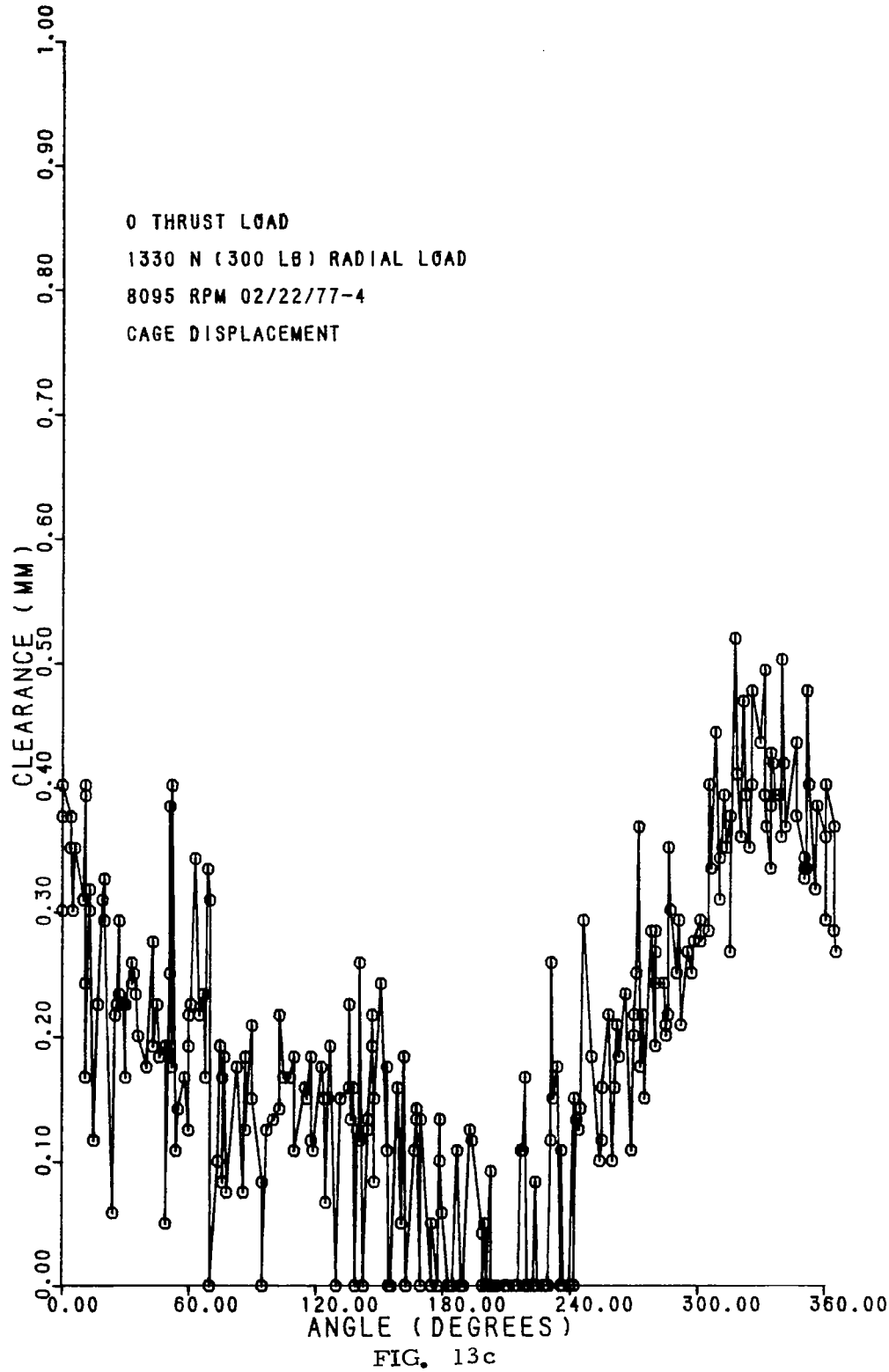
0 THRUST LOAD
1330 N (300 LB) RADIAL LOAD
8095 RPM 02/22/77-4
CAGE DISPLACEMENT
CLEARANCE (MM)
0.00
0.10
0.20
0.30
0.40
0.50
0.60
0.70
0.80
0.90
1.00
0.00
60.00
120.00
180.00
240.00
300.00
360.00
ANGLE (DEGREES)

FIG. 13c

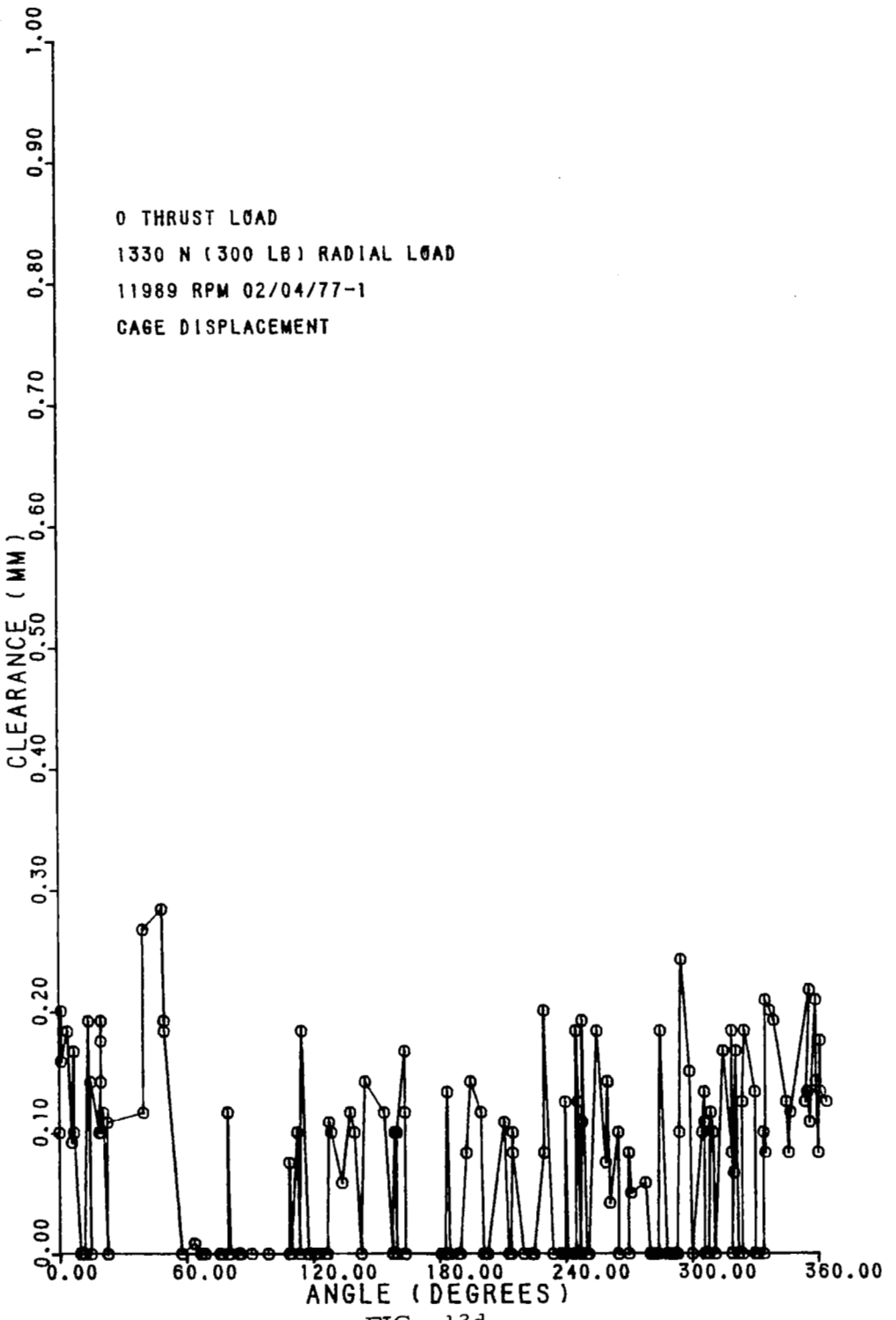
0 THRUST LOAD
1330 N (300 LB) RADIAL LOAD
11989 RPM 02/04/77-1
CAGE DISPLACEMENT
CLEARANCE (MM)
0.00
0.10
0.20
0.30
0.40
0.50
0.60
0.70
0.80
0.90
1.00
0.00
60.00
120.00
180.00
240.00
300.00
360.00
ANGLE (DEGREES)

FIG. 13d

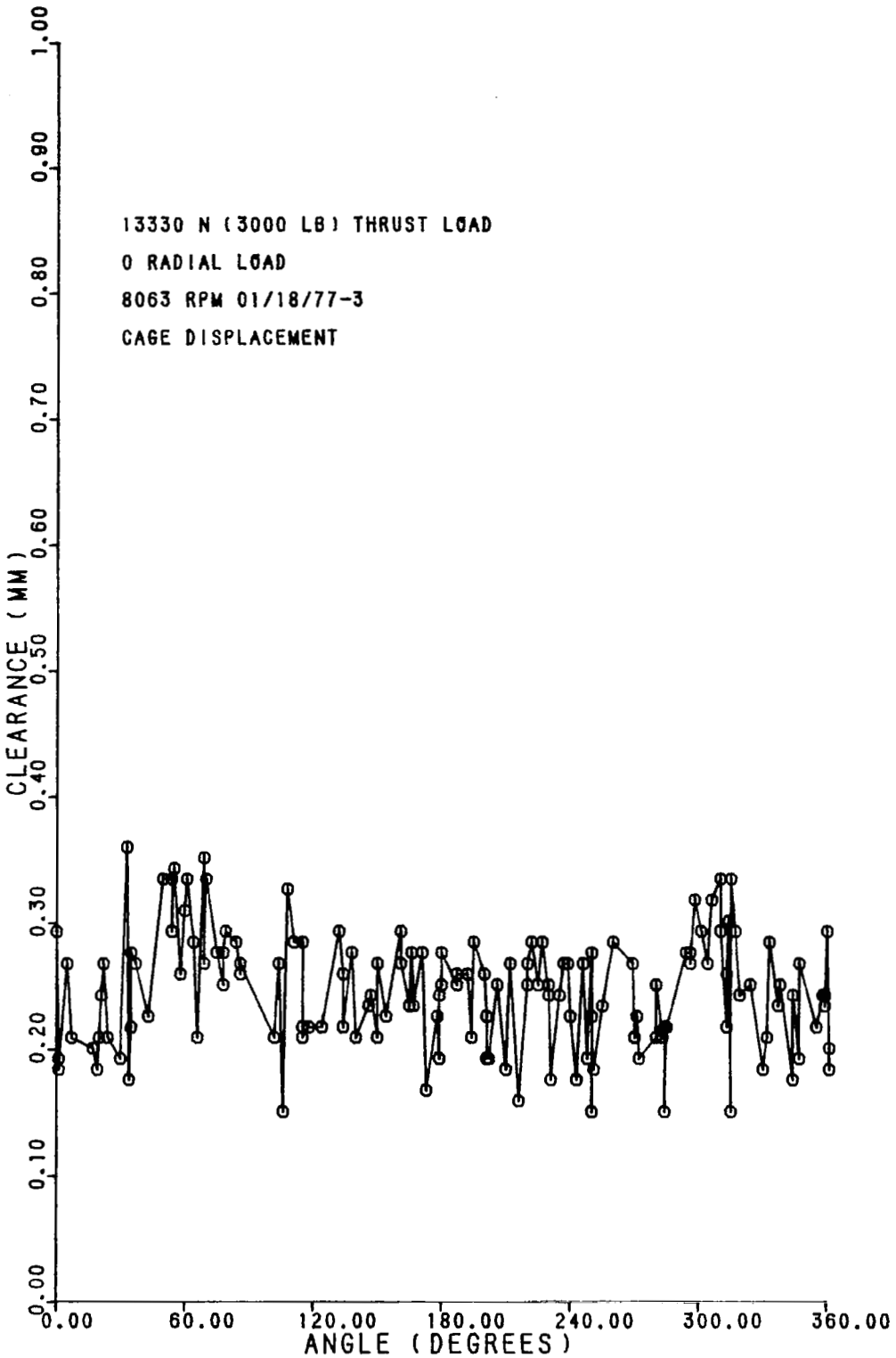
13330 N (3000 LB) THRUST LOAD
0 RADIAL LOAD
8063 RPM 01/18/77-3
CAGE DISPLACEMENT
CLEARANCE (MM)
0.00
0.10
0.20
0.30
0.40
0.50
0.60
0.70
0.80
0.90
1.00
0.00
60.00
120.00
180.00
240.00
300.00
360.00
ANGLE (DEGREES)

FIG. 13e

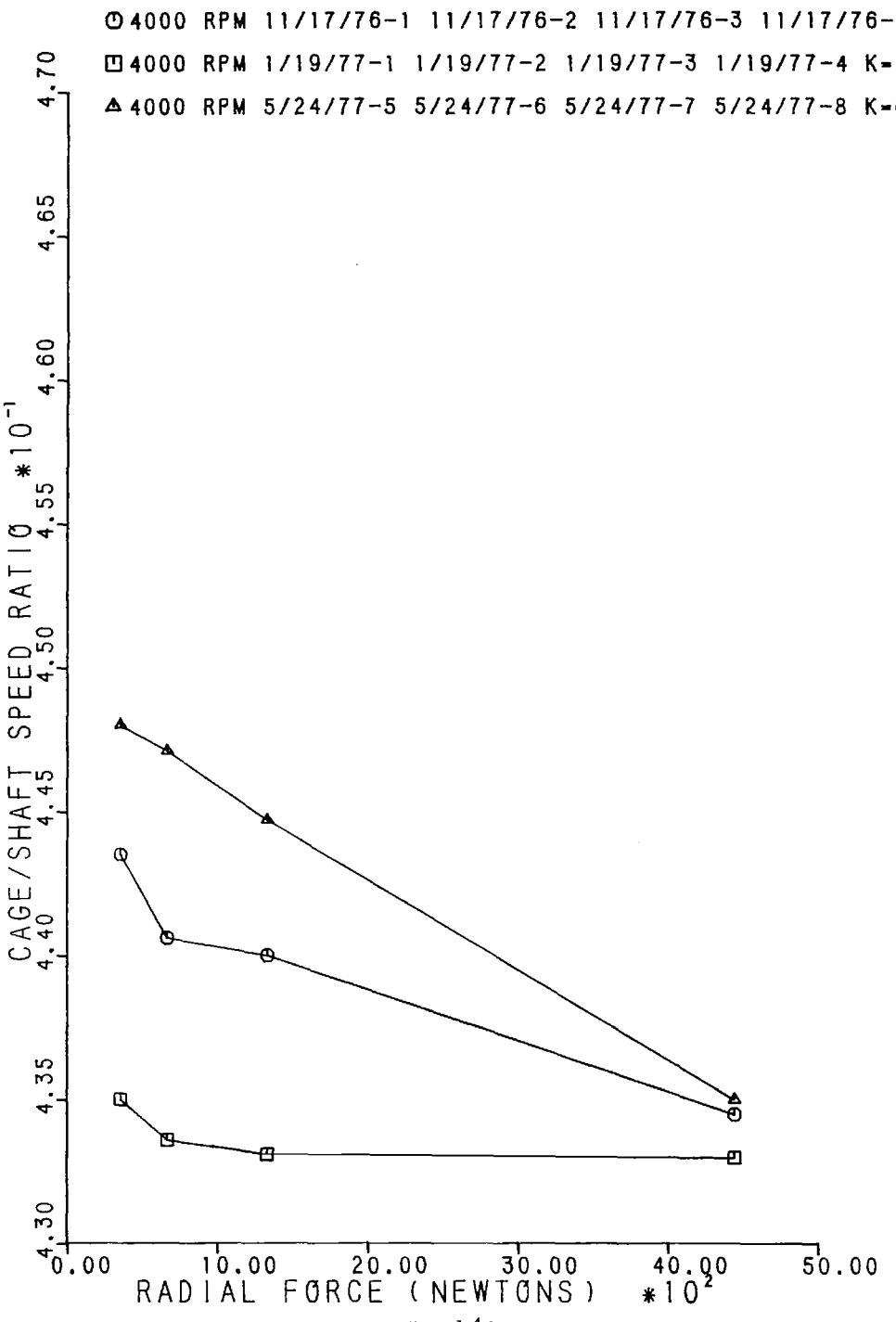
4000 RPM 11/17/76-1 11/17/76-2 11/17/76-3 11/17/76-4 K=4.7 N/MM
4000 RPM 1/19/77-1 1/19/77-2 1/19/77-3 1/19/77-4 K=17.2 N/MM
4000 RPM 5/24/77-5 5/24/77-6 5/24/77-7 5/24/77-8 K=61.8 N/MM
CAGE/SHAFT SPEED RATIO *10⁻¹
4.70
4.65
4.60
4.55
4.50
4.45
4.40
4.35
4.30
0.00
10.00
20.00
30.00
40.00
50.00
RADIAL FORCE (NEWTONS) *10²

FIG. 14a

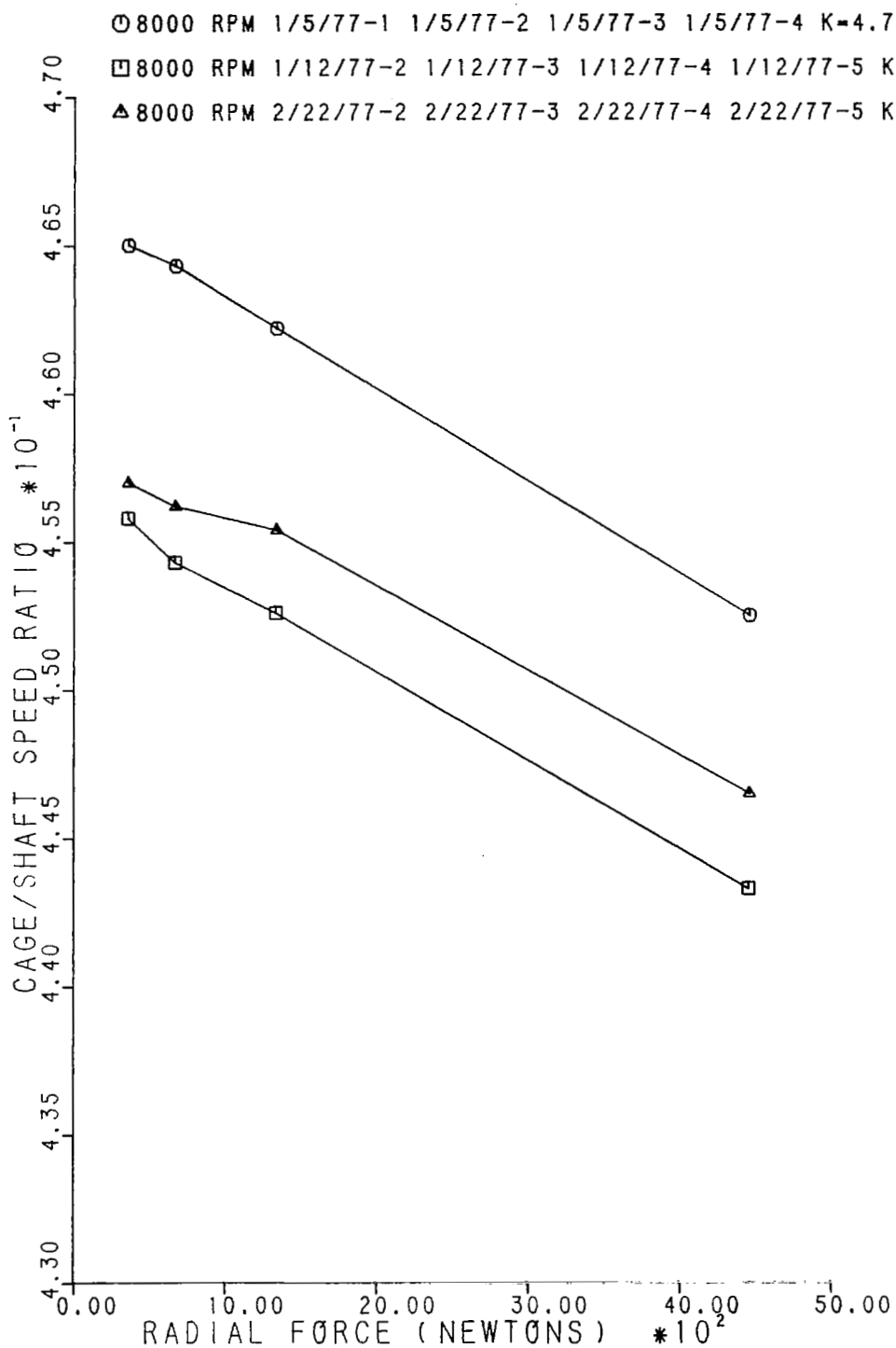
8000 RPM 1/5/77-1 1/5/77-2 1/5/77-3 1/5/77-4 K=4.7 N/MM
8000 RPM 1/12/77-2 1/12/77-3 1/12/77-4 1/12/77-5 K=17.2 N/MM
8000 RPM 2/22/77-2 2/22/77-3 2/22/77-4 2/22/77-5 K=61.8 N/MM
CAGE/SHAFT SPEED RATIO *10⁻¹
4.70
4.65
4.60
4.55
4.50
4.45
4.40
4.35
4.30
0.00
10.00
20.00
30.00
40.00
50.00
RADIAL FORCE (NEWTONS) *10²

FIG. 14b

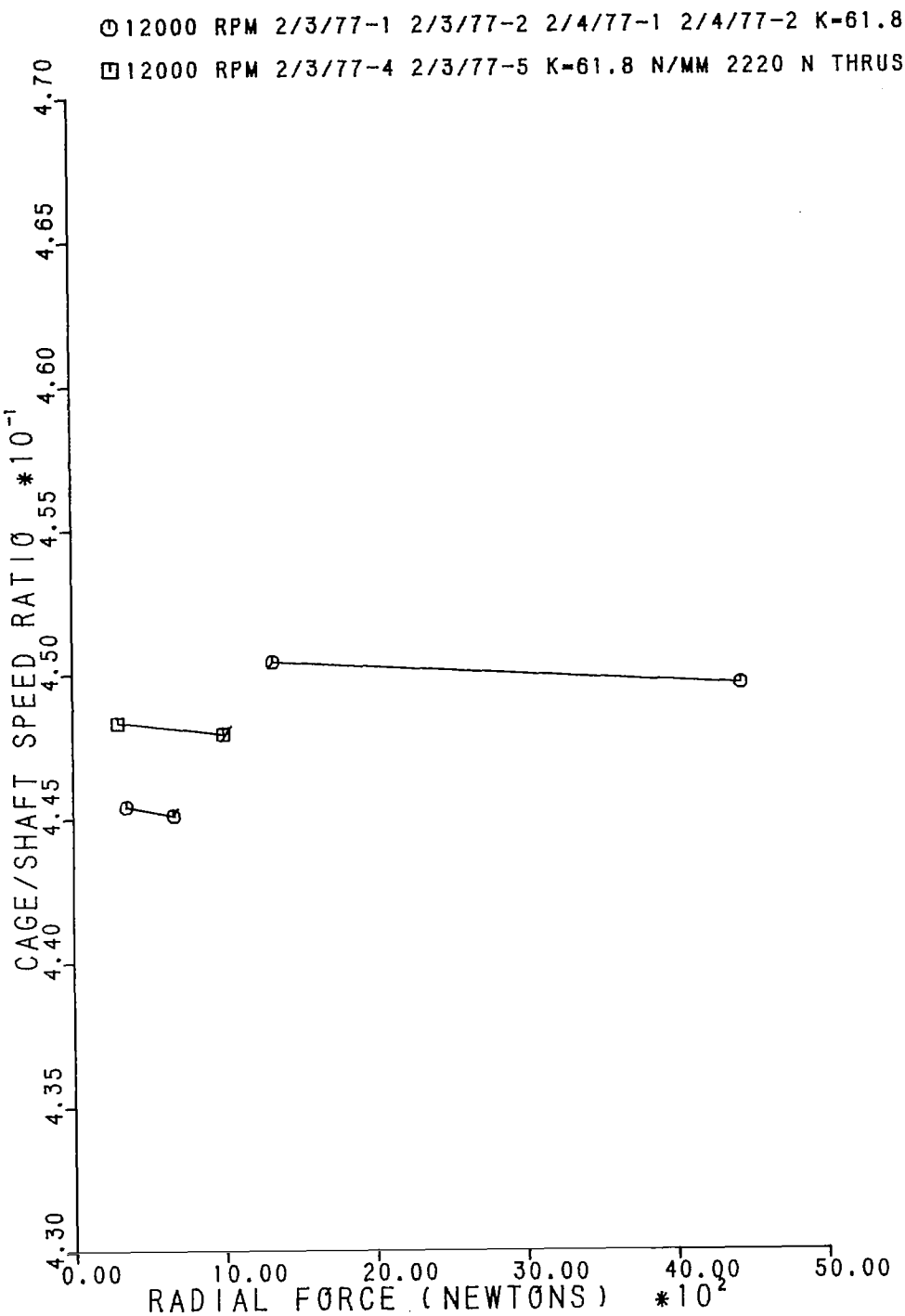
12000 RPM 2/3/77-1 2/3/77-2 2/4/77-1 2/4/77-2 K=61.8 N/MM
12000 RPM 2/3/77-4 2/3/77-5 K=61.8 N/MM 2220 N THRUST LOAD
CAGE/SHAFT SPEED RATIO *10^-1
4.70
4.65
4.60
4.55
4.50
4.45
4.40
4.35
4.30
0.00
10.00
20.00
30.00
40.00
50.00
RADIAL FORCE (NEWTONS) *10^2

FIG. 14c

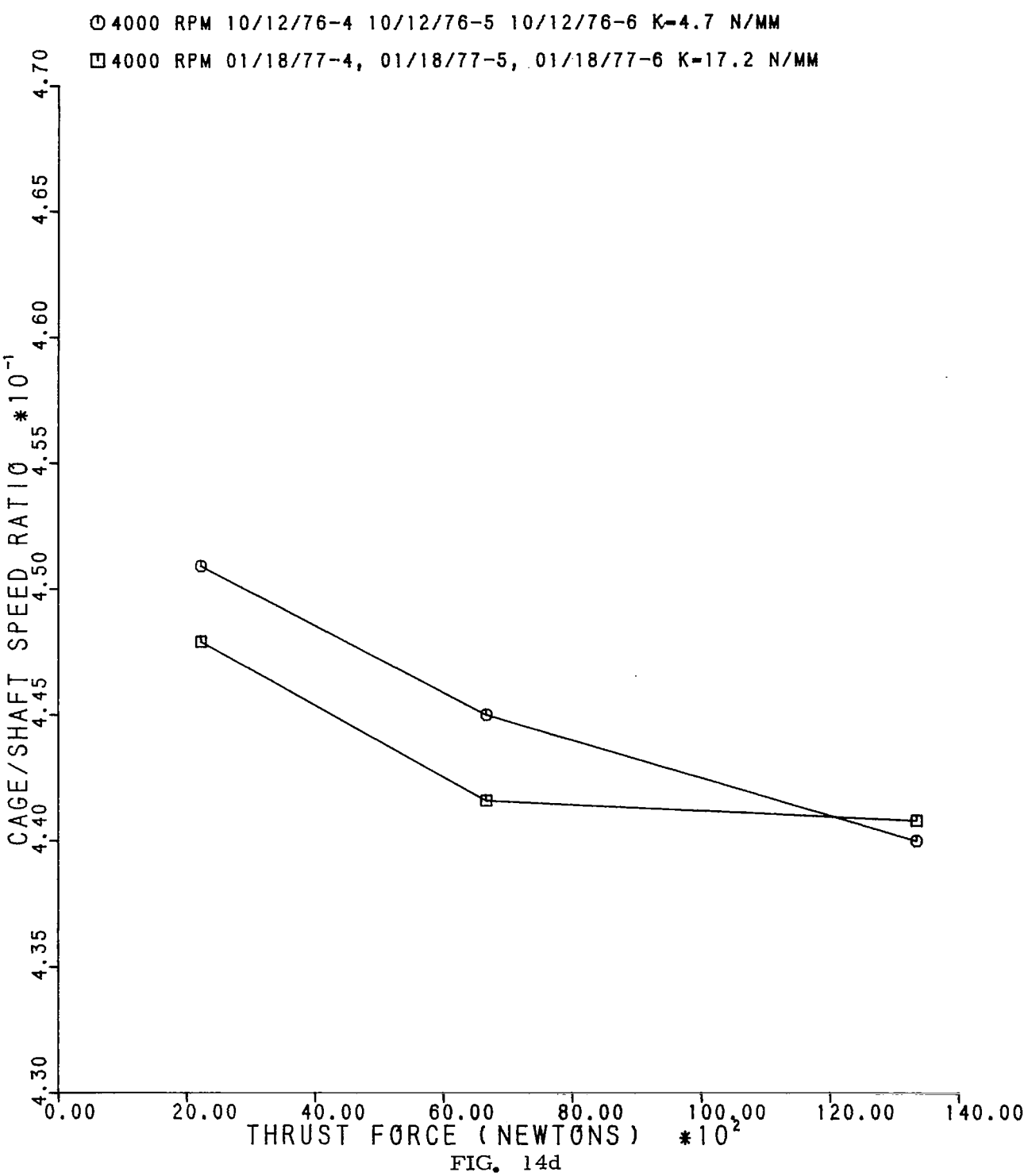
⊙4000 RPM 10/12/76-4 10/12/76-5 10/12/76-6 K=4.7 N/MM
⊡4000 RPM 01/18/77-4, 01/18/77-5, 01/18/77-6 K=17.2 N/MM
CAGE/SHAFT SPEED RATIO *10⁻¹
4.70
4.65
4.60
4.55
4.50
4.45
4.40
4.35
4.30
0.00
20.00
40.00
60.00
80.00
100.00
120.00
140.00
THRUST FORCE (NEWTONS) *10²
FIG. 14d

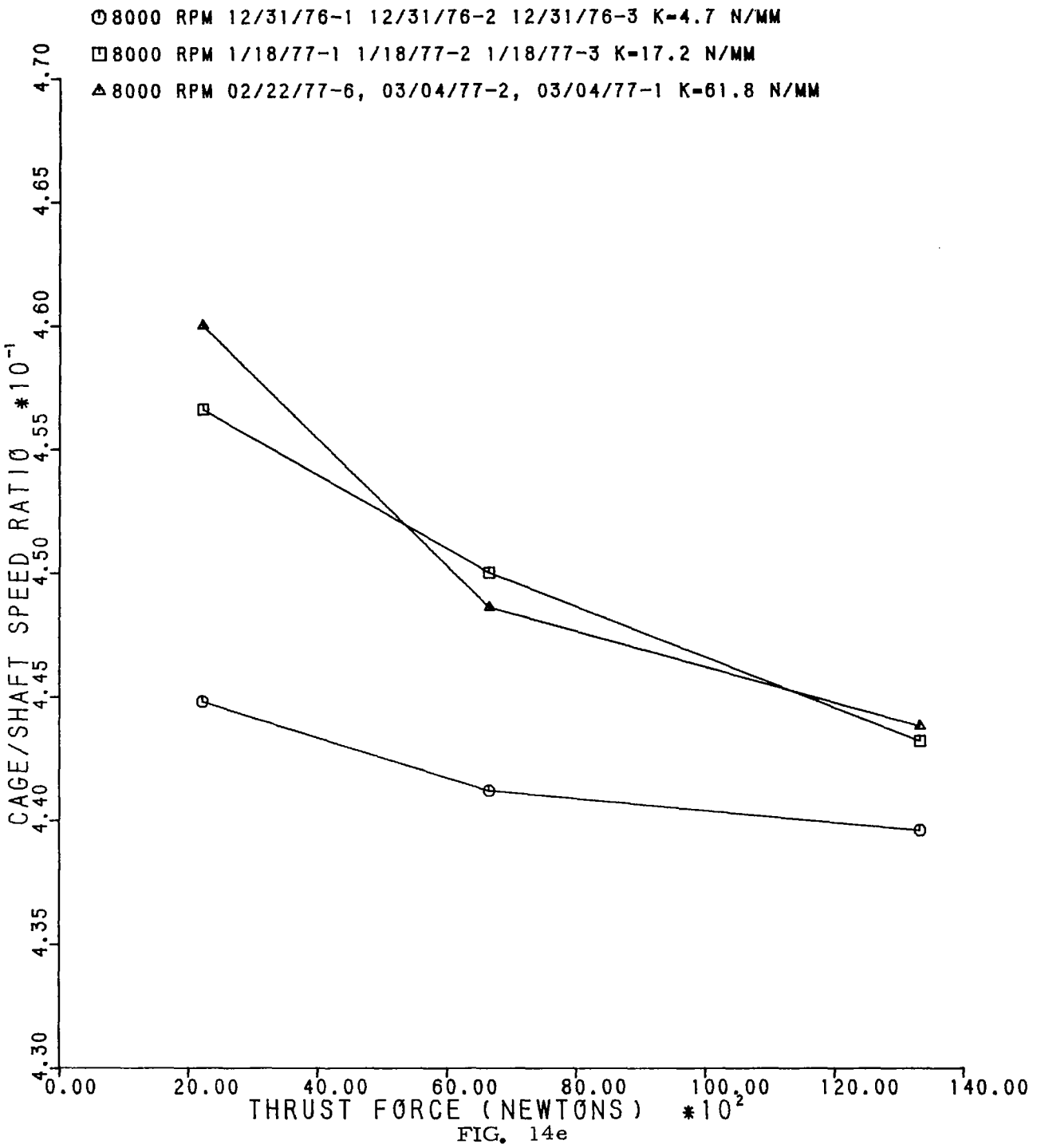
8000 RPM 12/31/76-1 12/31/76-2 12/31/76-3 K=4.7 N/MM
8000 RPM 1/18/77-1 1/18/77-2 1/18/77-3 K=17.2 N/MM
8000 RPM 02/22/77-6, 03/04/77-2, 03/04/77-1 K=61.8 N/MM
CAGE/SHAFT SPEED RATIO *10^-1
4.70
4.65
4.60
4.55
4.50
4.45
4.40
4.35
4.30
0.00
20.00
40.00
60.00
80.00
100.00
120.00
140.00
THRUST FORCE (NEWTONS) *10^2
FIG. 14e

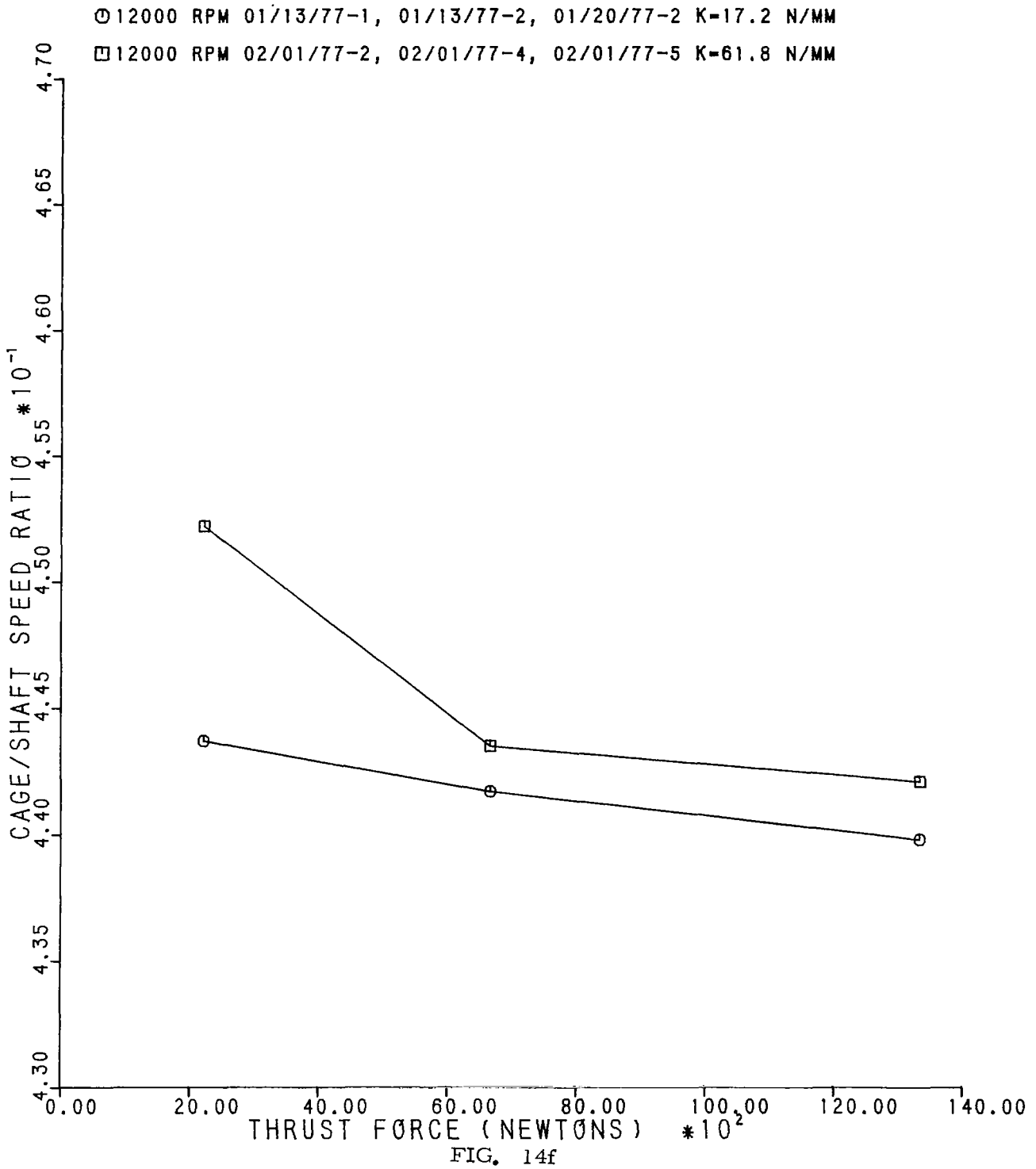
⊙12000 RPM 01/13/77-1, 01/13/77-2, 01/20/77-2 K=17.2 N/MM
⊡12000 RPM 02/01/77-2, 02/01/77-4, 02/01/77-5 K=61.8 N/MM
CAGE/SHAFT SPEED RATIO *10⁻¹
4.70
4.65
4.60
4.55
4.50
4.45
4.40
4.35
4.30
0.00
20.00
40.00
60.00
80.00
100.00
120.00
140.00
THRUST FORCE (NEWTONS) *10²

FIG. 14f

Table 1

Test Bearing Specifications

	P/N 506110	P/N 506111
Raceway Curvatures	52% Inner and Outer	52% Inner and Outer
Bearing Contact Angle	24°-27°**	24°-27°**
Bearing Mat'l, Races, Balls	CEVM-M-50-(R_c60 min)	CEVM-M-50 (R_c60 min)
Cage Mat'l	AMS-6415 (R_c 28-33)	AMS-6415 (R_c 28-33)
Cage Plating	Silver Plate Per AMS 2412	Silver Plate Per AMS 2412
Cage Plating Thickness, inches	.001-.002	.001-.002
Ball & Ring Stabilization Temp.	600°F	600°F
Balls		
Number	20	20
Nominal Dia.,inches	0.750	0.750
Allowable Variation in Any Indiv. Ball Dia. & Sphericity, inches	0.000020 max.	0.000020 max.
Internal Radial Clearance*	.0048-.0060***	.0054-.0060 ***
Axial Play inches	.026 max.****	.024 max ****
Diametral Cage Clearance, in.	.016-.026	.019-.025
Bearing Inner Dia., inches	4.33070-4.33045	4.33070-4.33045
Bearing Outer Dia., inches	6.8898-6.8894	6.8898-6.8894
Inner Race Land Dia., inches	5.343 min.	5.334 min.
Outer Race Shoulder Dia., inches	6.077 max.	6.090 max.
Ball Pitch Dia., in.	5.650	5.635
Bearing Width	1.1811-1.1761	1.1811-1.1761

*Same as Total Diametral Clearance
**Measured Under 60 lb Thrust Load
***Measured Under 33 lb Radial Load
****Measured Under 22 lb Thrust Load

Table 2

SPEED, LOAD, AND SPRING CONSTANTS

Figure 6
4000 RPM Nominal Shaft Speed

Figure	Spring Constant N/mm	Load N	Load (Lb)
6a	4.73	360	80 Radial
6a	17.2	360	80 Radial
6a	61.8	360	80 Radial
6b	4.73	667	150 Radial
6b	17.2	667	150 Radial
6b	61.8	667	150 Radial
6c	4.73	1330	300 Radial
6c	17.2	1330	300 Radial
6c	61.8	1330	300 Radial
6d	4.73	4450	1000 Radial
6d	17.2	4450	1000 Radial
6d	61.8	4450	1000 Radial
6e	4.73	2220	500 Thrust
6e	17.2	2220	500 Thrust
-	-	-	-
6f	4.73	6670	1500 Thrust
6f	17.2	6670	1500 Thrust
-	-	-	-
6g	4.73	13350	3000 Thrust
6g	17.2	13350	3000 Thrust
-	-	-	-

Figure 7
8000 RPM Nominal Shaft Speed

Figure	Spring Constant N/mm	Load N	Load (Lb)
7a	4.73	360	80 Radial
7a	17.2	360	80 Radial
7a	61.8	360	80 Radial
7b	4.73	667	150 Radial
7b	17.2	667	150 Radial
7b	61.8	667	150 Radial
7c	4.73	1330	300 Radial
7c	17.2	1330	300 Radial
7c	61.8	1330	300 Radial
7d	4.73	4450	1000 Radial
7d	17.2	4450	1000 Radial
7d	61.8	4450	1000 Radial
7e	4.73	2220	500 Thrust
7e	17.2	2220	500 Thrust
7e	61.8	2220	500 Thrust
7f	4.73	6670	1500 Thrust
7f	17.2	6670	1500 Thrust
7f	61.8	6670	1500 Thrust
7g	4.73	13350	3000 Thrust
7g	17.2	13350	3000 Thrust
7g	61.8	13350	3000 Thrust

Figure 8
12000 RPM Nominal Shaft Speed

Figure	Spring Constant N/mm	Load N	Load (Lb)
-	-	-	-
-	-	-	-
8a	61.8	360	80 Radial
-	-	-	-
-	-	-	-
8b	61.8	667	150 Radial
-	-	-	-
-	-	-	-
8c	61.8	1330	300 Radial
8c	61.8-2	1330	300+2220N(500lb)
-	-	-	- (Thrust)
8d	61.8	4450	1000 Radial
8d	61.8-2	4450	1000+2220N(500lb)
-	-	-	- (Thrust)
8e	61.8	2220	500 Thrust
-	-	-	-
-	-	-	-
8f	61.8	6670	1500 Thrust
-	-	-	-
-	-	-	-
8g	61.8	13350	3000 Thrust

Table 3

SPRING CONSTANTS AND BEARINGS USED

Date Installed in Machine	Spring Constant N/mm	Spring Constant Lb/in	Bearing
June 1976	1.49	8.51	PWA 506110
August 18, 1976	4.73	27.0	PWA 506111
Jan. 12, 1977	17.2	98.2	PWA 506110
Jan. 28, 1977	61.8	353.0	PWA 506110

Table 4

CALCULATED NUMBER OF SHAFT REVOLUTIONS BETWEEN PHOTOGRAPHS

$\Delta\theta_o$ rev	$W_s=(\Delta\theta_o)\frac{16 \times 60}{.441}$	$\Delta\theta_s$ rev	$W_s=(\Delta\theta_s)\frac{16 \times 60}{(-.559)}$
0 to 1	0 to 2,177 rpm	0 to -1	0 to 1,717 rpm
1 to 2	2,177 to 4,354	-1 to -2	1,717 to 3,435
2 to 3	4,354 to 6,531	-2 to -3	3,435 to 5,152
3 to 4	6,531 to 8,707	-3 to -4	5,152 to 6,869
4 to 5	8,707 to 10,884	-5 to -6	6,869 to 8,587
5 to 6	10,884 to 13,061	-6 to -7	8,587 to 10,304
		-7 to -8	10,304 to 12,021

*For a cage to shaft speed ratio of 0.441

Table 5

Force Ranges Measured

Speed RPM	Thrust Load N	Radial Load N	Spring Constant N/mm	Force and Range Max to Min N
4011	0	360	4.73	2 to -2
4068	0	360	17.2	7 to -10
4028	0	360	61.8	8 to -8
4017	0	670	4.73	2.5 to -2.5
4070	0	670	17.2	7 to -11
4037	0	670	61.8	10 to -9
4018	0	1330	4.73	2 to -2
4069	0	1330	17.2	5 to -12
4036	0	1330	61.8	10 to -9
4018	0	4450	4.73	2 to -2
4066	0	4450	17.2	2 to -11
4037	0	4450	61.8	5 to -10
4034	2220	0	4.73	1 to -3.5
3987	2220	0	17.2	-2 to -6
4041	6670	0	4.73	1 to -2
3987	6670	0	17.2	-2 to -4.5
4040	13350	0	4.75	1 to -1
3977	13340	0	17.2	-2 to -5
8095	0	360	4.73	5 to -4
8082	0	360	17.2	11 to -10
8090	0	360	61.8	14 to -11
8099	0	670	4.73	5 to -4
8089	0	670	17.2	12 to -13
8094	0	670	61.8	20 to -18
8097	0	1330	4.73	6 to -5
8087	0	1330	17.7	12 to -11
8095	0	1330	61.8	15 to -11
8084	0	4450	4.73	6 to -5
8078	0	4450	17.2	11 to -10
8085	0	4450	61.8	11 to 1-4
8000	2225	0	4.73	1 to -3
8063	2220	0	17.2	0 to -7
8070	2220	0	61.8	3 to -12
8000	6675	0	4.73	1 to -3
8063	6670	0	17.2	-2 to -7
8035	6670	0	61.8	2 to -17
8000	13350	0	4.73	-.5 to -2
8063	13330	0	17.2	-1 to -8
8023	13330	0	61.8	-1 to -12

Appendix I - Computer Program

```
      DIMENSION R(300,4),ANGLE(300),FORCE(300),ANGL(300)
      DIMENSION XLB(40),YLB(40)
      DIMENSION LINE1(8),LINE2(8),LINE3(6),LINE4(8)
      DIMENSION LINE5(4)
      INTEGER R,ANGLE
      ICN=0
      IC=0
      READ (5,30) S,AK,N
   30 FORMAT(2F10.0,I2)
      WRITE(6,31)S,AK
   31 FORMAT(1H1,8HNOTCH = ,F6.0,7H  AK = ,F6.4)
      WRITE(6,23)
   23 FORMAT(5X,110HZR1         ZR2         ZR3         ZR4       ZR2-ZR1    ZR
     1-ZR1    ZR4-ZR1    ZR3-ZR2    ZR4-ZR3    ZR4-ZR2
      ZUR1=0.
      ZUR2=0.
      ZUR3=0.
      ZUR4=0.
      ZU1=0.
      ZU2=0.
      ZU3=0.
      ZU4=0.
      ZU5=0.
      ZU6=0.
      DO 21 I=1,N
      READ(5,11)ZR1,ZR2,ZR3,ZR4
   11 FORMAT(4F10.0)
      Z1=ZR2-ZR1
      Z2=ZR3-ZR1
      Z3=ZR4-ZR1
      Z4=ZR3-ZR2
      Z5=ZR4-ZR3
      Z6=ZR4-ZR2
      WRITE(6,24)ZR1,ZR2,ZR3,ZR4,Z1,Z2,Z3,Z4,Z5,Z6
   24 FORMAT(11F10.0)
      ZUR1=ZUR1+ZR1
      ZUR2=ZUR2+ZR2
      ZUR3=ZUR3+ZR3
      ZUR4=ZUR4+ZR4
      ZU1=ZU1+Z1
      ZU2=ZU2+Z2
      ZU3=ZU3+Z3
      ZU4=ZU4+Z4
      ZU5=ZU5+Z5
      ZU6=ZU6+Z6
   21 CONTINUE
      AZR1=ZUR1/FLOAT(N)
      AZR2=ZUR2/FLOAT(N)
      AZR3=ZUR3/FLOAT(N)
      AZR4=ZUR4/FLOAT(N)
      AZ1=ZU1/FLOAT(N)
      AZ2=ZU2/FLOAT(N)
      AZ3=ZU3/FLOAT(N)
      AZ4=ZU4/FLOAT(N)
      AZ5=ZU5/FLOAT(N)
      AZ6=ZU6/FLOAT(N)
      F1=S/AZ3
      SCZ1=AZ1*F1
      SCZ2=AZ2*F1
      SCZ3=AZ3*F1
      SCZ4=AZ4*F1
      SCZ5=AZ5*F1
      SCZ6=AZ6*F1
      WRITE(6,25)AZR1,AZR2,AZR3,AZR4,AZ1,AZ2,AZ3,AZ4,AZ5,AZ6
   25 FORMAT(1H0,11F10.3)
      WRITE(6,32)F1,AZ3
   32 FORMAT(1H0,9HFACTOR = ,F10.4,5X,8HNOTCH =  ,F6.0)
      WRITE(6,25)SCZ1,SCZ2,SCZ3,SCZ4,SCZ5,SCZ6
      READ(5,33)LINE3,LINE1,LINE5
   33 FORMAT(6A4,6A4,4A4)
      READ(5,34)LINE2,LINE4
   34 FORMAT(8A4,8A4)
      WRITE(6,33)LINE3,LINE1
      WRITE(6,34)LINE2,LINE4
      WRITE(6,33)LINE5
      WRITE(6,26)
```

```
      26 FORMAT(1H0,*     R1          R2          R3          R4       R2-R1    R3-R1    R4-
     1R1     R3-R2   R4-R3    R4-R2   ANGLE   D3-Z3     D4-Z4*)
         SUD3=0.
         SUD4=0.
 1001    IC=IC+1
         READ(5,90)R(IC,1),R(IC,2),R(IC,3),R(IC,4),ANGLE(IC)
      90 FORMAT(2X,I4,6X,I4,6X,I4,6X,I4,6X,I3 )
      10 FORMAT(5F10.0)
         IF(IFEOF(5).EQ.-1) GO TO 50
         ANGL(IC)=ANGLE(IC)
         D1=R(IC,2)-R(IC,1)
         D2=R(IC,3)-R(IC,1)
         D3=R(IC,4)-R(IC,1)
         D4=R(IC,3)-R(IC,2)
         D5=R(IC,4)-R(IC,3)
         D6=R(IC,4)-R(IC,2)
         D7=D3-AZ3
         D8=D4-AZ4
         SUD3=SUD3+D3
         SUD4=SUD4+D4
      27 FORMAT(1H ,10F9.0,F5.0,2F8.0)
         GO TO 1001
      50 CONTINUE
         ID=IC-1
         AD3=SUD3/FLOAT(IC)
         AD4=SUD4/FLOAT(ID)
         F2=S/AD3
         WRITE(6,35)F2,AD3,AD4
      35 FORMAT(1HC,9HFACTOR = ,F10.4,5X,8HNOTCH =  ,F6.0,5X,6HPIN = ,F6.0)
         WRITE(6,20)
      20 FORMAT(1H ,*   SCD1    SCD2    SCD3    SCD4    SCD5    SCD6    DI1     DI2     D
     1   DI3     DI4   AVER   SDEV   POUNDS NEWTON ANGLE D3-AD3  D4-AD4*)
         I=0
         XFORLB=0.
         YFORLB=0.
         ICOUNT=0
C        NROLLS=NUMBER OF ROLLING ELEMENTS IN BEARING
         NROLLS=20
         DSECT=360./FLOAT(NROLLS)
         SECTOR=DSECT
         DO 51 IC=1,ID
         D1=R(IC,2)-R(IC,1)
         D2=R(IC,3)-R(IC,1)
         D3=R(IC,4)-R(IC,1)
         D4=R(IC,3)-R(IC,2)
         D5=R(IC,4)-R(IC,3)
         D6=R(IC,4)-R(IC,2)
         D7=D3-AD3
         D8=D4-AD4
         SCD1=D1*F2
         SCD2=D2*F2
         SCD3=D3*F2
         SCD4=D4*F2
         SCD5=D5*F2
         SCD6=D6*F2
         DI1         =(SCD1-SCZ1)
         DI2         =(SCD2-SCZ2)
         DI3         =(SCZ5-SCD5)
         DI4         =(SCZ6-SCD6)
         AD=(DI1+DI2+DI3+DI4)/4.
         SDEV=SQRT(((DI1-AD)*(DI1-AD)+(DI2-AD)*(DI2-AD)+(DI3-AD)*(DI3-AD)+(
        1DI4-AD)*(DI4-AD))/3.)
         FORCE(IC)=AD*AK*4.448
         FORLB=AD*AK
         ANGLER=ANGLE(IC)
         IF (ANGLER.LE.SECTOR)GO TO 100
         I=I+1
         XLB(I)=XFORLB/FLOAT(ICOUNT)
         YLB(I)=YFORLB/FLOAT(ICOUNT)
         SECTOR=SECTOR+DSECT
         XFORLB=0.
         YFORLB=0.
         ICOUNT=0
  100    RANGLE=ANGLE(IC)*.017453
         XFORLB=(FORLB*COS(RANGLE))+XFORLB
         YFORLB=(FORLB*SIN(RANGLE))+YFORLB
```

```
LN  0153            ICOUNT=ICOUNT+1
LN  0154            WRITE(6,22)SCD1,SCD2,SCD3,SCD4,SCD5,SCD6,CI1,CI2,CI3,CI4,AD,SDE
LN  0155           1FORCE(IC),ANGL (IC),07,08
LN  0156         22 FORMAT(1H ,6F7.2,6F6.1,2F7.2,F5.0,2F8.0)
LN  0157         51 CONTINUE
LN  0158            WRITE (6,99)
LN  0159         99 FORMAT (1H /1H )
LN  0160            WRITE(6,33)LINE3,LINE1
LN  0161            WRITE(6,34)LINE2,LINE4
LN  0162            WRITE(6,33)LINE5
LN  0163            TOTALX=0.
LN  0164            TOTALY=0.
LN  0165            SECTOR=0.
LN  0166            WRITE (6,101)
LN  0167       101  FORMAT (1H0,'SECTOR   X FORCES   Y FORCES')
LN  0168            DO 102 I=1,NROLLS
LN  0169            SECTOR=SECTOR+DSECT
LN  0170            WRITE (6,103)SECTOR,XLB(I),YLB(I)
LN  0171       103  FORMAT (1H0,F5.0,3X,F7.2,3X,F7.2)
LN  0172            TOTALX=TOTALX+XLB(I)
LN  0173            TOTALY=TOTALY+YLB(I)
LN  0174       102  CONTINUE
LN  0175            THETA=(ATAN(TOTALY/TOTALX))*57.297
LN  0176            FORCE1=SQRT(TOTALX**2+TOTALY**2)
LN  0177            WRITE (6,104)THETA,FORCE1
LN  0178       104  FORMAT (1H0,'ANGLE=',F5.0,3X,'FORCE=',F7.2)
LN  0179            CALL PLOTS
LN  0180            CALL PLOT(1.5,5.5,-3)
LN  0181            CALL FACTOR (.8)
LN  0182            ANGL (IC)=0.
LN  0183            ANGL (IC+1)=60.
LN  0184            CALL AXIS(0.,0.,15HANGLE (DEGREES),-15,06.,0.,0.,60. )
LN  0185            FORCE(IC)=0.
LN  0186            FORCE(IC+1)=5.
LN  0187            CALL AXIS(0., -5., 15HFORCE (NEWTONS) ,15,10.00,90.,-25.,5.)
LN  0188            CALL SYMBOL(-.6,-4.57,.10,105H-5.00     -4.00     -3.00     -2.00
LN  0189           1-1.00     0.00      1.00      2.00      3.00      4.00      5.00
LN  0190           2                          ,90.,105)
LN  0191            CALL SYMBOL(-.75,-1.06,.14,15HFORCE (POUNDS)      ,90.,15)
LN  0192            CALL SYMBOL(0.3,4.5,0.1  ,LINE1,0.0,32)
LN  0193            CALL SYMBOL(0.3,4.2,0.1  ,LINE2,0.0,32)
LN  0194            CALL SYMBOL(0.3,3.9,0.1  ,LINE3,0.0,24)
LN  0195            CALL SYMBOL(0.3,3.6,0.1  ,LINE4,0.0,32)
LN  0196            CALL SYMBOL(0.3,3.3,0.1,LINE5,0.0,16)
LN  0197            CALL PLOT(-.5,-4.45,3)
LN  0198            CALL PLOT(-.5,4.45,2)
LN  0199            CALL PLOT(-.56,-4.45,3)
LN  0200            CALL PLOT(-.5,-4.45,2)
LN  0201            CALL PLOT(-.56,-3.56,3)
LN  0202            CALL PLOT(-.5,-3.56,2)
LN  0203            CALL PLOT(-.56,-2.67,3)
LN  0204            CALL PLOT(-.5,-2.67,2)
LN  0205            CALL PLOT(-.56,-1.78,3)
LN  0206            CALL PLOT(-.5,-1.78,2)
LN  0207            CALL PLOT(-.56,-.89,3)
LN  0208            CALL PLOT(-.5,-0.89,2)
LN  0209            CALL PLOT(-.56,0.,3)
LN  0210            CALL PLOT(-.5,0.,2)
LN  0211            CALL PLOT(-.56,0.89,3)
LN  0212            CALL PLOT(-.5,0.89,2)
LN  0213            CALL PLOT(-.56,1.78,3)
LN  0214            CALL PLOT(-.5,1.78,2)
LN  0215            CALL PLOT(-.56,2.67,3)
LN  0216            CALL PLOT(-.5,2.67,2)
LN  0217            CALL PLOT(-.56,3.56,3)
LN  0218            CALL PLOT(-.5,3.56,2)
LN  0219            CALL PLOT(-.56,4.45,3)
LN  0220            CALL PLOT(-.5,4.45,2)
LN  0221            NPTS=IC-1
LN  0222            CALL LINE( ANGL ,FORCE,NPTS,1,1,1)
LN  0223            CALL PLOT(0.,0.,999)
LN  0224            END
```

1. Report No.	2. Government Accession No.	3. Recipient's Catalog No.
NASA CR-2976		

4. Title and Subtitle	5. Report Date
BALL TO SEPARATOR CONTACT FORCES IN ANGULAR CONTACT BALL BEARINGS UNDER THRUST AND RADIAL LOADS	April 1978
	6. Performing Organization Code

7. Author(s)	8. Performing Organization Report No.
Lester J. Nypan	None
	10. Work Unit No.

9. Performing Organization Name and Address	11. Contract or Grant No.
California State University, Northridge Northridge, California 91330	NSG-3065
	13. Type of Report and Period Covered

12. Sponsoring Agency Name and Address	14. Sponsoring Agency Code
National Aeronautics and Space Administration Washington, D.C. 20546	Contractor Report

15. Supplementary Notes

Final report. Project manager, Harold H. Coe, Fluid System Components Division, NASA Lewis Research Center, Cleveland, Ohio.

16. Abstract

Experimental data is reported on ball to cage contact forces in a 110 mm bore ball bearing operating at speeds to 12 000 rpm under radial and thrust loads. Information is also reported on cage to inner race land contact force, cage to inner race land clearance, and cage to shaft speed ratios.

17. Key Words (Suggested by Author(s))	18. Distribution Statement
Ball bearings Cage forces Cage speed Ball-cage contact	Unclassified - unlimited STAR Category 37

19. Security Classif. (of this report)	20. Security Classif. (of this page)	21. No. of Pages	22. Price*
Unclassified	Unclassified	108	A06

* For sale by the National Technical Information Service, Springfield, Virginia 22161

NASA-Langley, 1978